Supporting Information

Nanocluster-regulated porous ionic rotaxane assemblies with solvent-adaptability for selective adsorption and conductivity

Jiaxu Wang, Mingfeng Wei, Zexi Zhu, Bao Li,* Lixin Wu*

State Key Laboratory of Supramolecular Structure and Materials, College of Chemistry, Jilin University, Changchun, P. R. China.

**E-mail: wulx@jlu.edu.cn; libao@jlu.edu.cn*

Table of Contents

S1. Materials……..…..……2

S2. Measurements……...……...……2

S3. Synthesis……...……3

S4. Preparation and structure analysis of CR·PF_6/Cl/Br/I/SO_4……...……...……...……7

S5. Preparation and structure analysis of porous rotaxane assemblies….……...……...…21

S6. Solvent-adaptability for selective adsorption..……...…….……27

S7. Reversible crystalline transformation triggered by DMSO……..……43

S8. Computational details……..……54

S9. Induced proton conductivity variations……..55

S10. Reference……56

S1. Materials

The general chemicals, 1,12-dibromododecane, α-cyclodextrin, pentamethyldiethylenetriamine (PMDETA), KPF_6, CH_3COOH, and Sephadex G-25 were purchased from Shanghai Aladdin Biochemical Technology Company Limited. NaN_3, $CuSO_4$, triethylamine, were purchased from Tianjin Fuyu Fine Chemical Company Limited. Propargyl bromide (stabilized with MgO) was purchased from Anhui Senrise Technologies Company Limited. Sodium ascorbate was purchased from Chengdu Huaxia Chemical Reagent Company Limited. Copper(I) iodide was purchased from Shanghai Macklin Biochemical Company Limited. $MgSO_4$, CH_3COOK, and K_2SO_4 were purchased from Tianjin Fuchen Chemical Reagent Factory. NaCl, NaBr, NaI were purchased from Tianjin Huadong Reagent Factory. Organic solvents were purchased from Tianjin Tiantai Chemical Reagent Company Limited. $H_4SiW_{12}O_{40}$ and $H_3PMo_{12}O_{40}$ were purchased from Sinopharm Chemical Reagent Company Limited. $H_4PMo_{11}VO_{40}$, $H_5PMo_{10}V_2O_{40}$ and $H_6PMo_9V_3O_{40}$ were synthesized according to the literature.[1,2]

S2. Measurements

^{1}H NMR and COSY were recorded on a CAS Oxford 400 MHz spectrometer by using tetramethylsilane (TMS) as an internal reference. ^{1}H NMR, DOSY, and 2D NOESY NMR spectra were recorded on a Bruker Avance 500 MHz spectrometer (Germany) by using tetramethylsilane (TMS) as internal reference (s = singlet, d = doublet, t = triplet, q = quartet, m = multiplet). ESI-MS was tested by Agilent1290-Bruker micrOTOF QII. FT-IR spectra (KBr pellet) were collected on a Bruker Vertex 80 V spectrometer (Germany) equipped with a DTGS detector (32 scans) in a resolution of 4 cm^{-1}. Scanning electronic microscopic (SEM) measurement was performed on a JEOL-6700F (Japan) field emission scanning electron microscope. Transmission electronic microscopic (TEM) images were obtained on a JEOL JEM-2100F (Japan) field emission electron microscope. Atomic force microscopic (AFM) images were taken with a Dimension FastScan™ atomic force microscope (Bruker, USA) under ambient conditions. Powder X-ray diffraction (PXRD) data were recorded on Rigaku SmartLab 3 (Japan) X-ray diffractometer using Cu$K\alpha_1$ radiation at the wavelength of 1.543 Å. Organic elemental analysis (C, N, H and S) was carried out on a Flash EA1112 from Thermo-Quest Italia S.P.A. Inorganic elemental analysis (Mo and V) was carried out on Thermo Scientific™ iCAP™ 7400 ICP-OES. N_2 and CO_2 sorption experiment were carried out on a Micromeritics ASAP 2460 instrument. The proton conductivity was measured with a Solartron 1260A impedance/gain-phase analyzer by a two-probe AC impedance from 0.1 to 100 kHz with the amplitude voltage of the signal at 20 mV. The samples were covered between two round copper electrodes (d = 0.8 cm) and maintained at 98% relative humidity (provided by saturated K_2SO_4 solution) for measurement.

Single-crystal X-ray diffraction data were collected at 100 K using a Bruker D8 Venture imaging plate diffractometer with graphite-monochromated Mo$K\alpha$ (λ = 0.71073 Å). Data were collected using Bruker APEX 3 and integrated with SAINT (Bruker, *SAINT*, *V8.40A*, Bruker AXS Inc., Madison, Wisconsin, USA). Multi-scan semi-empirical absorption correction was performed using SADABS-2016/2,[3] and the space group and instruction files were generated by Bruker XPREP. The structure was solved by direct method using the SHELXS,[4] and refined by full-matrix least-squares methods against F^2 by the SHELXL[5] refinement package, implemented in OLEX 2.[6] All non-hydrogen atoms were refined with anisotropic displacement parameters, while C-bound hydrogen atoms were refined isotropic on calculated positions using a riding model with their U_{iso} values constrained to 1.5 times the U_{eq} of their pivot atoms for terminal sp^3 carbon atoms and 1.2 times for all other carbon atoms. Due to the difficulty in distinguishing vanadium atoms from molybdenum atoms in the V-substituted polyoxometalates, co-occupancy of V and Mo was applied. Some crystal structure contained voids, and solvents in these voids were disordered and could not be modeled. Therefore, solvents were removed using the PLATON "SQUEEZE" command.[7] The type and quantity of solvent removed were confirmed by elemental analysis. Distances and angles in the crystal were measured using the Mercury and Diamond.

S3. Synthesis

The rotaxanes used in the work are prepared following the route presented in Fig. S1a.

1,12-diazidododecane: 1,12-dibromododecane (5.0 g) and sodium azide (4.0 g) were dissolved in DMF (50.0 mL) and then stirred at 80°C for about 72 h. The solvent was removed through vacuum distillation, and then dichloromethane and water were added. The organic layer was collected and washed with water several times, then dried with anhydrous $MgSO_4$, filtered, and concentrated. 1,12-diazidododecane was obtained in 87.34% yield (3.36 g) as a pale-yellow oil; ^{1}H NMR (500 MHz, DMSO-d_6): δ 3.32 (t, J = 6.9 Hz, 4H), 1.53 (p, J = 6.9 Hz, 4H), 1.33–1.26 (m, 16H).

Triethylpropargylammonium bromide: Triethylamine (7.75 mL, 5.64 g) and propargyl bromide (3.63 mL, 5.52 g) were dropwise added to 50 mL ice-cooled $CHCl_3$ successively. After stirring overnight at room temperature, a white precipitate appeared and was collected by vacuum suction filtration. The crude product was dissolved in CH_3OH and separated by adding a large amount of ethyl acetate. Triethylpropargylammonium bromide was obtained in 84.58% yield (8.64 g) as a white powder; ^{1}H NMR (500 MHz, DMSO-d_6): δ 4.32 (m, 2H), 4.02 (t, J = 2.52 Hz, 1H), 3.33 (q, J = 7.25 Hz, 6H), 1.22 (t, J = 7.25 Hz, 9H).

***N,N'*-((Dodecane-1,12-diylbis(1*H*-1,2,3-triazole-1,4-diyl-))bis(methylene))bis(*N,N*-diethylethanaminium):** 1,12-diazidododecane (2.3 g), CuI (0.18 g) and few drops of triethylamine were dissolved in ethanol, and then triethylpropargylammonium bromide (2.55 g) was added to the solution, the solution was heated at 75°C for 90 h, a orange oil was obtained by adding a large amount of ethyl acetate in yield of 33.7% (2.12 g); ^{1}H NMR (500 MHz, DMSO-d_6): δ 8.45 (s, 2H), 4.55 (s, 4H), 4.40 (t, J = 7.1 Hz, 12H), 1.83 (p, J = 7.1 Hz, 4H), 1.30 (t, J = 7.2 Hz, 18H), 1.24 (s, 16H).

CR·SO_4: 1,12-diazidododecane (3.36 g) was dropwise added to an aqueous solution (250 mL) of α-cyclodextrin (28.66 g) and then stirred with ultrasound for 1 hour to obtain a viscous white turbid solution. Aqueous solutions of triethylpropargylammonium bromide (6.54 g), $CuSO_4$ (1.96 g), and sodium ascorbate (3.08 g) were added successively and then pentamethylldiethylenetriamine (2.8 mL) was added dropwise. The mixture was stirred at room temperature for 90 hours, the precipitate was removed and the solution was concentrated by rotary evaporation. A large amount of acetone was added to the concentrated aqueous solution to separate pale blue powder. The crude product was further purified by Sephadex G-25 several times and recrystallized in MeOH/H_2O. CR·SO_4 was obtained as a white powder in 16.23% yield (5.70 g);^{1}H NMR (500 MHz, D_2O): δ 8.29 (s 2H), 4.99 (s 12H), 4.51 (s 4H), 4.34 (t, J = 7.8 Hz, 4H), 3.83 (t, J = 9.3 Hz, 12H), 3.80–3.65 (m, 36H), 3.58 (t, J = 9.2 Hz, 12H), 3.52–3.45 (m, 12H), 3.20 (q, J = 7.1 Hz, 12H), 1.92 (s, 4H), 1.45 (s, 16H), 1.34 (t, J = 7.2 Hz, 18H); ^{1}H NMR (500 MHz, DMSO-d_6): δ 8.05 (s, 2H), 6.15 (s, 12H), 6.06 (s, 12H), 4.79 (s, 12H), 4.46 (t, J = 7.02 Hz, 16H), 4.31 (s, 4H), 3.77 (t, J = 9.1 Hz, 12H), 3.59–3.50 (m, 36H), 3.35 (m, 12H), 3.27 (s, 12H), 3.17 (d, J = 7.3 Hz, 12H), 2.10 (s, 4H), 1.52–1.45 (m, 16H), 1.29 (t, J = 7.1 Hz, 18H); ^{13}C NMR (500MHz, D_2O): δ 135.15, 127.95, 102.39, 81.09, 74.04, 72.40, 71.89, 59.98, 52.70, 50.75, 50.32, 31.79, 31.70, 31.56, 31.27, 28.09, 6.85; ESI-MS, (*m/z*) $[C_{30}H_{60}N_8(C_{36}H_{60}O_{30})_2]^{2+}$: 1238.6; Elemental anaylsis for $C_{30}H_{60}N_8(C_{36}H_{60}O_{30})_2SO_4 \cdot 9H_2O$ (%): Anal. Calcd: C 44.76, H 7.292, N 4.09, S 1.172; Found: C 44.72, H 6.991, N 4.09, S 1.143.

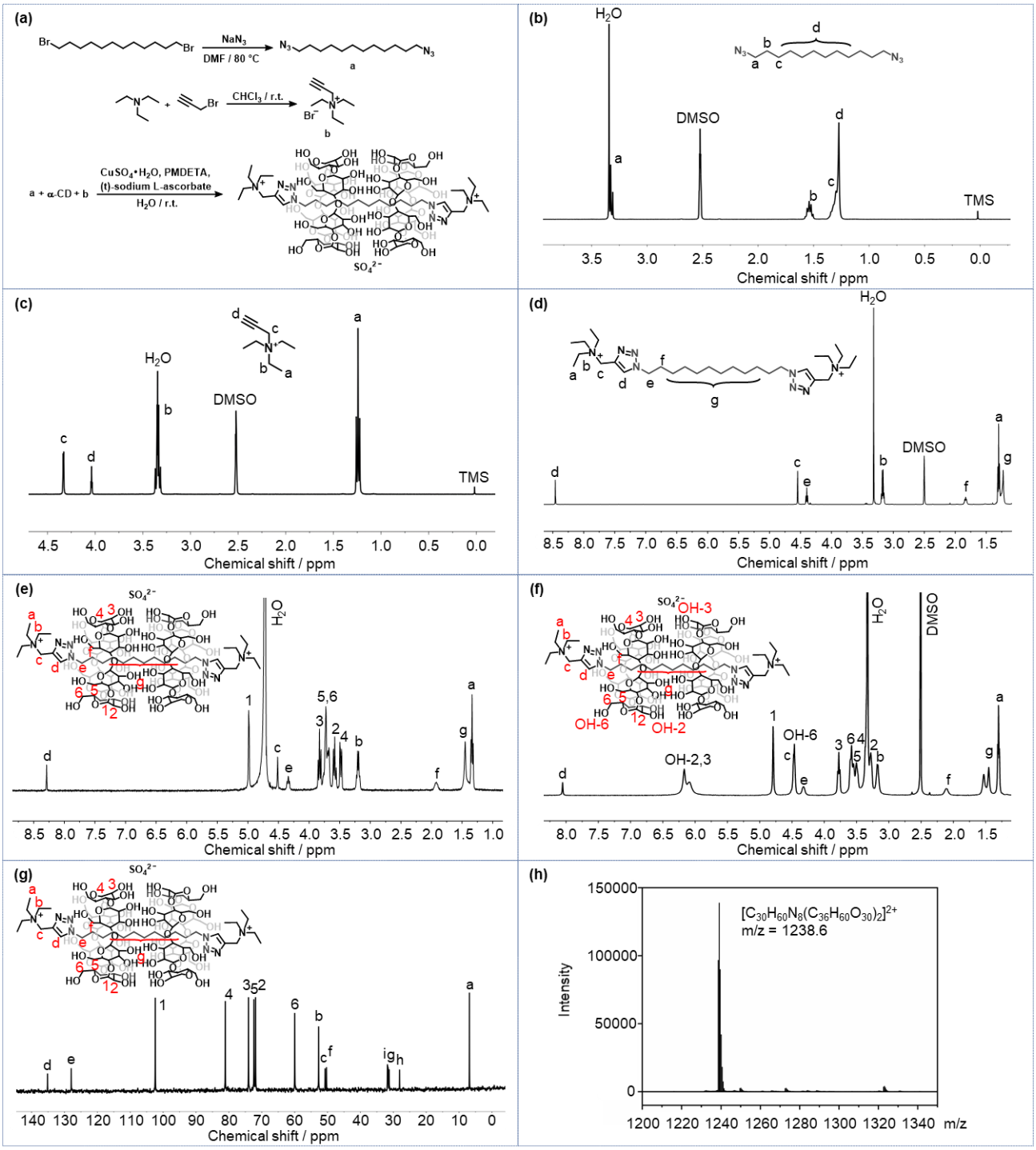

Fig. S1 Synthetic route of cationic rotaxane (CR) sulfate. (a) Synthetic route of CR·SO_4; (b) ^{1}H NMR spectrum of 1,12-diazidododecane (400 MHz, DMSO-d_6); (c) ^{1}H NMR spectrum of triethylpropargylammonium bromide (400 MHz, DMSO-d_6); (d) ^{1}H NMR spectrum of guest moiety *N,N'*-((dodecane-1,12-diylbis(1*H*-1,2,3-triazole-1,4-diyl))bis(methylene))bis(*N,N*-diethyl-ethanaminium) (500 MHz, DMSO-d_6); (e) ^{1}H NMR spectrum of CR·SO_4 (400 MHz, D_2O); (f) ^{1}H NMR spectrum of CR·SO_4 (400 MHz, DMSO-d_6); (g) ^{13}C NMR spectrum of CR·SO_4 (500 MHz, D_2O); (H) ESI-MS spectrum of CR·SO_4.

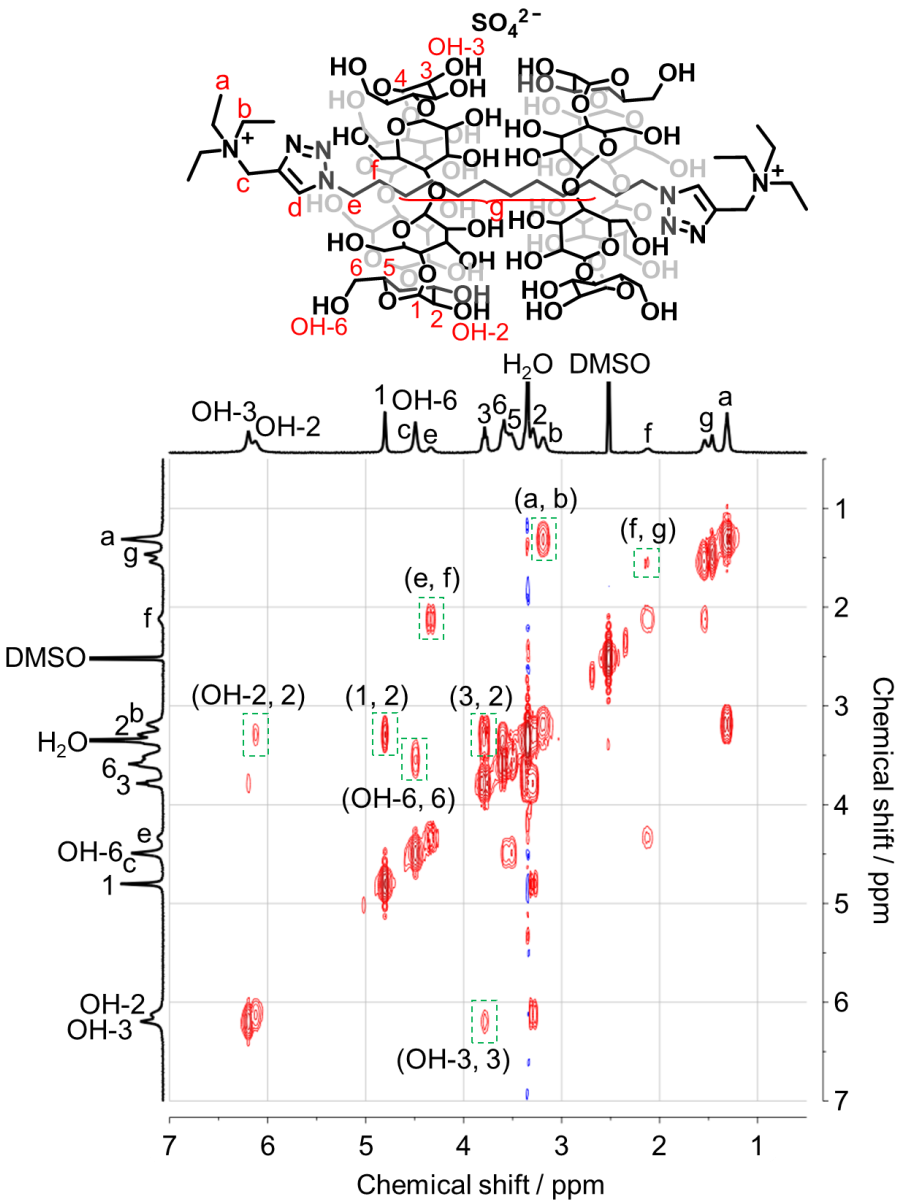

Fig. S2 2D correlation spectroscopy (COSY) spectrum (400 MHz, DMSO-d_6) of CR·SO_4.

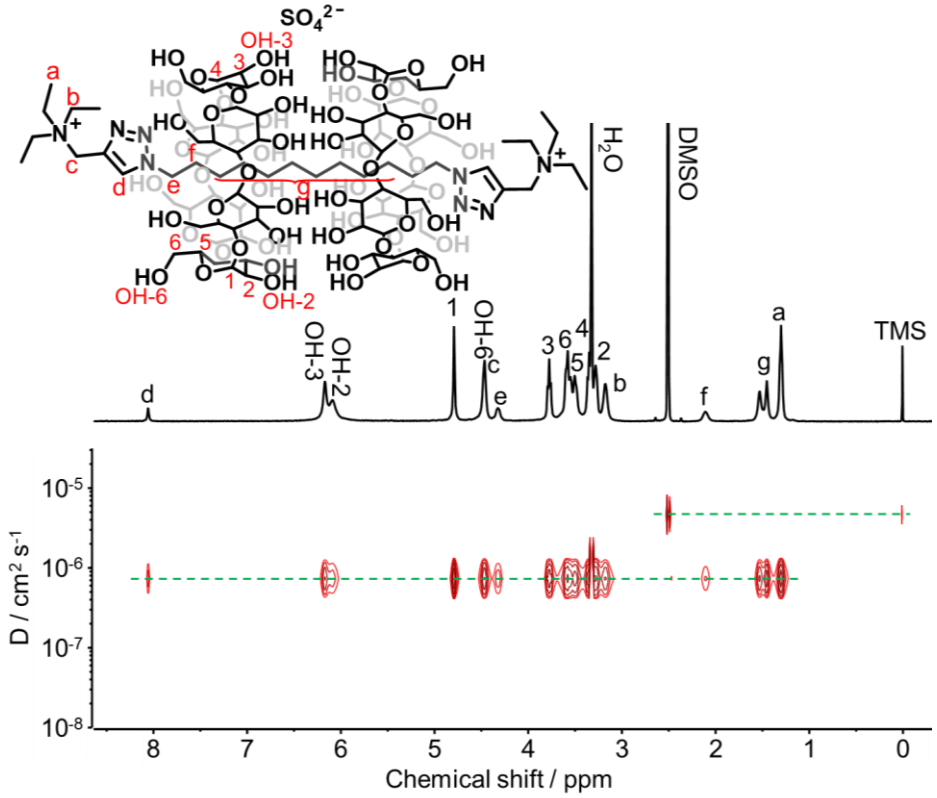

Fig. S3 Diffusion-ordered spectroscopy (DOSY) spectrum (500 MHz, DMSO-d_6) of CR·SO_4.

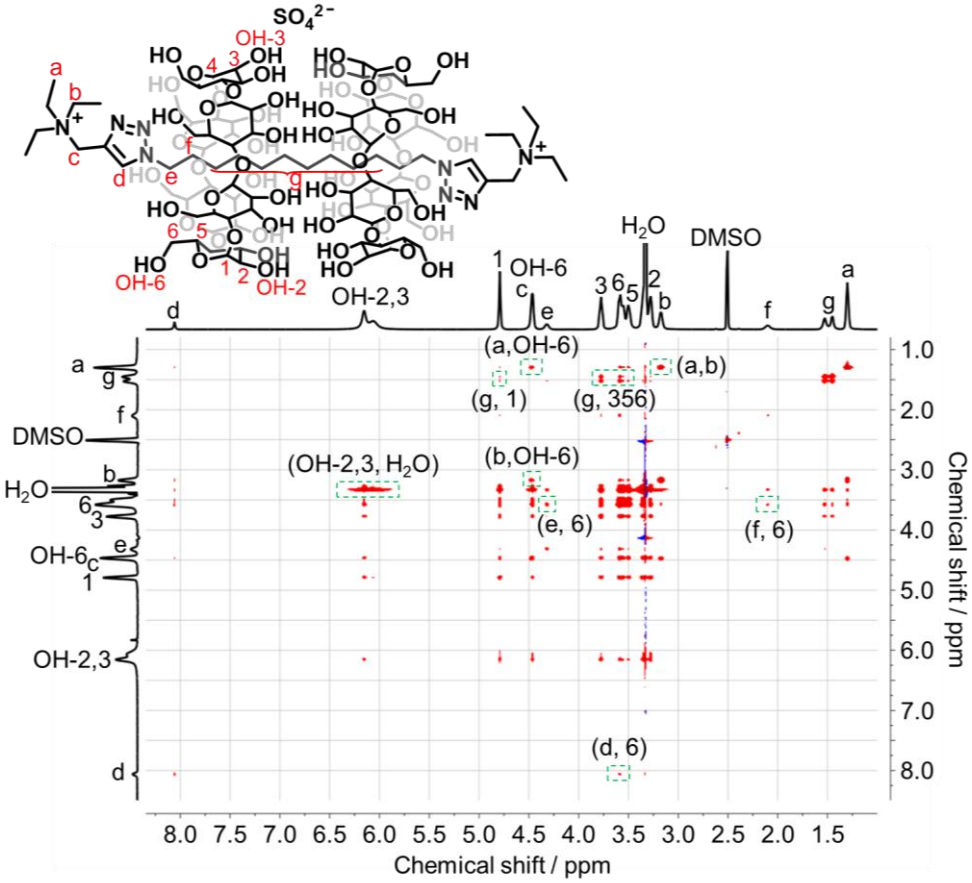

Fig. S4 2D nuclear Overhauser effect spectroscopic (NOESY) spectrum (500 MHz, DMSO-d_6) of CR·SO_4.

S4. Preparation and structure analysis of CR·PF_6/Cl/Br/I/SO_4

Preparation of CR·PF_6 single crystal: CR·SO_4 (294 mg) and KPF_6 (50 mg) were dissolved in water to obtain a clear solution, and evaporated for one day to get colorless block crystals; ^{1}H NMR (500 MHz, DMSO-d_6): δ 8.16 (s, 2H), 5.87 (s, 12H), 5.51 (s, 12H), 4.78 (d, J = 3.2 Hz, 12H), 4.47 (d, J = 5.8 Hz, 16H), 4.26 (t, J = 8.4 Hz, 4H), 3.77 (t, J = 9.3 Hz, 12H), 3.66–3.47 (m, 36H), 3.39 (t, J = 9.0 Hz, 12H), 3.25 (t, J = 9.9 Hz, 12H), 3.16 (q, J = 6.0 Hz, 12H), 1.94 (s, 4H), 1.48–1.42 (m, 16H), 1.30 (t, J = 7.12 Hz, 18H). Elemental analysis for $C_{30}H_{60}N_8(C_{36}H_{60}O_{30})_2(PF_6)_2\cdot 14H_2O$ (%): Anal. Calcd: N 3.69, C 40.65, H 6.943; Found: N 3.70, C 40.56, H 6.941.

Preparation of CR·Cl/Br/I: CR·SO_4 aqueous solution was treated with activated ion exchange resins (by NaCl/NaBr/NaI) for one day, the resins were removed by filtration and the ion-substituted CR was precipitated in acetone.

Preparation of CR·Cl/Br/I/SO_4 single crystal: Ethanol vapor was slowly volatilized into the CR·Cl/Br/I/SO_4 alkaline aqueous solution, resulting in colorless needle or block crystals. Elemental analysis for $C_{30}H_{60}N_8(C_{36}H_{60}O_{30})_2Cl_2\cdot 10H_2O$ (%): Anal. Calcd: N 4.11, C 44.88, H 7.385; Found: N 4.00, C 44.84, H 7.224; $C_{30}H_{60}N_8(C_{36}H_{60}O_{30})_2Br_2\cdot 10H_2O$ (%): Anal. Calcd: N 4.05, C 44.32, H 7.073; Found: N 3.98, C 44.56, H 6.990; $C_{30}H_{60}N_8(C_{36}H_{60}O_{30})_2I_2\cdot 5H_2O$ (%): Anal. Calcd: N 3.97, C 43.41, H 6.785; Found: N 3.90, C 43.56, H 6.867; $C_{30}H_{60}N_8(C_{36}H_{60}O_{30})_2SO_4\cdot 43H_2O$ (%): Anal. Calcd: N 3.41, C 37.25, H 6.313, S 0.975; Found: N 3.36, C 37.25, H 6.368, S, 1.384.

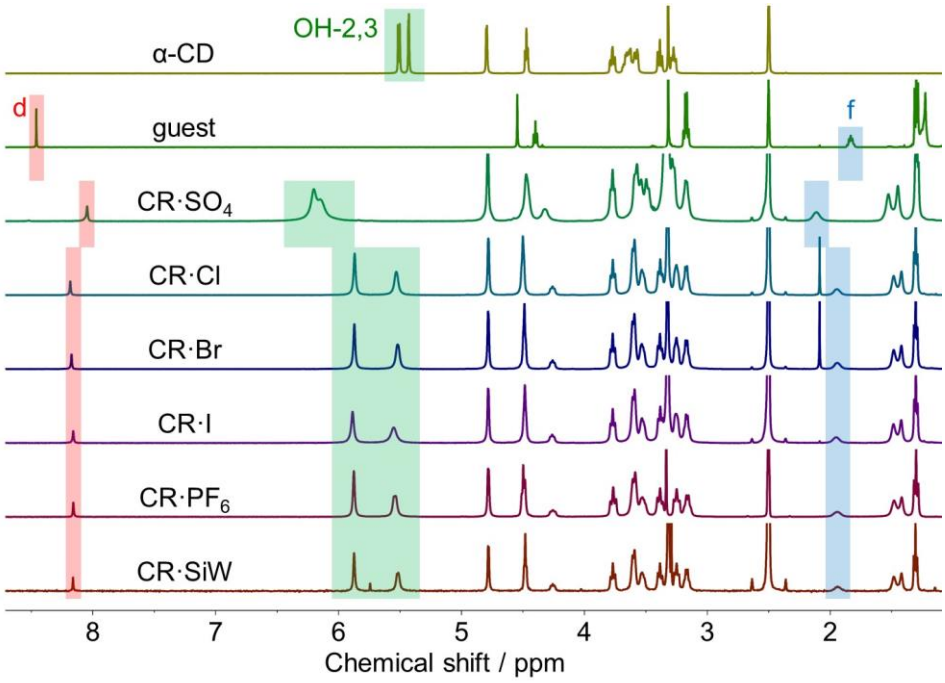

Fig. S5 Comparison of ^{1}H NMR spectra of α-CD, guest, CR·SO_4, CR·Cl, CR·Br, CR·I, CR·PF_6, CR·SiW in DMSO-d_6.

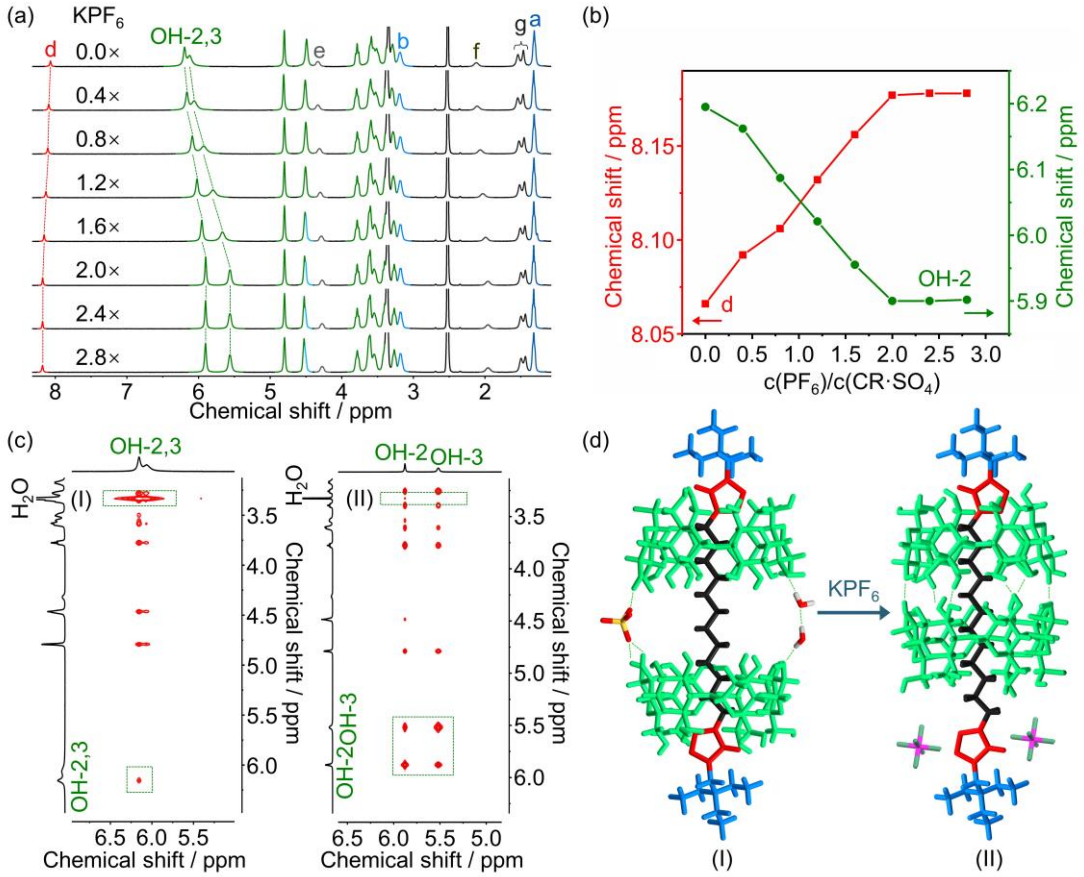

Fig. S6 (a) ^{1}H NMR of CR·SO_4 with the addition of 0–2.8 eq. KPF_6 (DMSO-d_6); (b) Chemical shift variations of H_d and $H_{OH\text{-}2}$ relative to the ratio of c(PF_6)/c(CR·SO_4); (c) Comparison of 2D NOESY spectra of CR·SO_4 and CR·PF_6; (d) Possible conformational changes.

Table S1 Crystal data and structure refinement for CR·PF_6.

Formula	$C_{30}H_{60}N_8(C_{36}H_{60}O_{30})_2(PF_6)_2 \cdot 13H_2O$
CCDC number	2320352
Formula weight	3002.68
Temperature/ K	100.15
Crystal system	Orthorhombic
Space group	$P2_12_12_1$
color of crystal	colourless
a/ Å	14.3808(14)
b/ Å	23.220(2)
c/ Å	40.897(4)
α/°	90
β/°	90
γ/°	90
Volume/ Å^3	13656(2)
Z	4
ρ_{calc}/ g·cm^{-3}	1.460
μ/ mm^{-1}	0.154
F(000)	6384
Radiation	Mo$K\alpha$ (λ = 0.71073 Å)
2θ range for data collection/°	4.89–50.05 (0.84 Å)
Index ranges	$-17 \le h \le 17$, $-27 \le k \le 27$, $-48 \le l \le 48$
Reflections collected	471403
Independent reflections	24035 [R_{int} = 0.1112, R_{sigma} = 0.0369]
Goodness of fit on F^2	1.932
Final R index.	R_1 = 0.1368, wR_2 = 0.4084
Largest diff. peak/hole/e Å^{-3}	1.78/−0.83

$R_1 = \sum|F_o| - |F_c|/\sum|F_o|$. $wR_2 = \{(F_o{}^2 - F_c{}^2)^2/\sum w(F_o{}^2)^2\}^{1/2}$.

Table S2 Crystal data and structure refinement for CR·Cl.

Formula	$C_{102}H_{180}Cl_2N_8O_{73}$
CCDC number	2421017
Formula weight	2757.43
Temperature/ K	100.15
Crystal system	Orthorhombic
Space group	$P2_12_12_1$
color of crystal	colourless
a/ Å	14.5575(13)
b/ Å	23.1145(18)
c/ Å	41.496(4)
α/°	90
β/°	90
γ/°	90
Volume/ Å^3	13963(2)
Z	4
ρ_{calc}/ g·cm^{-3}	1.312
μ/ mm^{-1}	0.148
F(000)	5864
Radiation	Mo*Kα* (λ = 0.71073 Å)
2θ range for data collection/°	4.91–50.05 (0.84 Å)
Index ranges	$-17 \le h \le 17$, $-27 \le k \le 27$, $-49 \le l \le 49$
Reflections collected	771895
Independent reflections	24654 [R_{int} = 0.0608, R_{sigma} = 0.0144]
Goodness of fit on F^2	1.084
Final *R* index.	R_1 = 0.0647, wR_2 = 0.1796
Largest diff. peak/hole/e Å^{-3}	1.40/−0.77

$R_1 = \sum|F_o| - |F_c|/\sum|F_o|$. $wR_2 = \{\left(F_o{}^2 - F_c{}^2\right)^2/\sum w\left(F_o{}^2\right)^2\}^{1/2}$.

Table S3 Crystal data and structure refinement for CR·Br.

Formula	$C_{102}H_{180}Br_2N_8O_{76.50}$
CCDC number	2421014
Formula weight	2902.35
Temperature/ K	100.00
Crystal system	Orthorhombic
Space group	$P2_12_12_1$
color of crystal	colourless
a/ Å	14.5353(7)
b/ Å	23.1364(10)
c/ Å	41.710(2)
α/°	90
β/°	90
γ/°	90
Volume/ Å^3	14026.8(11)
Z	4
ρ_{calc}/ g·cm^{-3}	1.374
μ/ mm^{-1}	0.682
F(000)	6120
Radiation	Mo*Kα* (λ = 0.71073 Å)
2θ range for data collection/°	4.81–50.05 (0.84 Å)
Index ranges	$-17 \le h \le 17$, $-27 \le k \le 27$, $-49 \le l \le 49$
Reflections collected	562424
Independent reflections	24768 [R_{int} = 0.0626, R_{sigma} = 0.0236]
Goodness of fit on F^2	1.060
Final *R* index.	R_1 = 0.0866, wR_2 = 0.2413
Largest diff. peak/hole/e Å^{-3}	1.49/−2.99

$R_1 = \sum|F_o| - |F_c|/\sum|F_o|$. $wR_2 = \{(F_o{}^2 - F_c{}^2)^2/\sum w(F_o{}^2)^2\}^{1/2}$.

Table S4 Crystal data and structure refinement for CR·I.

Formula	$C_{102}H_{180}I_2N_8O_{73.50}$
CCDC number	2421018
Formula weight	2948.33
Temperature/ K	100.00
Crystal system	Orthorhombic
Space group	$P2_12_12_1$
color of crystal	colourless
a/ Å	14.6275(15)
b/ Å	23.029(2)
c/ Å	41.431(4)
α/°	90
β/°	90
γ/°	90
Volume/ Å^3	13956(2)
Z	4
ρ_{calc}/ g·cm^{-3}	1.403
μ/ mm^{-1}	0.553
F(000)	6168
Radiation	Mo*Kα* (λ = 0.71073 Å)
2θ range for data collection/°	4.91–50.05 (0.84 Å)
Index ranges	$-17 \le h \le 17$, $-27 \le k \le 27$, $-49 \le l \le 49$
Reflections collected	530729
Independent reflections	24638 [R_{int} = 0.0721, R_{sigma} = 0.0214]
Goodness of fit on F^2	1.078
Final *R* index.	R_1 = 0.0972, wR_2 = 0.2722
Largest diff. peak/hole/e Å^{-3}	2.48/−1.40

$R_1 = \sum|F_o| - |F_c|/\sum|F_o|$. $wR_2 = \{(F_o{}^2 - F_c{}^2)^2/\sum w(F_o{}^2)^2\}^{1/2}$.

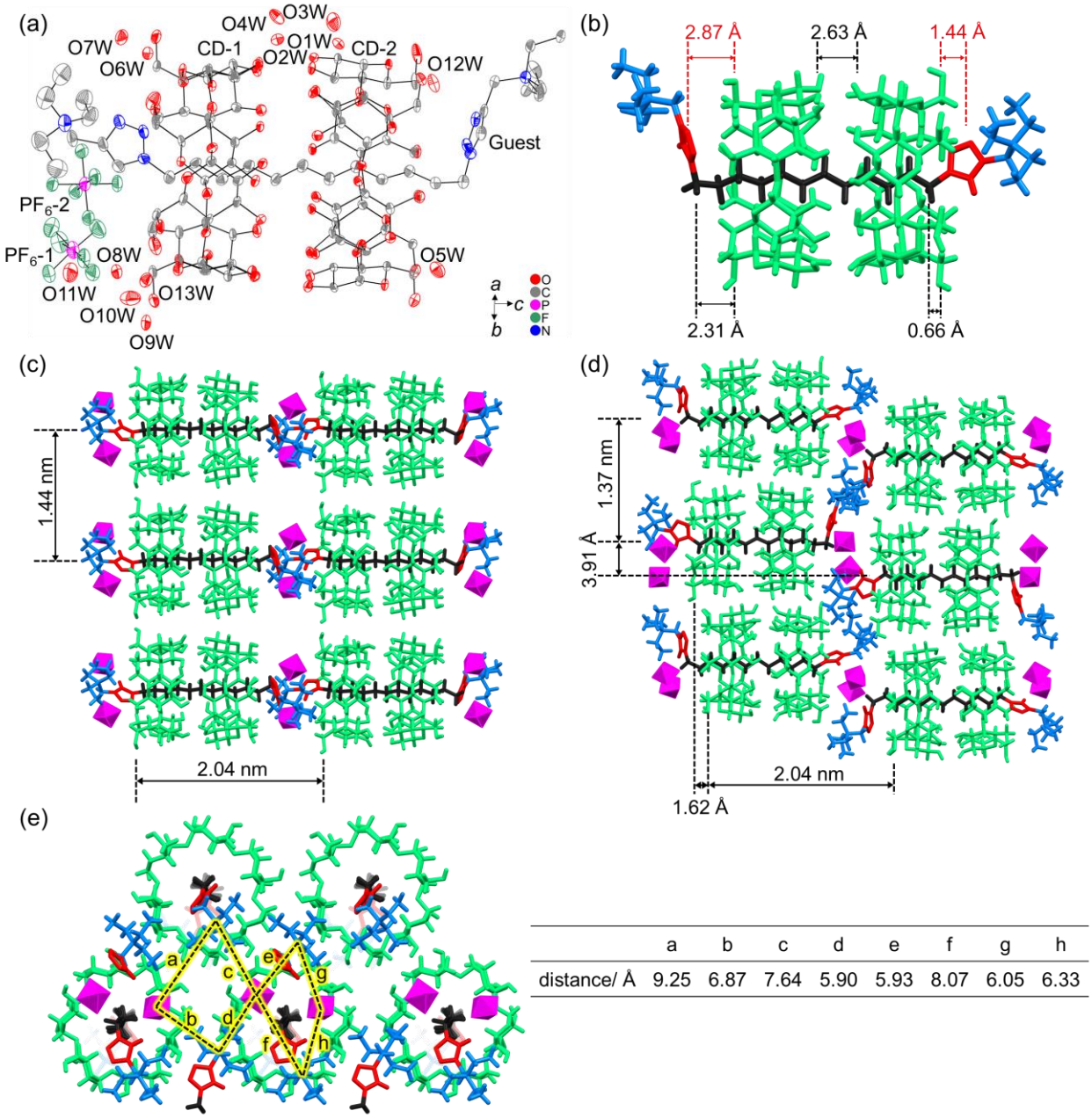

	a	b	c	d	e	f	g	h
distance/ Å	9.25	6.87	7.64	5.90	5.93	8.07	6.05	6.33

Fig. S7 X-ray crystal structure of CR·PF_6. (a) Asymmetric unit (ORTEP Type 30%); (b) The relative position between the guest and CD; (c) Arrangement on the (010) plane; (d) Arrangement on the (110) plane; (e) Arrangement of PF_6^- and triethylamine group, and their distances, on the (001) plane.

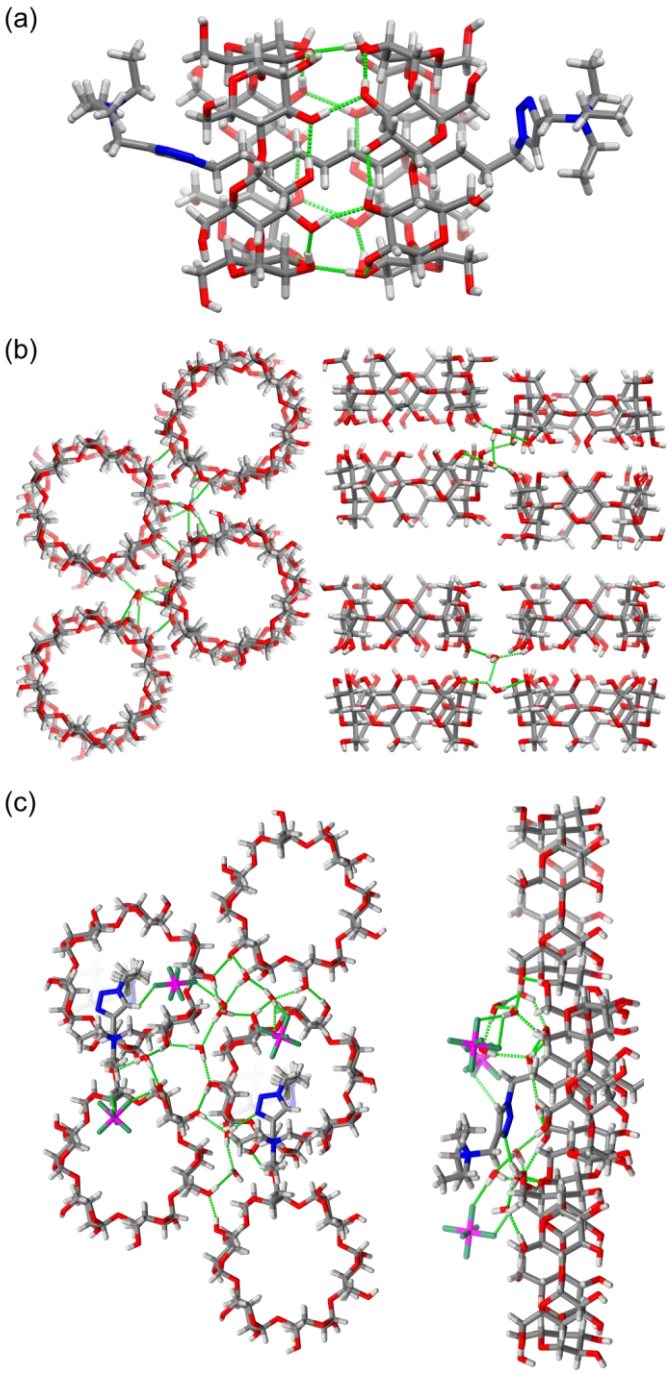

Fig. S8 Hydrogen bonds in CR·PF_6. (a) Intramolecular hydrogen bonds between the secondary side of cyclodextrins on CR; (b) Intermolecular hydrogen bonds among the secondary side of cyclodextrins on CR and crystalline H_2O; (c) Intermolecular hydrogen bonds among the primary side of cyclodextrins on CR, PF_6^-, triazole group and crystalline H_2O.

Table S5 Intramolecular hydrogen bonds list between the secondary side of cyclodextrins on CR.

D	A	d(D−A)/Å	D	A	d(D−A)/Å
O103	O107	2.976(14)	O203	O118	2.923(13)
O108	O213	2.828(12)	O207	O203	2.912(13)
O112	O108	2.792(13)	O208	O212	2.776(13)
O113	O208	2.857(13)	O213	O217	2.781(12)
O117	O113	2.778(14)	O218	O103	2.803(12)
O118	O122	2.789(15)	O222	O218	2.846(13)
O123	O127	2.834(15)	O223	O128	2.837(13)
O128	O102	2.765(14)	O227	O223	2.765(13)
O202	O228	2.719(13)	O228	O123	2.878(13)

Table S6 Intermolecular hydrogen bonds list among the secondary side of cyclodextrins on CR and crystalline H_2O.

D	A	d(D−A)/Å	D	A	d(D−A)/Å
O122	$O1W^{\#1}$	2.704(14)	O2W	$O228^{\#4}$	3.026(15)
O127	$O2W^{\#2}$	2.94(2)	O2W	O112	2.918(14)
O102	$O2W^{\#3}$	2.773(14)	O4W	$O203^{\#4}$	3.099(16)
O107	O4W	2.732(15)	O4W	O3W	2.71(2)
O212	$O202^{\#4}$	2.749(13)	O4W	$O223^{\#5}$	3.026(16)
O217	$O227^{\#5}$	2.693(13)	O3W	$O117^{\#4}$	3.02(3)
O1W	O2W	2.907(15)	O3W	O213	2.93(2)
O1W	O208	2.963(14)			

Symmetry codes: (#1) 1−*x*, 0.5+*y*, 0.5−*z*; (#2) −*x*, 0.5+*y*, 0.5−*z*; (#3) −1+*x*, +*y*, +*z*; (#4) 1−*x*, −0.5+*y*, 0.5−*z*; (#5) −*x*, −0.5+*y*, 0.5−*z*.

Table S7 Intermolecular hydrogen bonds list among the primary side of cyclodextrins on CR, PF_6^-, triazole group and crystalline H_2O in CR·PF_6 single crystal.

D	A	d(D−A)/Å	D	A	d(D−A)/Å
C124	F5B	3.163(19)	O130	O10W	2.80(3)
C22	F6A$^{\#7}$	3.16(2)	O120	O215$^{\#1}$	2.83(2)
O6W	F3B$^{\#8}$	3.018(18)	C5	O115$^{\#8}$	2.94(4)
O6W	F4B$^{\#8}$	2.988(17)	O6W	O7W	2.82(2)
O8W	F2B	2.902(19)	O13W	O120	2.64(2)
O11W	F1A	2.93(3)	O13W	O8W	2.83(2)
O9W	N7$^{\#2}$	2.93(2)	O9W	O10W	2.99(3)
O205	O5W$^{\#6}$	2.879(18)	O12W	O210	2.642(16)
O210	O13W$^{\#4}$	2.700(16)	O12W	O220$^{\#6}$	2.89(2)
O225	O6W$^{\#2}$	2.733(15)	O8W	O124	3.098(16)
O220	O125$^{\#5}$	2.789(16)	O7W	O110	2.725(19)
O230	O105$^{\#2}$	2.820(14)	O7W	O11W$^{\#9}$	2.85(3)
O110	O205$^{\#4}$	2.801(17)	O5W	O225	2.669(18)
O125	O9W	2.80(2)	O5W	O12W$^{\#3}$	3.21(2)
O105	O6W	2.719(16)	O11W	O5W$^{\#10}$	3.06(3)
O215	O9W$^{\#5}$	3.04(2)	O10W	O11W	3.11(3)
O115	O130$^{\#6}$	2.84(2)			

Symmetry codes: (#1) 1−*x*, 0.5+*y*, 0.5−*z*; (#2) −*x*, 0.5+*y*, 0.5−*z*; (#3) −1+*x*, +*y*, +*z*; (#4) 1−*x*, −0.5+*y*, 0.5−*z*; (#5) −*x*, −0.5+*y*, 0.5−*z*; (#6) 1+*x*, +*y*, +*z*; (#7) 0.5−*x*, 2−*y*, 0.5+*z*; (#8) −0.5+*x*, 1.5−*y*, −*z*; (#9) 0.5+*x*, 1.5−*y*, −*z*; (#10) −0.5−*x*, 2−*y*, −0.5+*z*.

Table S8 Crystal data and structure refinement for CR·SO_4.

Formula	$C_{30}H_{60}N_8(C_{36}H_{60}O_{30})_2SO_4 \cdot 16.4H_2O$
CCDC number	2421019
Formula weight	2869.91
Temperature/ K	100.00
Crystal system	Orthorhombic
Space group	$P2_12_12_1$
color of crystal	colourless
a/ Å	22.125(2)
b/ Å	23.865(2)
c/ Å	26.217(3)
α/°	90
β/°	90
γ/°	90
Volume/ Å^3	13843(2)
Z	4
ρ_{calc}/ g·cm^{-3}	1.377
μ/ mm^{-1}	0.133
F(000)	6159
Radiation	Mo$K\alpha$ (λ = 0.71073 Å)
2θ range for data collection/°	4.82–50.05 (0.84 Å)
Index ranges	$-26 \le h \le 26$, $-28 \le k \le 28$, $-31 \le l \le 31$
Reflections collected	708613
Independent reflections	24458 [R_{int} = 0.1224, R_{sigma} = 0.0311]
Goodness of fit on F^2	1.075
Final R index.	R_1 = 0.0982, wR_2 = 0.2613
Largest diff. peak/hole/e Å^{-3}	1.67/−0.78

$R_1 = \sum|F_o| - |F_c|/\sum|F_o|$. $wR_2 = \{(F_o{}^2 - F_c{}^2)^2/\sum w(F_o{}^2)^2\}^{1/2}$.

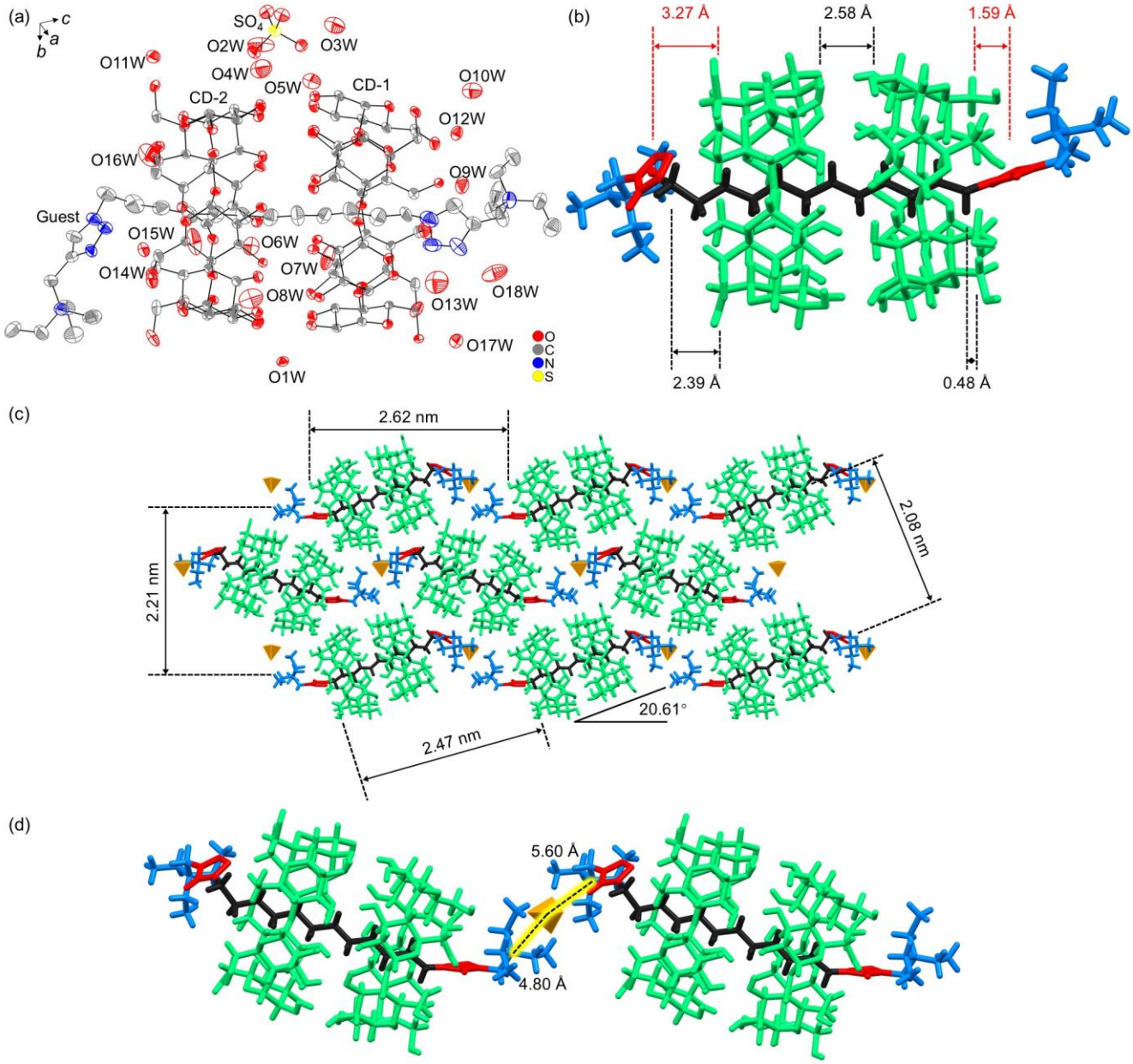

Fig. S9 X-ray crystal structure of CR·SO_4. (a) Asymmetric unit (ORTEP Type 30%); (b) The relative position between the guest and CD; (c) Arrangement on the (010) plane; (d). Electrostatic interaction distance between SO_4^{2-} and triethylamino groups.

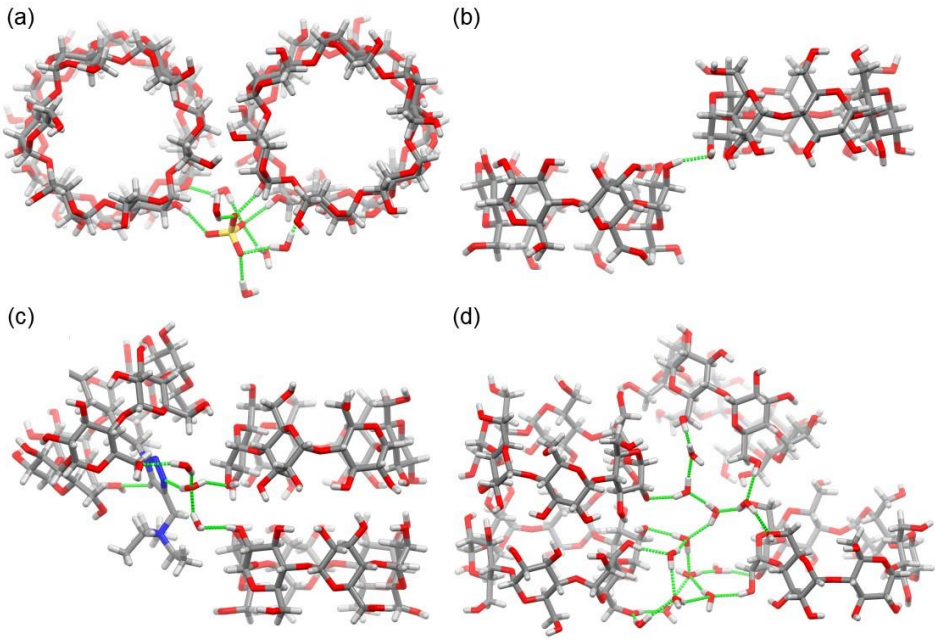

Fig. S10 Hydrogen bonds in CR·SO_4. (a, b) Intermolecular hydrogen bonds among the secondary side of cyclodextrins on CR and SO_4^{2-} in CR·SO_4 single crystal; (c, d) Intermolecular hydrogen bonds among the cyclodextrins, triazole group and crystalline H_2O.

Table S9 Intramolecular hydrogen bonds list between the secondary side of cyclodextrins on CR.

D	A	d(D−A)/Å	D	A	d(D−A)/Å
O103	O107	2.877(8)	O202	O228	2.780(9)
O108	O112	2.924(9)	O203	O128	2.787(9)
O113	O218	2.811(9)	O207	O203	2.901(10)
O117	O113	2.958(9)	O212	O208	2.929(10)
O118	O213	2.816(10)	O213	O217	2.883(9)
O122	O118	2.912(9)	O218	O222	2.794(8)
O123	O208	2.756(9)	O223	O108	2.710(8)
O127	O123	2.798(10)	O227	O223	2.874(9)
O128	O102	2.898(9)	O228	O103	2.846(9)

Table S10 Intermolecular hydrogen bonds list among the secondary side of cyclodextrins on CR and SO_4^{2-}

D	A	d(D−A)/Å	D	A	d(D−A)/Å
O102	O4S$^{\#2}$	2.738(11)	O2W	O3S	2.817(15)
O112	O1S	2.768(10)	O3W	O1S	2.76(4)
O222	O2S	2.745(11)	O12W	O2S$^{\#3}$	2.886(12)
O1W	O1S$^{\#2}$	2.666(11)	O16W	O2S$^{\#3}$	2.92(2)
O1W	O202	2.622(9)	O107	O127$^{\#1}$	2.705(8)

Symmetry codes: (#1) 1−*x*, −0.5+*y*, 0.5−*z*; (#2) 1−*x*, 0.5+*y*, 0.5−*z*; (#3) 0.5−*x*, −*y*, 0.5+*z*.

Table S11 Intermolecular hydrogen bonds list among the cyclodextrins, triazole group and crystalline H_2O.

D	A	d(D−A)/Å	D	A	d(D−A)/Å
O105	O9W	2.931(16)	O14W	O15W	2.844(16)
O7W	O9W$^{\#5}$	2.80(3)	O15W	O2W$^{\#10}$	2.637(18)
O7W	O122	2.74(2)	O2W	O218	2.864(14)
O11W	O7W$^{\#8}$	2.62(2)	O13W	O210$^{\#11}$	2.82(2)
O11W	O6W$^{\#8}$	2.806(15)	O13W	O18W	2.91(5)
O110	O10W	2.937(17)	O18W	O4W$^{\#7}$	2.98(4)
O10W	O11W$^{\#3}$	2.882(15)	O4W	O15W$^{\#8}$	2.95(3)
O10W	O215$^{\#3}$	2.941(17)	O217	O4W	2.789(18)
O220	O11W	2.766(12)	C9	O115	3.08(2)
O6W	O15W	2.723(17)	O5W	N2$^{\#5}$	2.69(3)
O6W	O212	2.885(12)	O5W	O117	2.682(17)
O208	O8W	2.880(17)	O17W	O5W$^{\#7}$	2.686(17)
O8W	O6W	2.79(2)	O17W	O125	2.793(13)
O8W	O18W$^{\#9}$	2.93(4)	O4W	O5W	2.95(3)
O210	O14W	2.751(15)			

Symmetry codes: (#3) 0.5−*x*, −*y*, 0.5+*z*; (#5) −0.5+*x*, 0.5−*y*, 1−*z*; (#7) 0.5+*x*, 0.5−*y*, 1−*z*; (#8) −*x*, −0.5+*y*, 0.5−*z*; (#9) 0.5−*x*, 1−*y*, −0.5+*z*; (#10) −*x*, 0.5+*y*, 0.5−*z*; (#11) 0.5−*x*, 1−*y*, 0.5+*z*.

S5. Preparation and structure analysis of porous rotaxane assemblies

Preparation of CR·SiW single crystal: CR·SO_4 (10.56 mg, 4 μmol), $H_4SiW_{12}O_{40}$ (5.8 mg, 2 μmol), and CH_3COOK (100 mg, 1.02 mmol) were mixed in 10 mL H_2O, and then 200 μL CH_3COOH was added to adjust pH to about 4. The suspension was transferred to a Teflon-lined reactor and kept at 102 ˚C for 3 days. The reactor was cooled to room temperature slowly and colorless crystals of CR SiW_{12} State A were obtained in 84.85% yield (13.29 mg).

Preparation of CR·PMo/$PMo_{11}V$/$PMo_{10}V_2$/PMo_9V_3 single crystal: The single crystal with different POMs can be obtained by just changing the POMs with the same preparation method as CR·SiW single crystal, but the diffraction of crystals is too weak to solve the exact structure and its structure is further confirmed by PXRD.

Preparation of CR·$PMo_{11}V$ assembly: The assembly was constructed by simply dropwise adding an aqueous solution of CR·SO_4 (5.28 mg, 2 mL) into an aqueous solution of $H_4PMo_{11}VO_{40}$ (1.78 mg, 8 mL) at 50 °C for 30 min stewing. The assemblies were further collected by filtration to obtain yellow powder in 81.37% yield (5.48 mg); ^{1}H NMR (500 MHz, DMSO-d_6): δ 8.17 (s, 2H), 5.90 (s, 12H), 5.51 (s, 12H), 4.78 (s, 12H), 4.51 (s, 16H), 4.25 (s, 4H), 3.77 (t, J = 9.2 Hz, 12H), 3.60 (d, J = 9.4 Hz, 24H), 3.52 (d, J = 10.6 Hz, 12H), 3.40 (d, J = 10.0 Hz, 12H), 3.24 (t, J = 8.6 Hz, 12H), 3.18 (s, 12H), 1.92 (s, 4H), 1.48 (s, 8H), 1.42 (s, 8H), 1.32 (t, J = 6.7 Hz, 18H). Elemental analysis for $C_{30}H_{60}N_8(C_{36}H_{60}O_{30})_2(PMo_{11}VO_{40})_{0.5}\cdot 7H_2O$ (%): Anal. Calcd: N 3.21, C 35.07, H 5.60, Mo 15.11, V 0.73; Found: N 3.19, C 34.61, H 5.22, Mo 15.29, V 0.88.

Preparation of CR·SiW/PMo/$PMo_{10}V_2$/PMo_9V_3 assemblies: The assemblies with different POMs can be obtained by just changing the POMs with the same preparation method as CR·$PMo_{11}V$ assembly. Yield: 84.28% for SiW_{12}; 81.06% for PMo_{12}; 83.57% for $PMo_{10}V_2$; 82.36% for PMo_9V_3. Elemental analysis for $C_{30}H_{60}N_8(C_{36}H_{60}O_{30})_2(SiW_{12}O_{40})_{0.5}\cdot 8H_2O$ (%): Anal. Calcd: N 2.76, C 30.18, H 4.87; Found: N 2.73, C 29.95, H 4.46; Elemental analysis for $C_{30}H_{60}N_8(C_{36}H_{60}O_{30})_2(SO_4)_{0.25}(PMo_{12}O_{40})_{0.5}\cdot 10H_2O$ (%): Anal. Calcd: N 3.12, C 34.09, H 5.609, Mo 16.02; Found: N 3.07, C 33.61, H 5.129, Mo 16.30; Elemental analysis for $C_{30}H_{60}N_8(C_{36}H_{60}O_{30})_2(HPMo_{10}V_2O_{40})_{0.5}\cdot 9H_2O$ (%): Anal. Calcd: N 3.19, C 34.93, H 5.71, Mo 13.68, V 1.45; Found: N 3.20, C 34.55, H 5.29, Mo 13.70, V 1.45; Elemental analysis for $C_{30}H_{60}N_8(C_{36}H_{60}O_{30})_2(H_2PMo_9V_3O_{40})_{0.5}\cdot 9H_2O$ (%): Anal. Calcd: N 3.22, C 35.15, H 5.76, Mo 12.39, V 2.19; Found: N 3.19, C 34.83, H 5.36, Mo 12.38, V 2.33.

Table S12 Crystal data and structure refinement for CR·SiW single crystal.

Formula	$(C_{30}H_{60}N_8(C_{36}H_{60}O_{30})_2)_2SiW_{12}O_{40}\cdot 11H_2O$
CCDC number	2320351
Formula weight	8029.52
Temperature/ K	273.15
Crystal system	Monoclinic
Space group	*C*2
color of crystal	colourless
a/ Å	44.113(9)
b/ Å	14.038(3)
c/ Å	23.812(5)
α/°	90
β/°	95.909(13)
γ/°	90
Volume /Å^3	14667(5)
Z	2
ρ_{calc}/ g·cm^{-3}	1.818
μ/ mm^{-1}	4.799
F(000)	7976
Radiation	Mo*Kα* (λ = 0.71073 Å)
2θ range for data collection/°	5.10–50.06 (0.84 Å)
Index ranges	$-52 \le h \le 52$, $-16 \le k \le 16$, $-28 \le l \le 28$
Reflections collected	253088
Independent reflections	25912 [R_{int} = 0.1937, R_{sigma} = 0.0938]
Goodness of fit on F^2	1.054
Final R index.	R_1 = 0.0862, wR_2 = 0.2105
Largest diff. peak/hole/e Å^{-3}	1.94/−1.86

$R_1 = \sum|F_o| - |F_c|/\sum|F_o|$. $wR_2 = \{(F_o{}^2 - F_c{}^2)^2/\sum w(F_o{}^2)^2\}^{1/2}$.

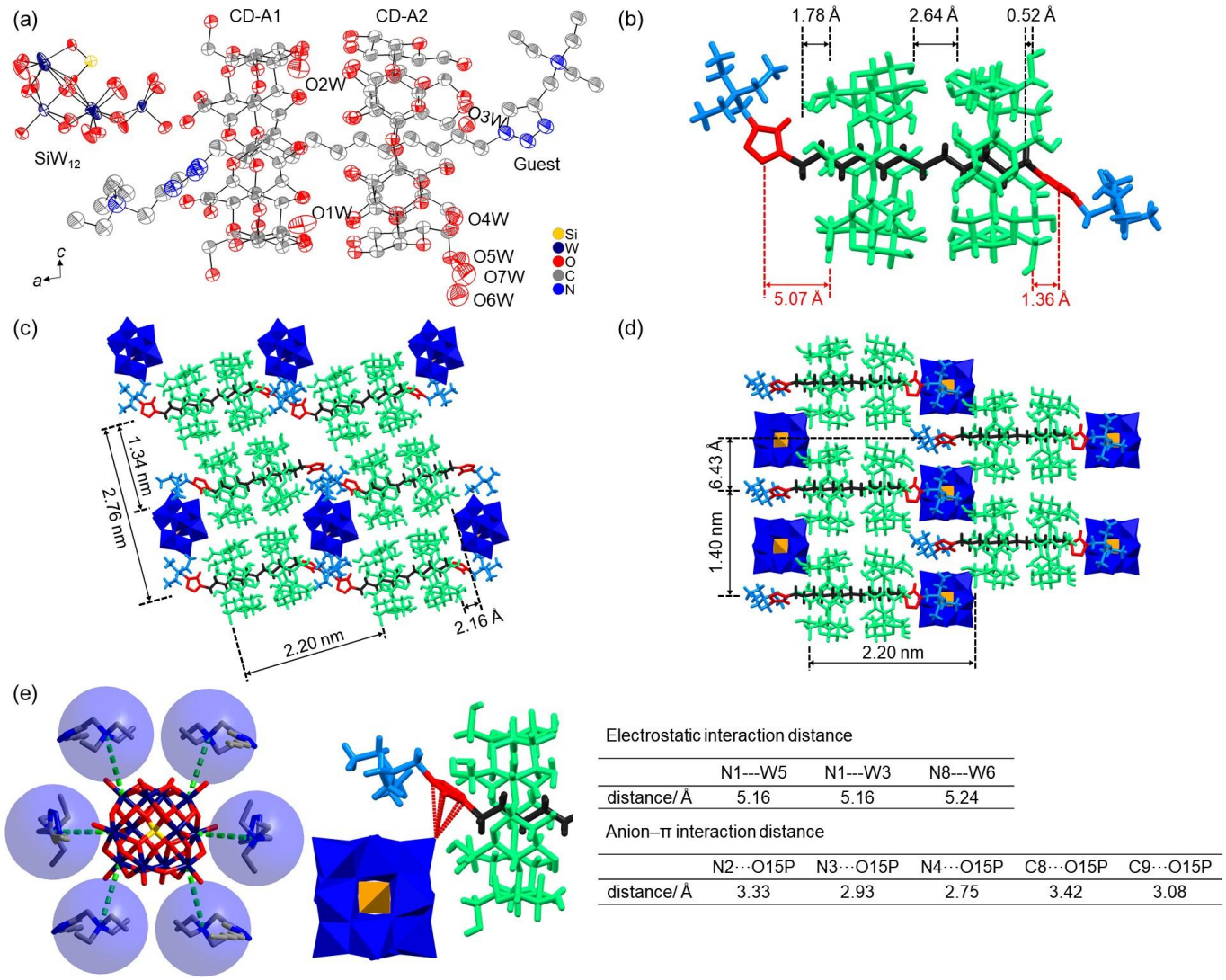

Electrostatic interaction distance

	N1---W5	N1---W3	N8---W6
distance/ Å	5.16	5.16	5.24

Anion–π interaction distance

	N2···O15P	N3···O15P	N4···O15P	C8···O15P	C9···O15P
distance/ Å	3.33	2.93	2.75	3.42	3.08

Fig. S11 X-ray crystal structure of CR·SiW. (a) Asymmetric unit (ORTEP Type 30%); (b) The relative position between the guest and cyclodextrin; (c) Arrangement on the (011) plane; (d) Arrangement on the (001) plane; (e) Distance measurement of electrostatic and anion–π interaction.

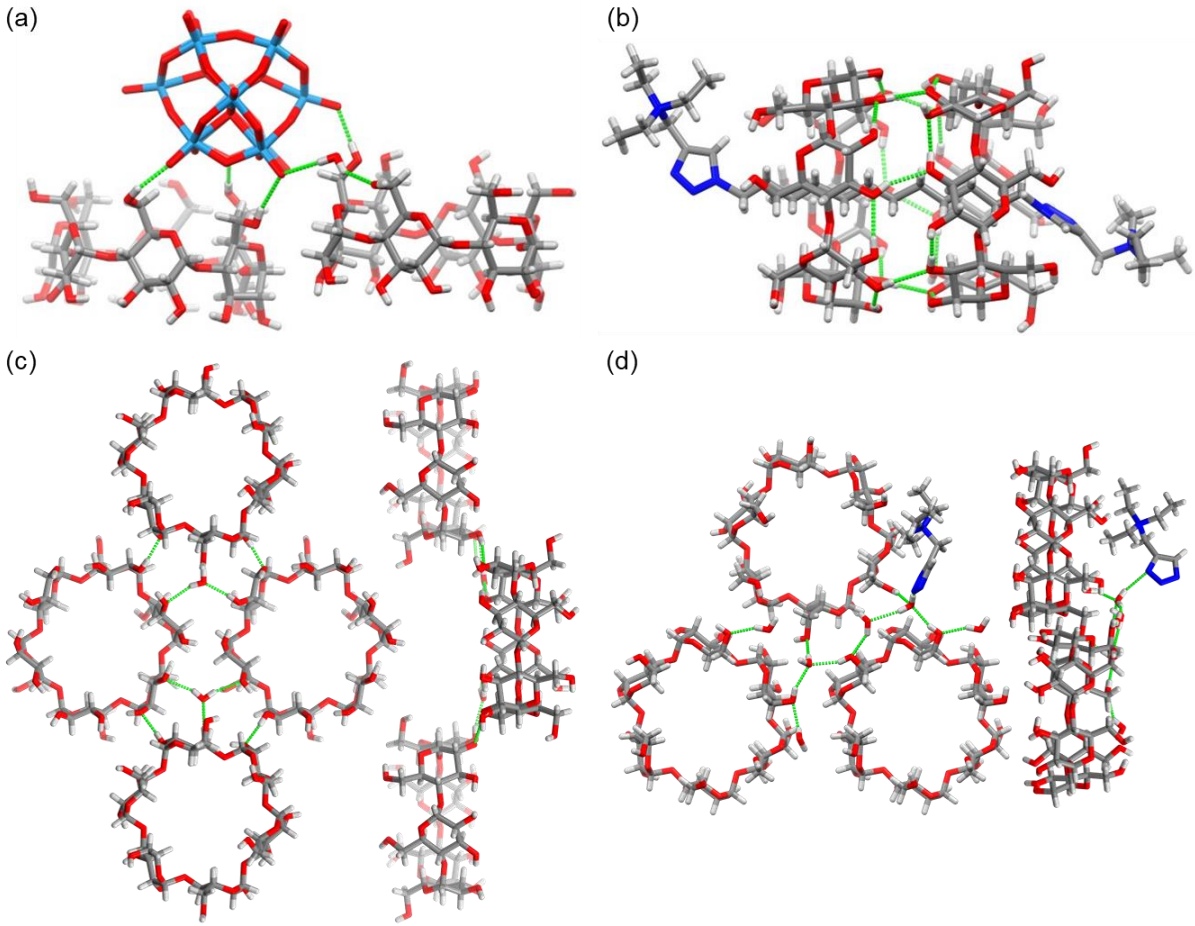

Fig. S12 Hydrogen bonds in CR·SiW. (a) Intermolecular hydrogen bonds among the primary side of cyclodextrins on CR and POM; (b) Intramolecular hydrogen bonds between the secondary side of cyclodextrins on CR; (c) Intermolecular hydrogen bonds among the secondary side of cyclodextrins on CR and crystalline H_2O; (d) Intermolecular hydrogen bonds among the primary side of cyclodextrins on CR, crystalline H_2O, and triazole group.

Table S13 Intermolecular hydrogen bonds list among the primary side of cyclodextrins on CR and POM.

D	A	d(D−A)/Å	D	A	d(D−A)/Å
O120	O5P$^{\#4}$	3.15(4)	O3W	O5P$^{\#5}$	3.06(8)
O215	O14P$^{\#5}$	2.90(4)	O115	O19P	3.10(4)
O125	O1P$^{\#4}$	2.87(4)			

Symmetry codes: (#4) 2−*x*, +*y*, 1−*z*; (#5) −0.5+*x*, 0.5+*y*, +*z*.

Table S14 Intramolecular hydrogen bonds list between the secondary side of cyclodextrins on CR.

D	A	d(D−A)/Å	D	A	d(D−A)/Å
O217	O213	3.03(4)	O122	O213	3.10(4)
O212	O208	2.91(4)	O228	O108	2.94(4)
O213	O123	3.02(4)	O202	O228	2.85(4)
O208	O128	2.86(4)	O118	O122	2.88(4)
O218	O118	2.86(4)	O127	O123	2.92(4)
O207	O203	2.82(4)	O107	O103	2.70(5)
O222	O218	2.89(5)	O128	O102	2.77(4)
O223	O113	3.07(4)	O113	O117	2.85(4)
O203	O103	2.83(4)	O108	O112	2.84(4)
O227	O223	2.97(4)			

Table S15 Intermolecular hydrogen bonds list among the secondary side of cyclodextrins on CR and crystalline H_2O.

D	A	d(D−A)/Å	D	A	d(D−A)/Å
O123	O2W	2.80(6)	O2W	O118$^{\#7}$	2.87(6)
O102	O107$^{\#1}$	2.70(4)	O2W	O113$^{\#8}$	2.92(6)
O112	O127$^{\#2}$	2.79(5)	O1W	O108	2.94(6)
O103	O1W$^{\#1}$	2.82(6)	O1W	O128$^{\#2}$	2.93(6)
O117	O122$^{\#3}$	2.68(4)			

Symmetry codes: (#1) 1.5−*x*, 0.5+*y*, −*z*; (#2) +*x*, −1+*y*, +*z*; (#3) 1.5−*x*, −0.5+*y*, 1−*z*; (#7) 1.5−*x*, 0.5+*y*, 1−*z*; (#8) +*x*, 1+*y*, +*z*.

Table S16 Intermolecular hydrogen bonds list among the primary side of cyclodextrins on CR and crystalline H_2O.

D	A	d(D−A)/Å	D	A	d(D−A)/Å
O230	O4W$^{\#2}$	2.85(5)	O3W	O210	2.59(8)
O210	O4W	2.73(5)	O6W	O7W	2.85(16)
O205	O6W	2.77(7)	O6W	N7$^{\#10}$	3.03(7)
O130	O6W$^{\#1}$	2.72(7)	O5W	O205	2.84(10)
O4W	O105$^{\#1}$	2.69(5)	O7W	O230	2.79(15)

Symmetry codes: (#1) 1.5−*x*, 0.5+*y*, −*z*; (#2) +*x*, −1+*y*, +*z*; (#10) 1−*x*, +*y*, −*z*.

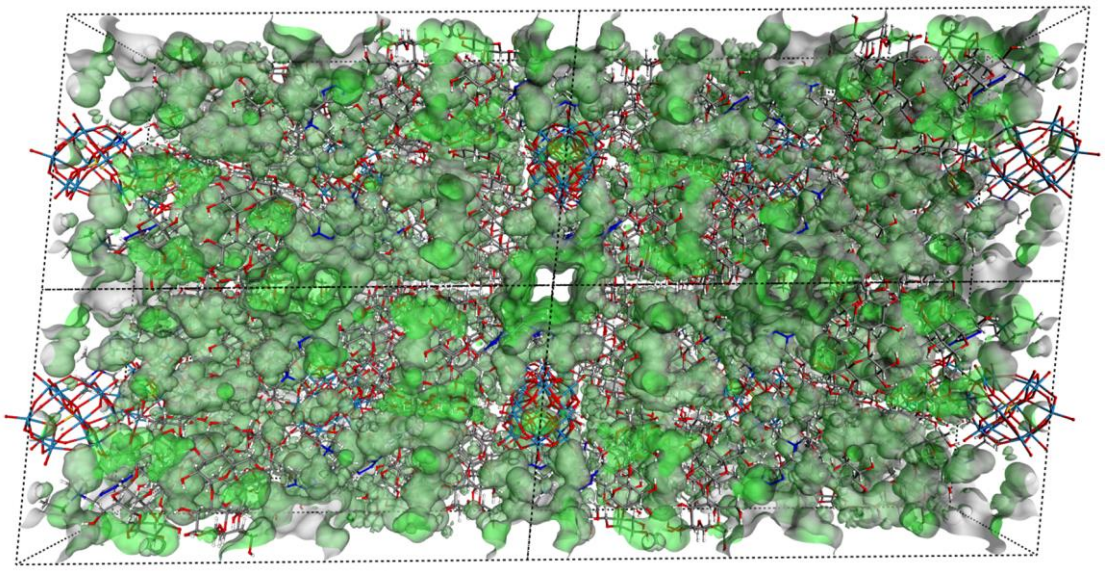

Fig. S13 Voids of CR·SiW single crystal (diameter of 1D channel pore: 0.6 nm).

Table S17 Elemental analysis for CR·SiW single crystal.

CR·SiW	N (%)	C (%)	H (%)
Found	2.61	28.24	4.874
Calcd	2.63	28.71	4.796
Error	0.02	0.47	−0.008

Formula: $C_{30}H_{60}N_8(C_{36}H_{60}O_{30})_2(SiW_{12}O_{40})_{0.55}\cdot 11.5H_2O$

Table S18 Solvent mask information for CR·SiW single crystal.

Number	Volume/Å^3	Electron Count	Content/Unit Cell
1	738	190	23 H_2O
3	48	12	1 H_2O
7	40	0	
9	44	0	

A solvent mask was calculated and 202 electrons were found in a volume of 870 Å^3 in 4 voids per unit cell. This is consistent with the presence of 24[H_2O] per Unit Cell which account for 190 electrons per unit cell.

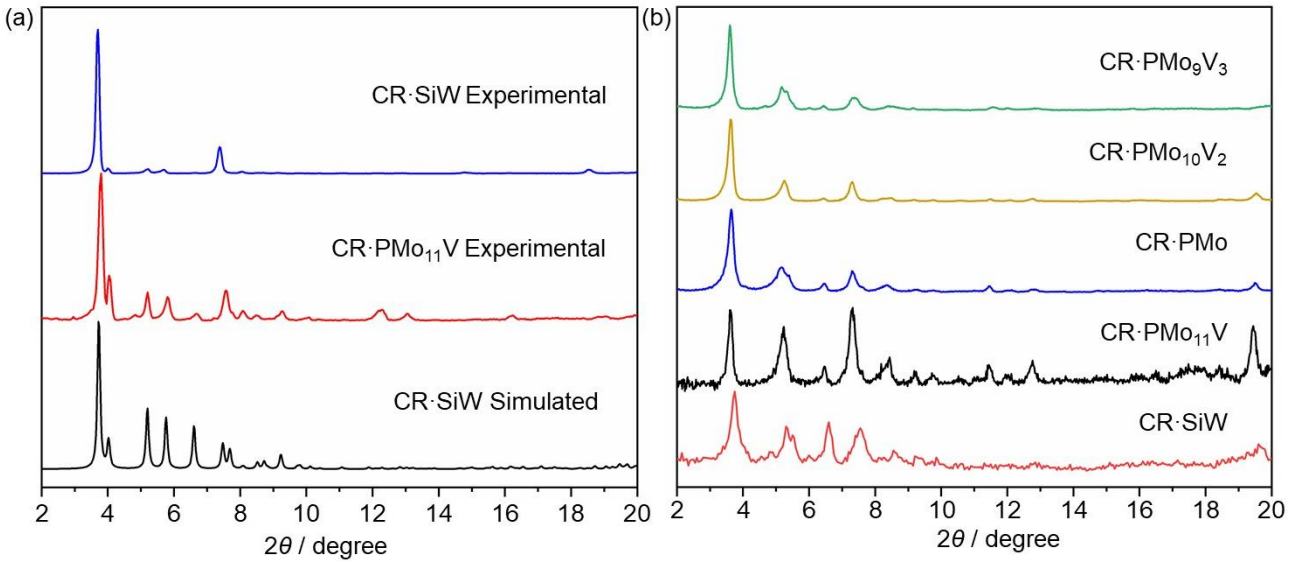

Fig. S14 (a) PXRD of CR·SiW single crystal, CR·$PMo_{11}V$ single crystal and simulated pattern of CR·SiW single crystal; (b) Comparison between PXRD of CR·SiW/$PMo_{11}V$/PMo/$PMo_{10}V_2$/PMo_9V_3 assemblies.

S6. Solvent-adaptability for selective adsorption

Vacuum degassing of CR·$PMo_{11}V$ assembly

The as-prepared CR·$PMo_{11}V$ assembly powder was vacuum-dried at 100°C for 4 hours, and after which PXRD analysis was performed to confirm the structure changes.

Solvent vapor adsorption

3 mg of vacuum-degassed CR·$PMo_{11}V$ assembly was placed in a vial, which was then sealed within a larger vial containing the solvents. The solvent vapor was allowed to gradually diffuse into the powder for 72 hours at room temperature. Subsequently, NMR analysis was conducted to calculate the maximum adsorption amount.

Butanol-selective multicomponent adsorption

Breakthrough experiments of H_2O, ethanol, acetone, and butanol vapors were conducted under constant temperature conditions of 25 °C using the Micromeritics ASAP 2920 system paired with the HPR-20 R&D mass spectrometer detector. PRAs was accurately weighed and loaded into the experimental setup. The vapor generator's temperature conditions were set to prepare the desired vapor concentrations (e.g., H_2O at 25 °C; ethanol at 20 °C; acetone at 25 °C; butanol at 30 °C), and the carrier gas (N_2) flow rate was adjusted to 10 mL/min to ensure a constant gas flow. The sample was then exposed to the target vapor flow, and real-time monitoring of the outlet gas composition was performed to record the breakthrough curves and sample adsorption amounts for each vapor. After the experiment, the equipment was cleaned, and data was recorded and analyzed.

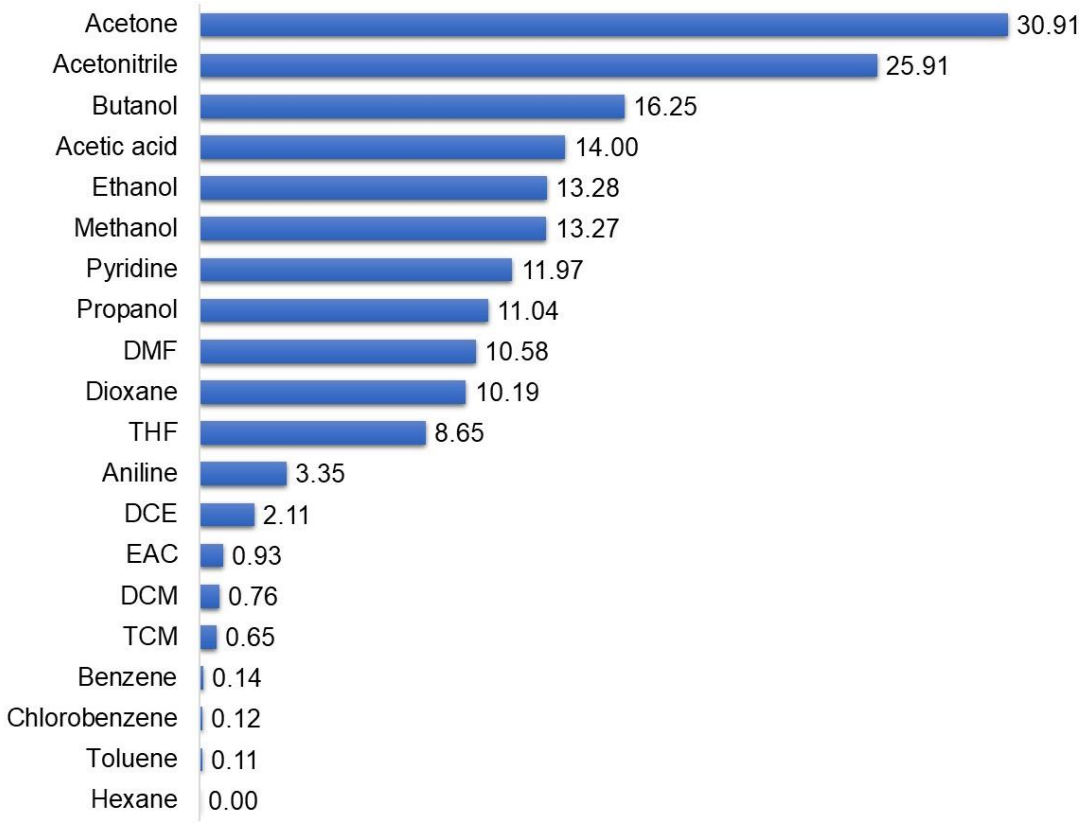

Fig. S15 The maximum adsorption amount of CR·PMo$_{11}$V assembly per unit lattice for different solvent vapors: acetone, acetonitrile, butanol, acetic acid, ethanol, methanol, pyridine, propanol, N,N-Dimethylformamide (DMF), dioxane, tetrahydrofuran (THF), aniline, dichloroethane (DCE), ethyl acetate (EAC), dichloromethane (DCM), trichloromethane (TCM), benzene, chlorobenzene, toluene, hexane calculated through NMR integration.

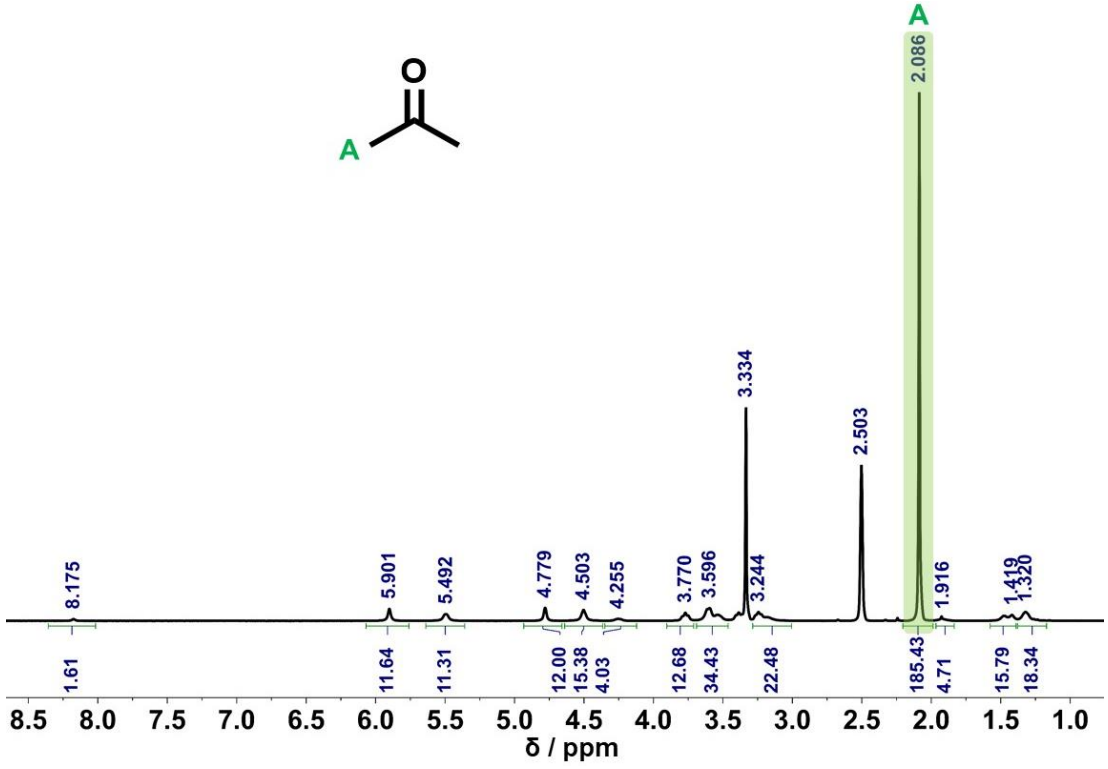

Fig. S16 ^{1}H NMR specture of CR·PMo$_{11}$V assembly after acetone sorption.

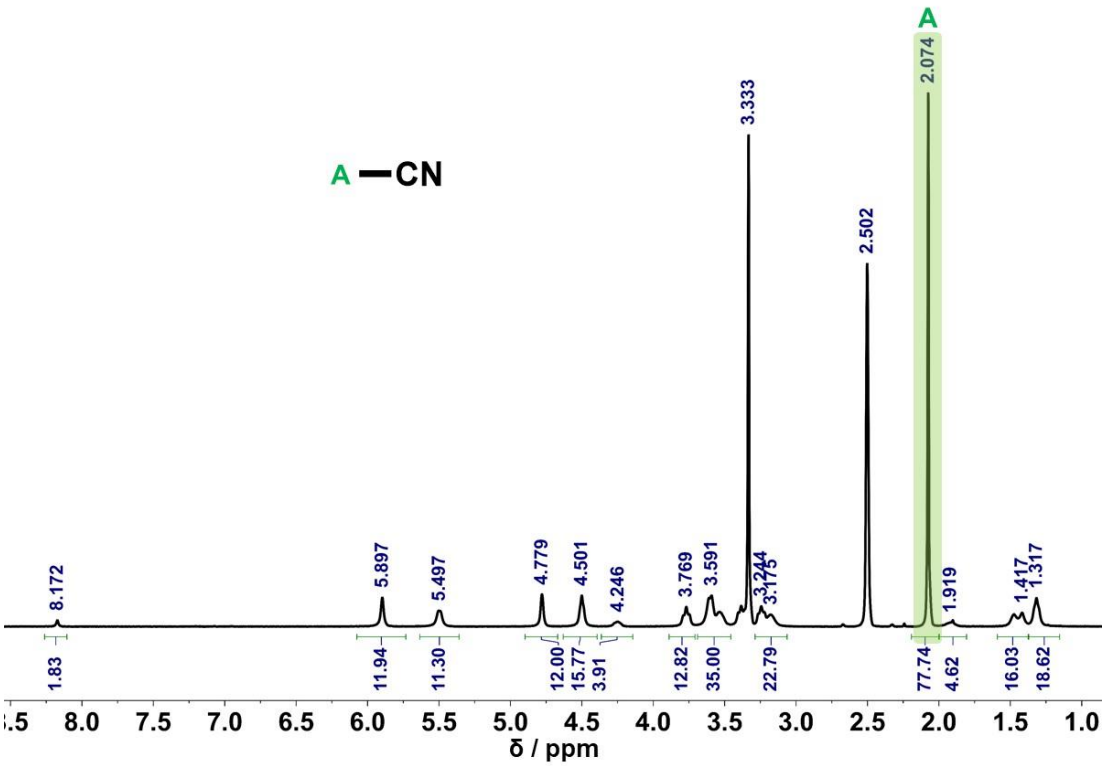

Fig. S17 ^{1}H NMR specture of CR·PMo$_{11}$V assembly after acetonitrile sorption.

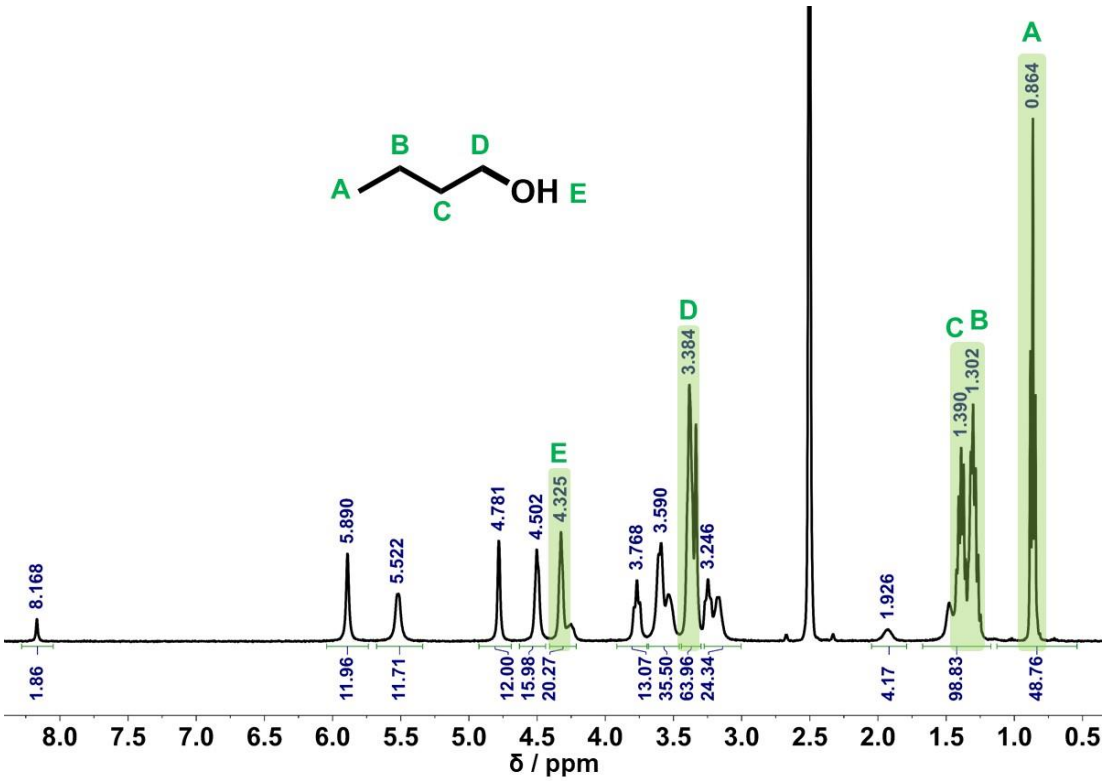

Fig. S18 ^{1}H NMR specture of CR·PMo$_{11}$V assembly after butanol sorption.

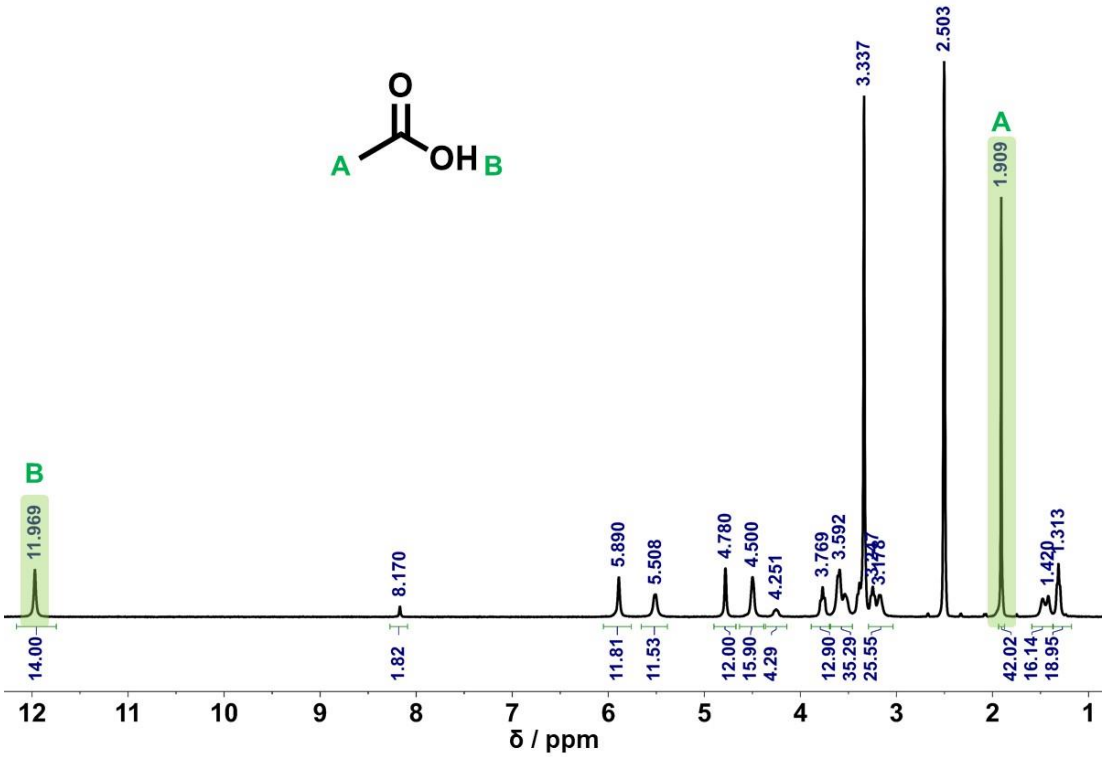

Fig. S19 ^{1}H NMR specture of CR·PMo$_{11}$V assembly after acetic acid sorption.

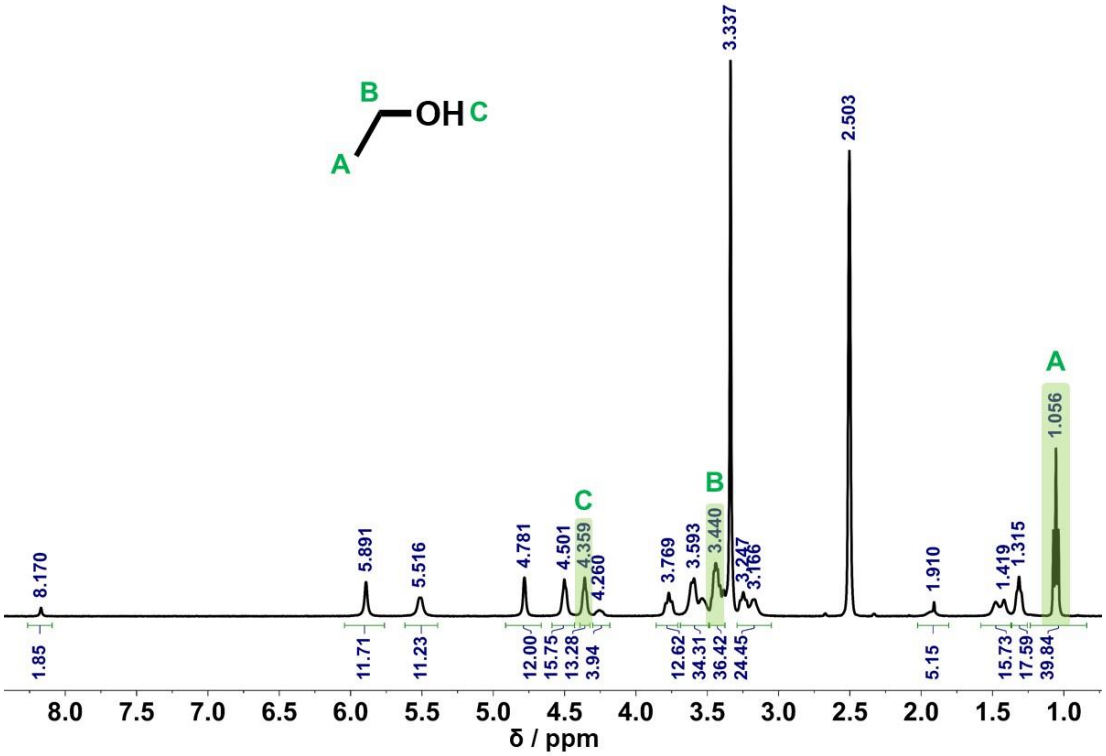

Fig. S20 ^{1}H NMR specture of CR·PMo$_{11}$V assembly after ethanol sorption.

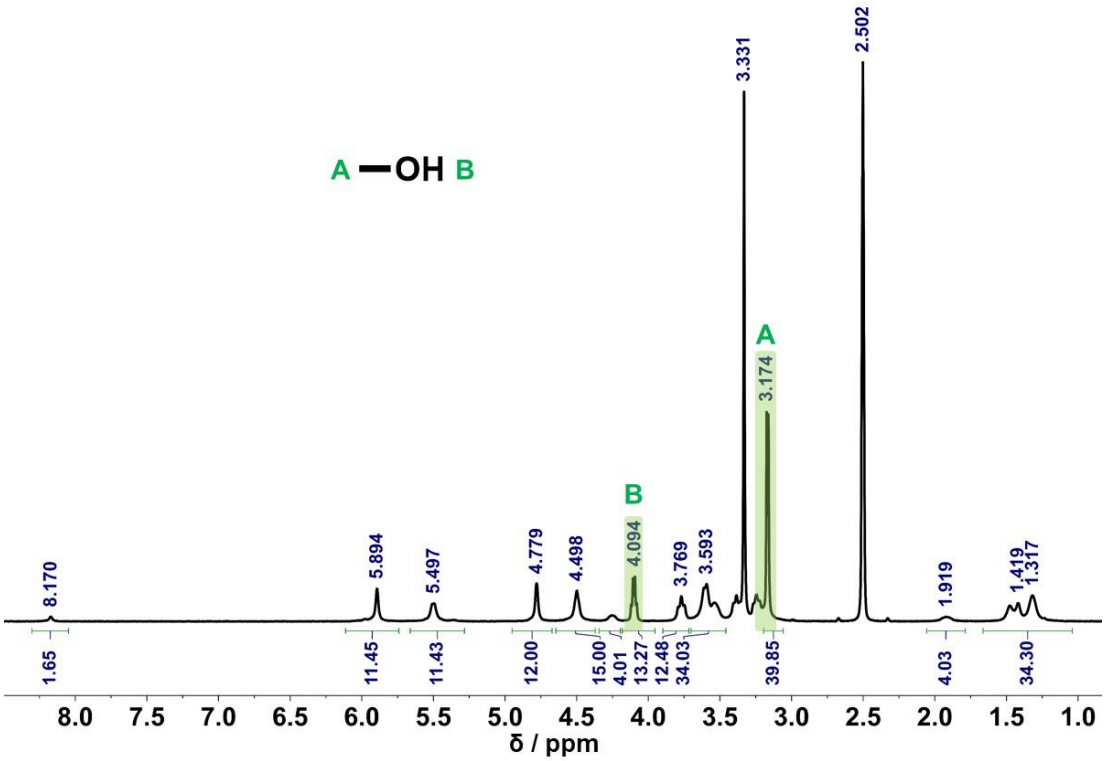

Fig. S21 ^{1}H NMR specture of CR·PMo$_{11}$V assembly after methanol sorption.

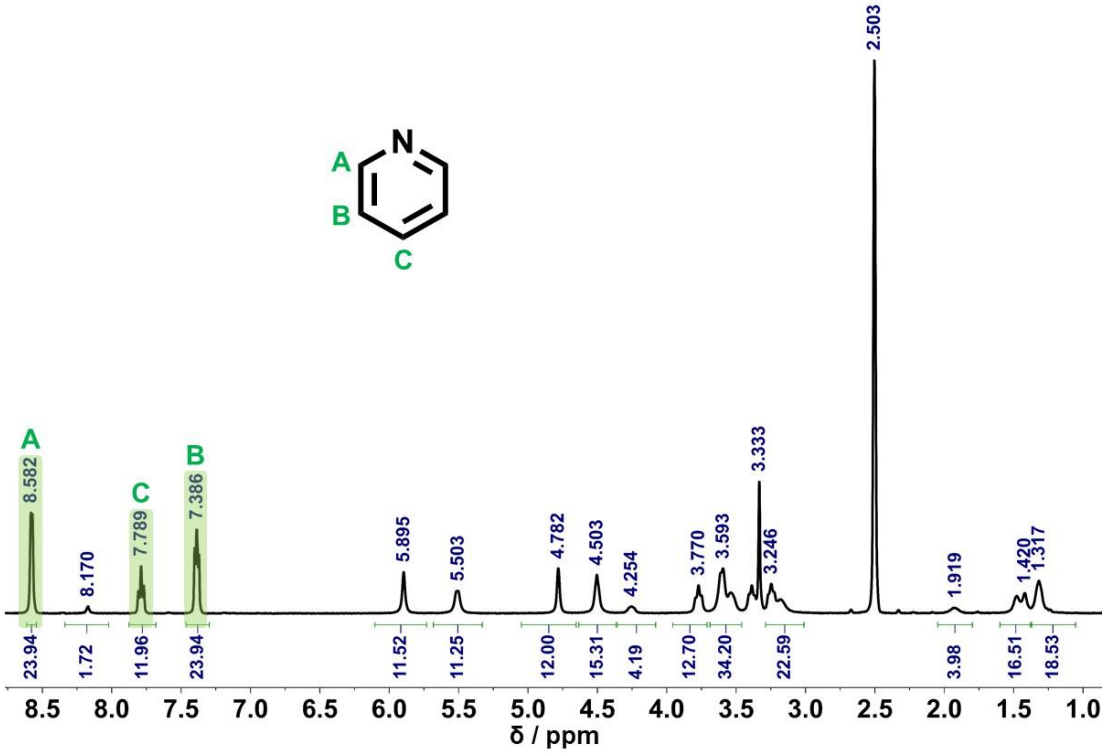

Fig. S22 ^{1}H NMR specture of CR·PMo$_{11}$V assembly after pyridine sorption.

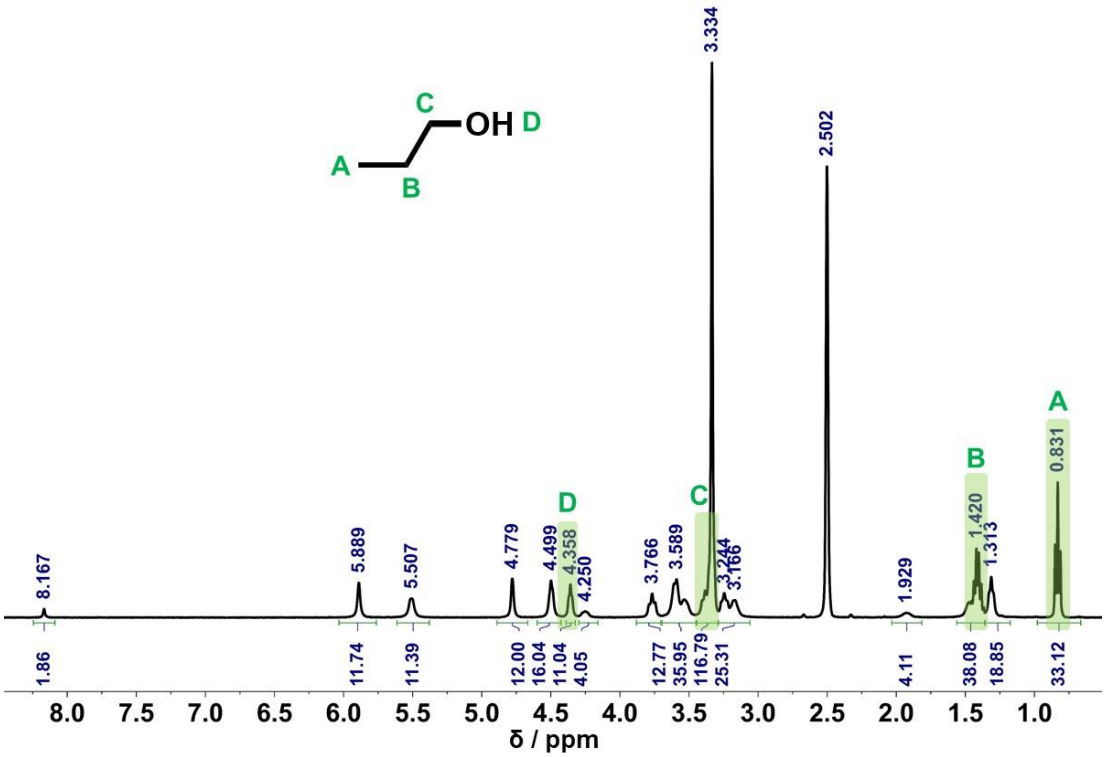

Fig. S23 ^{1}H NMR specture of CR·PMo$_{11}$V assembly after propanol sorption.

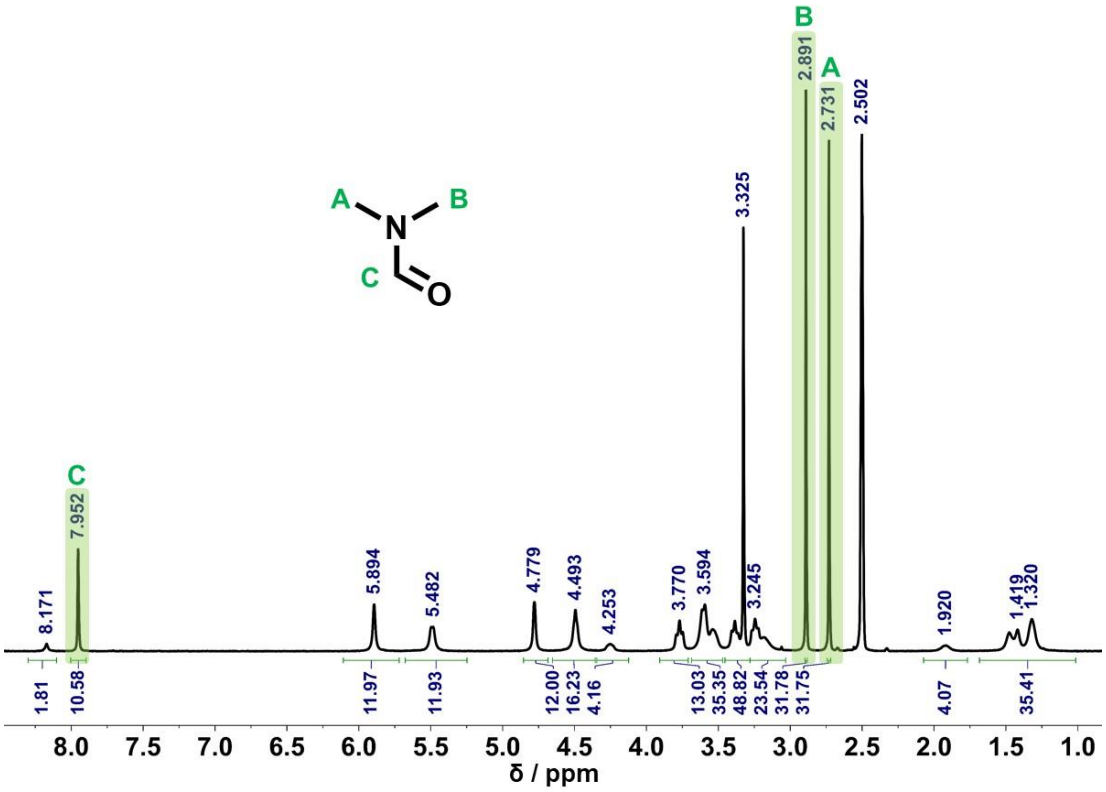

Fig. S24 ^{1}H NMR specture of CR·PMo$_{11}$V assembly after N,N-Dimethylformamide (DMF) sorption.

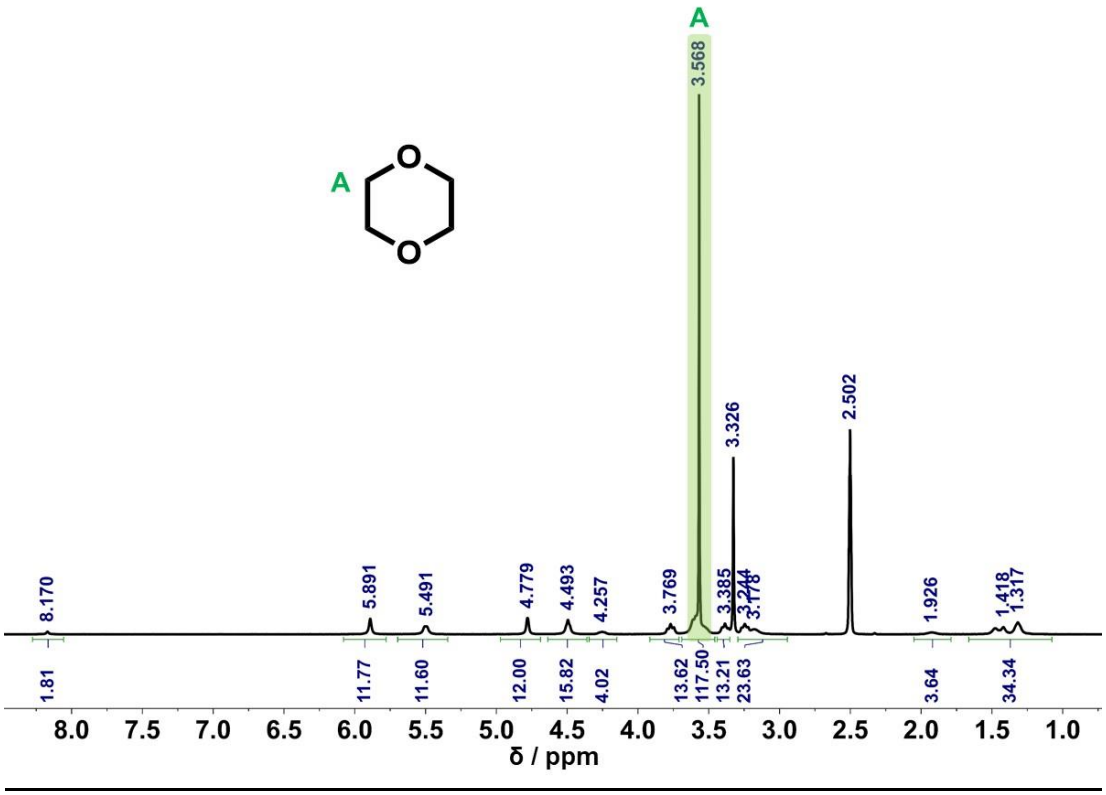

Fig. S25 ^{1}H NMR specture of CR·PMo$_{11}$V assembly after dioxane sorption.

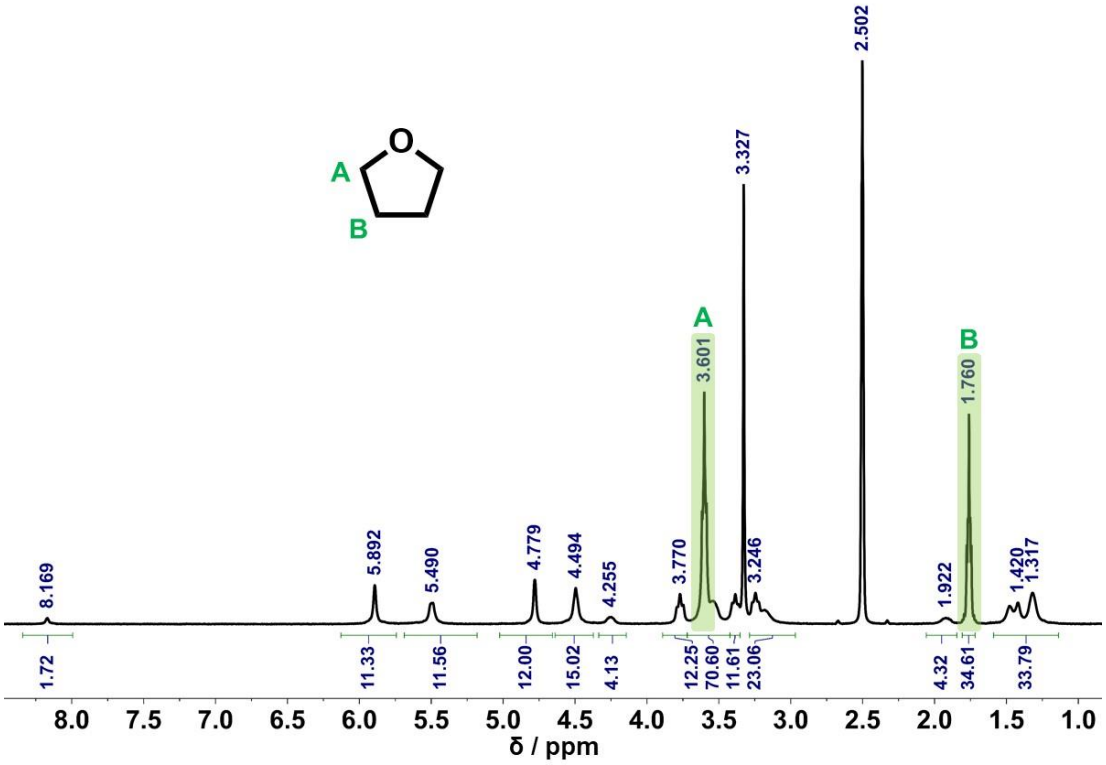

Fig. S26 ^{1}H NMR specture of CR·PMo$_{11}$V assembly after tetrahydrofuran (THF) sorption.

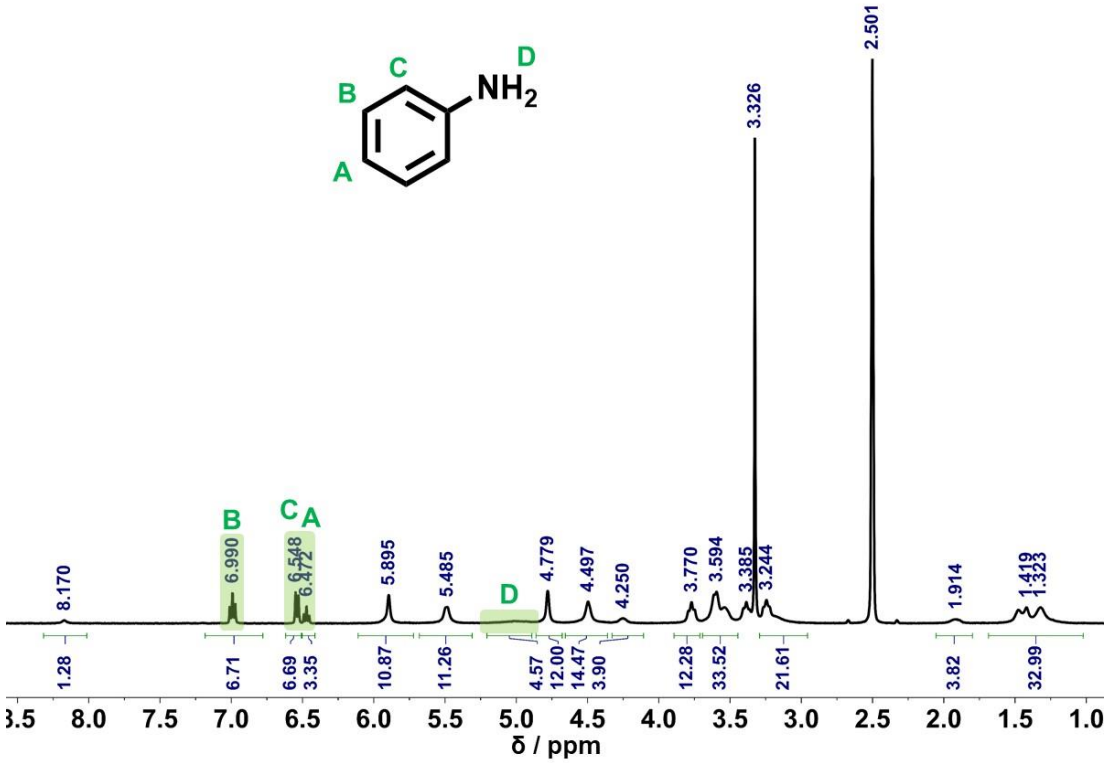

Fig. S27 ^{1}H NMR specture of CR·PMo$_{11}$V assembly after aniline sorption.

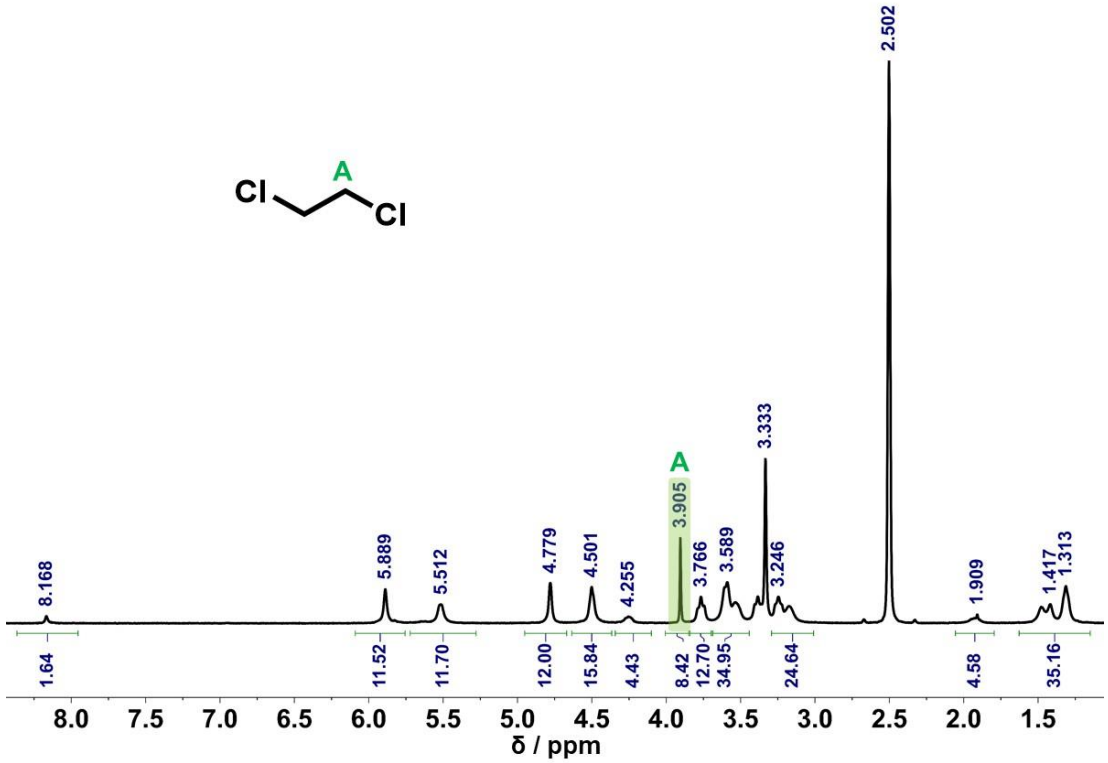

Fig. S28 ^{1}H NMR specture of CR·PMo$_{11}$V assembly after dichloroethane (DCE) sorption.

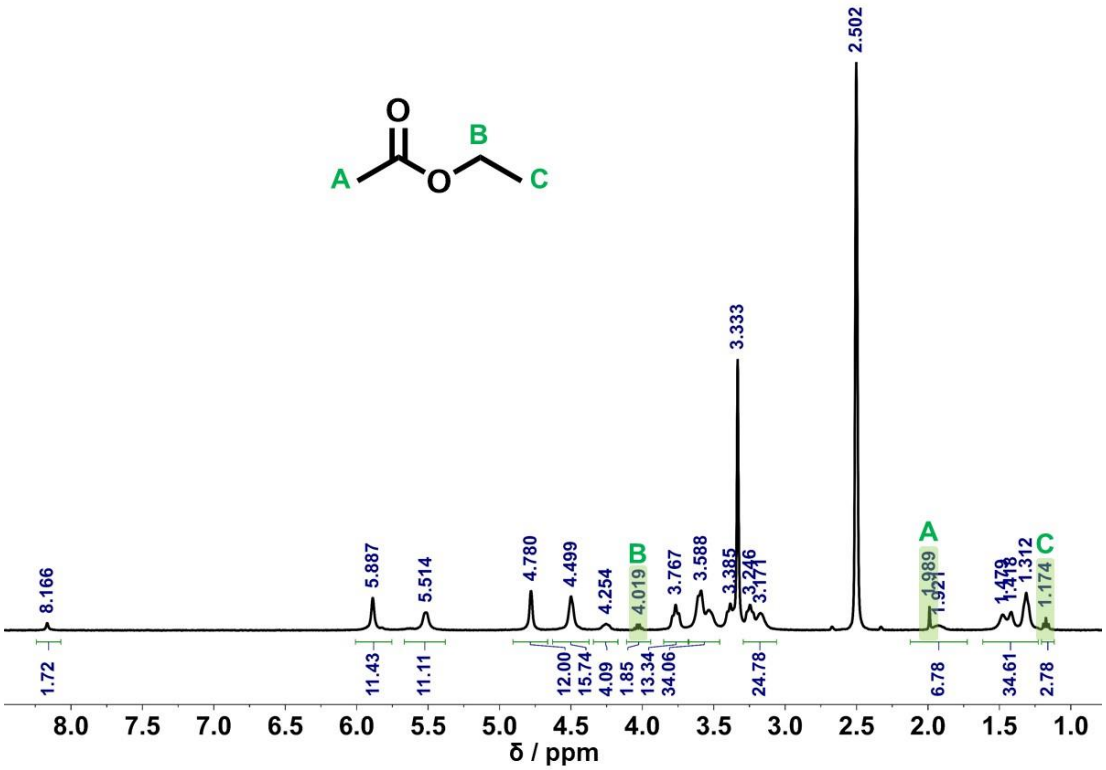

Fig. S29 ^{1}H NMR specture of CR·PMo$_{11}$V assembly after ethyl acetate (EAC) sorption.

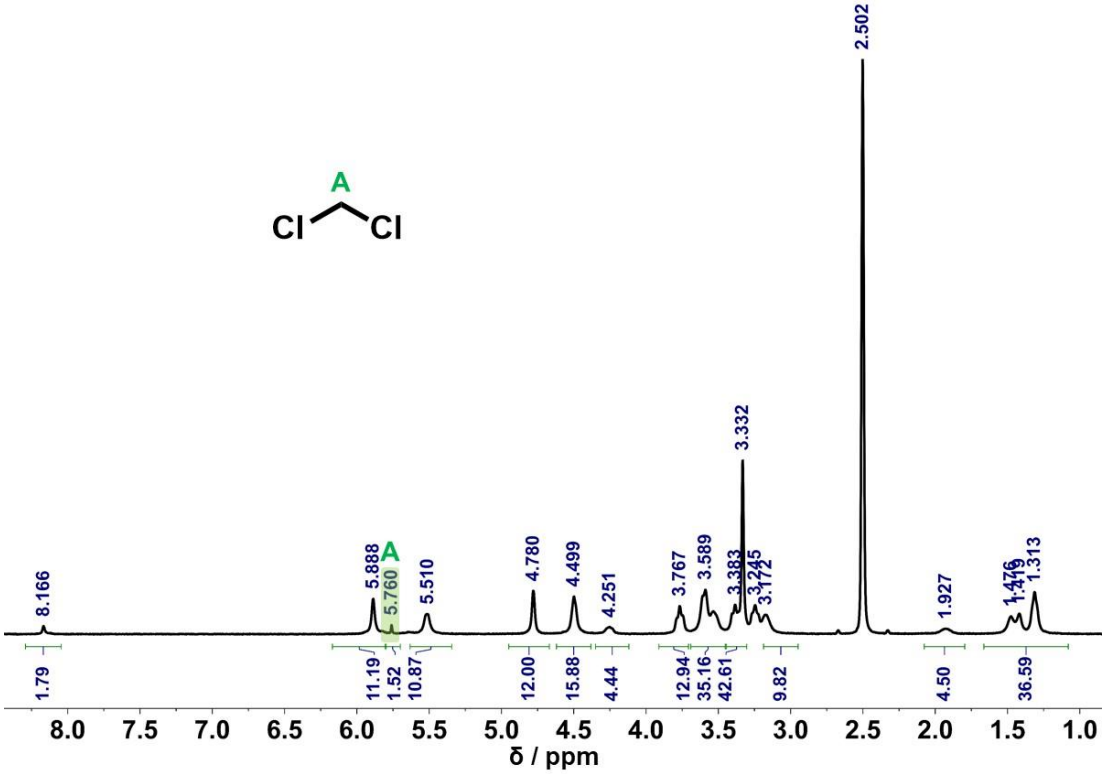

Fig. S30 ^{1}H NMR specture of CR·PMo$_{11}$V assembly after dichloromethane (DCM) sorption.

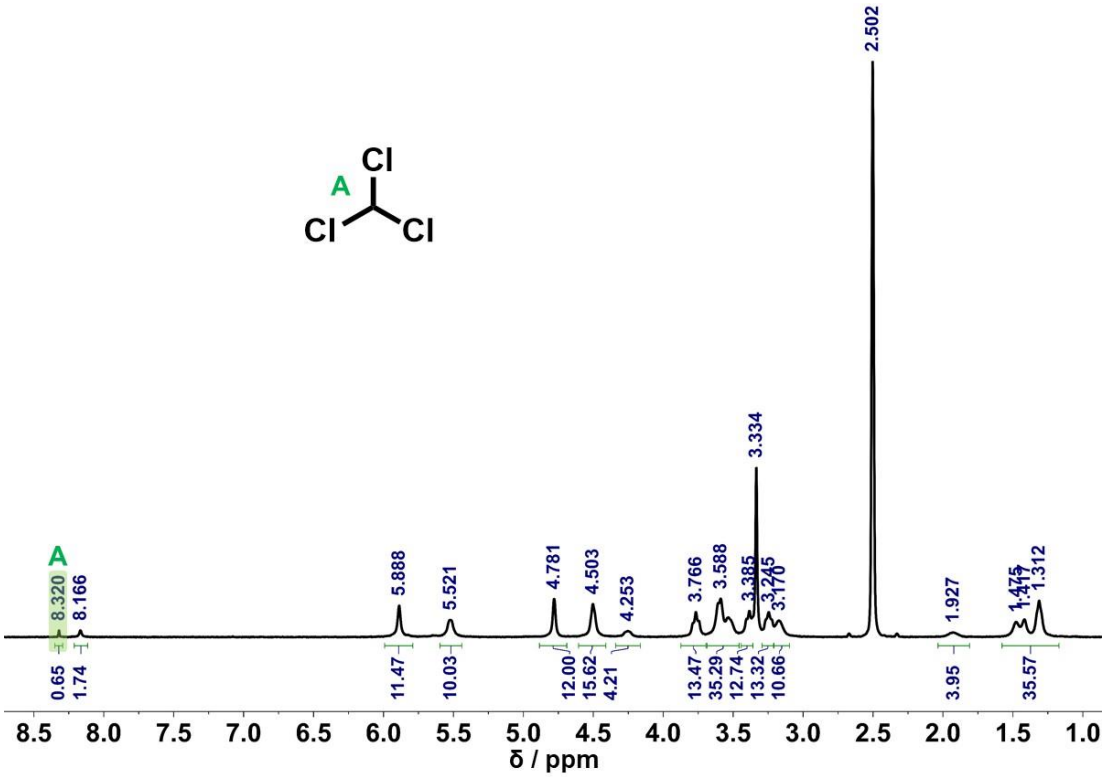

Fig. S31 ^{1}H NMR specture of CR·PMo$_{11}$V assembly after trichloromethane (TCM) sorption.

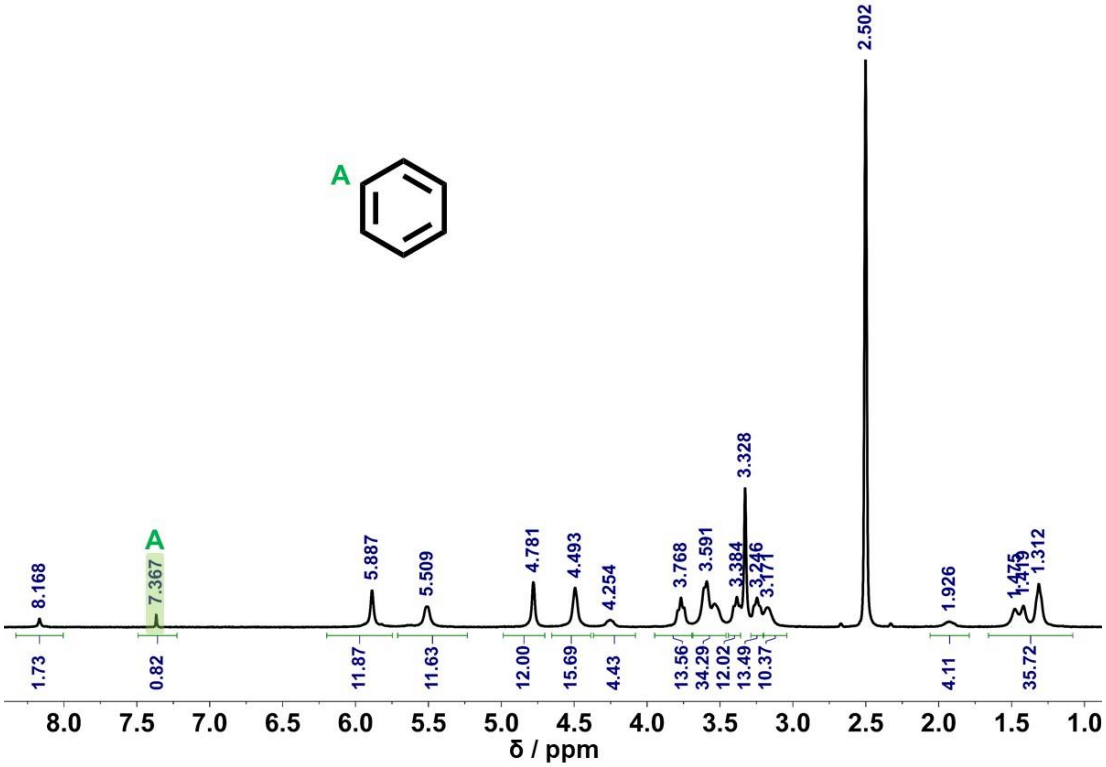

Fig. S32 ^{1}H NMR specture of CR·PMo$_{11}$V assembly after benzene sorption.

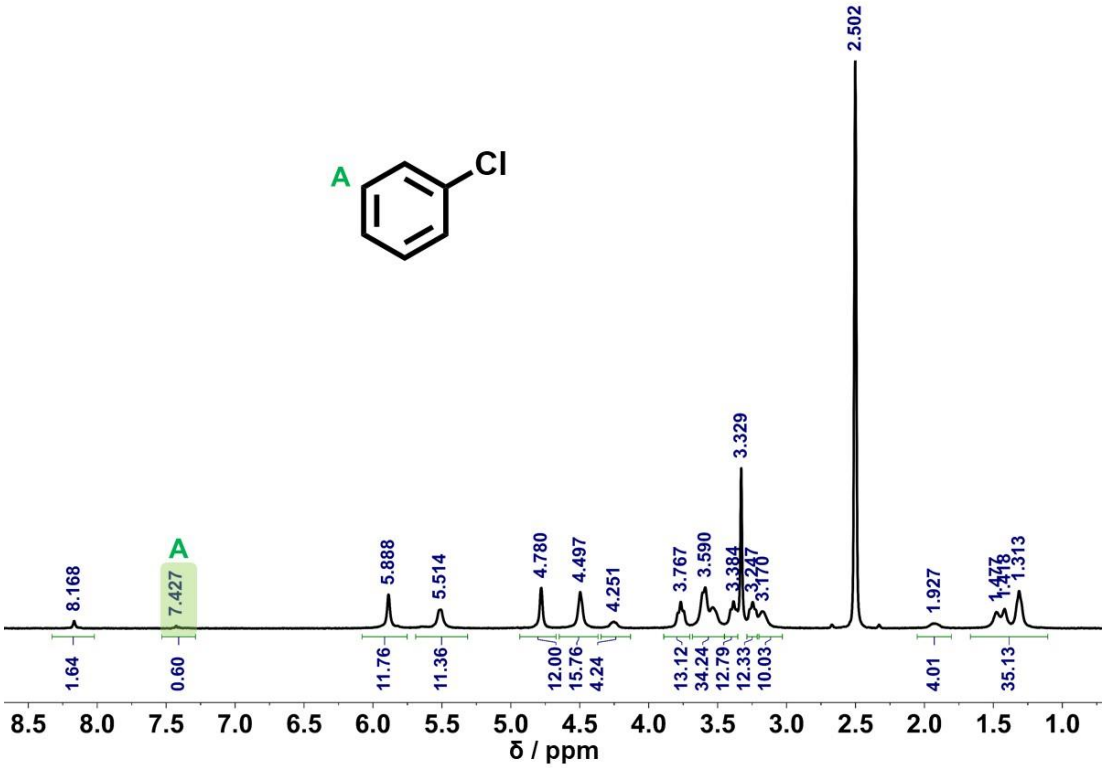

Fig. S33 ^{1}H NMR specture of CR·PMo$_{11}$V assembly after chlorobenzene sorption.

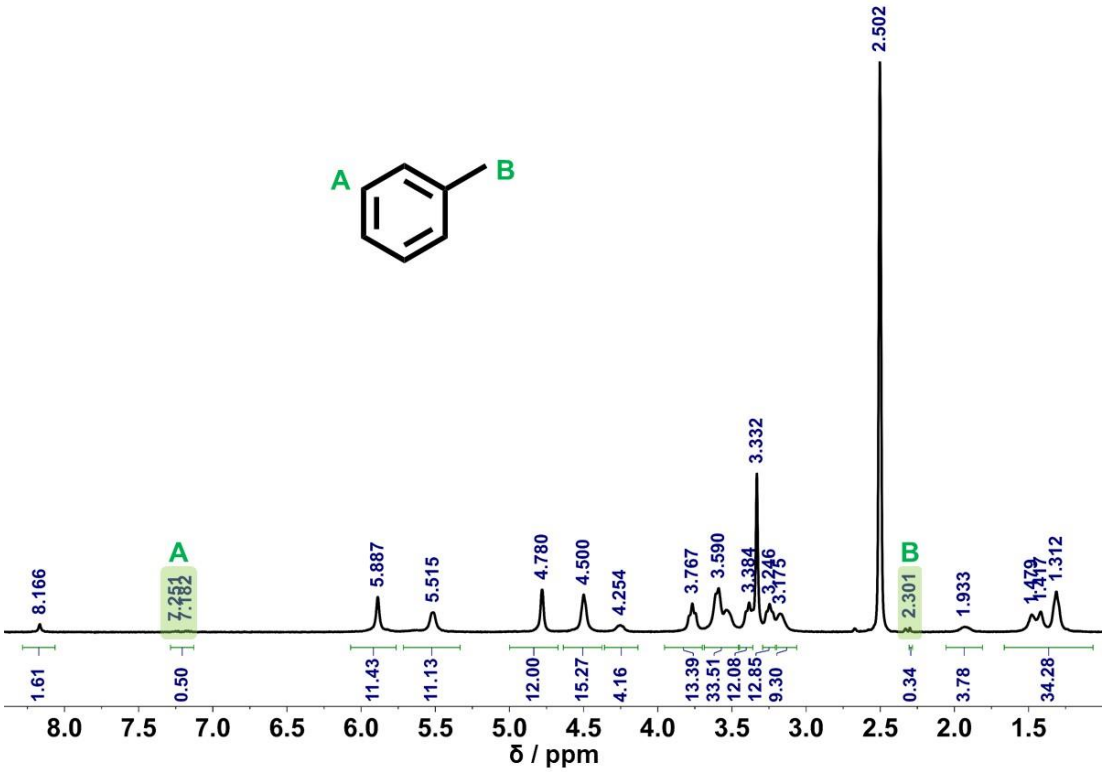

Fig. S34 ^{1}H NMR specture of CR·PMo$_{11}$V assembly after toluene sorption.

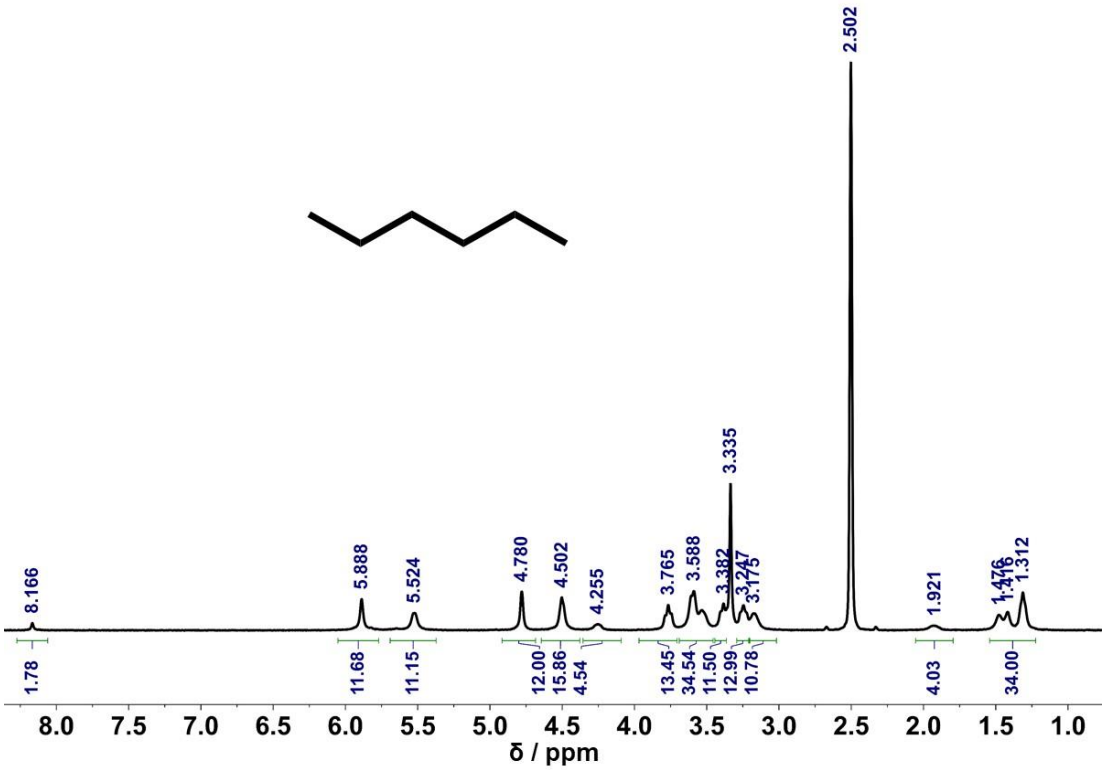

Fig. S35 ^{1}H NMR specture of CR·PMo$_{11}$V assembly after hexane sorption.

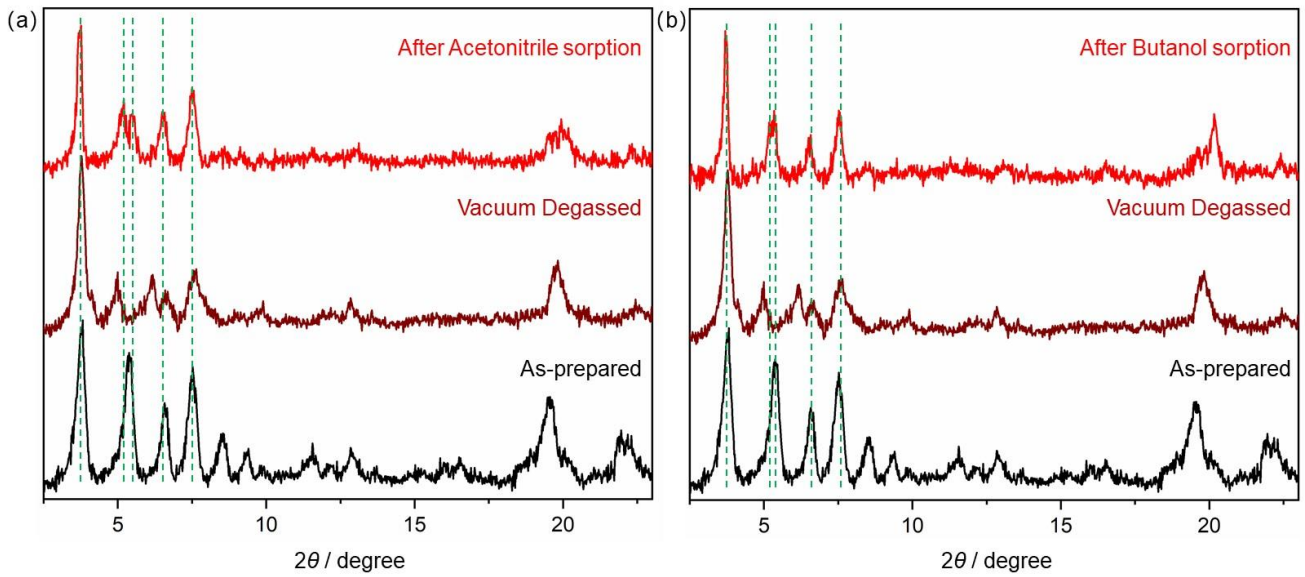

Fig. S36 Comparison of the PXRD patterns of CR·PMo$_{11}$V assembly: as-prepared, vaccum degassed, and after (a) Acetonitrile; (b) Butanol sorption.

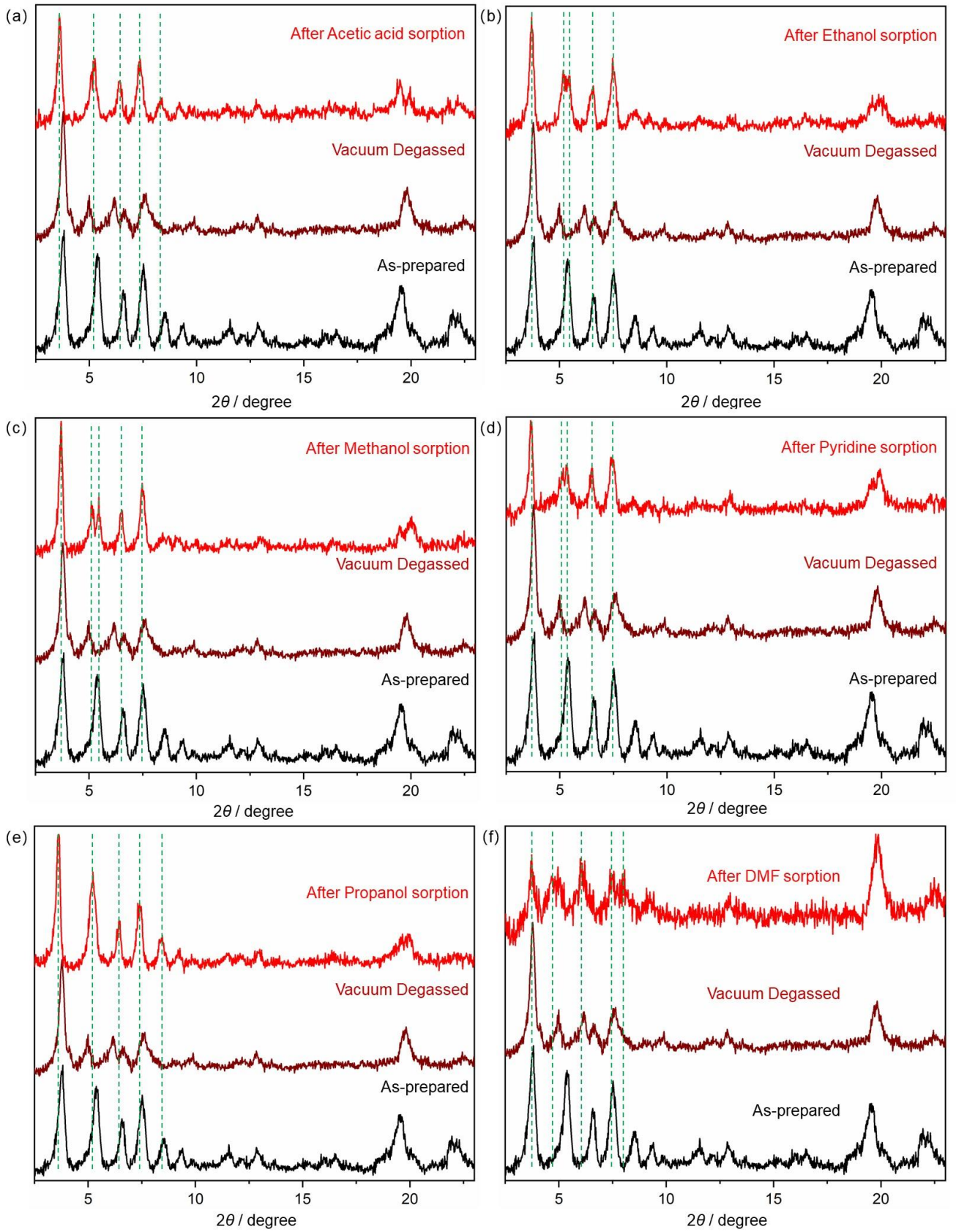

Fig. S37 Comparison of the PXRD patterns of CR·$PMo_{11}V$ assembly: as-prepared, vaccum degassed, and after (a) Acetic acid; (b) Ethanol; (c) Methanol; (d) Pyridine; (e) Propanol; (f) N,N-Dimethylformamide (DMF) sorption.

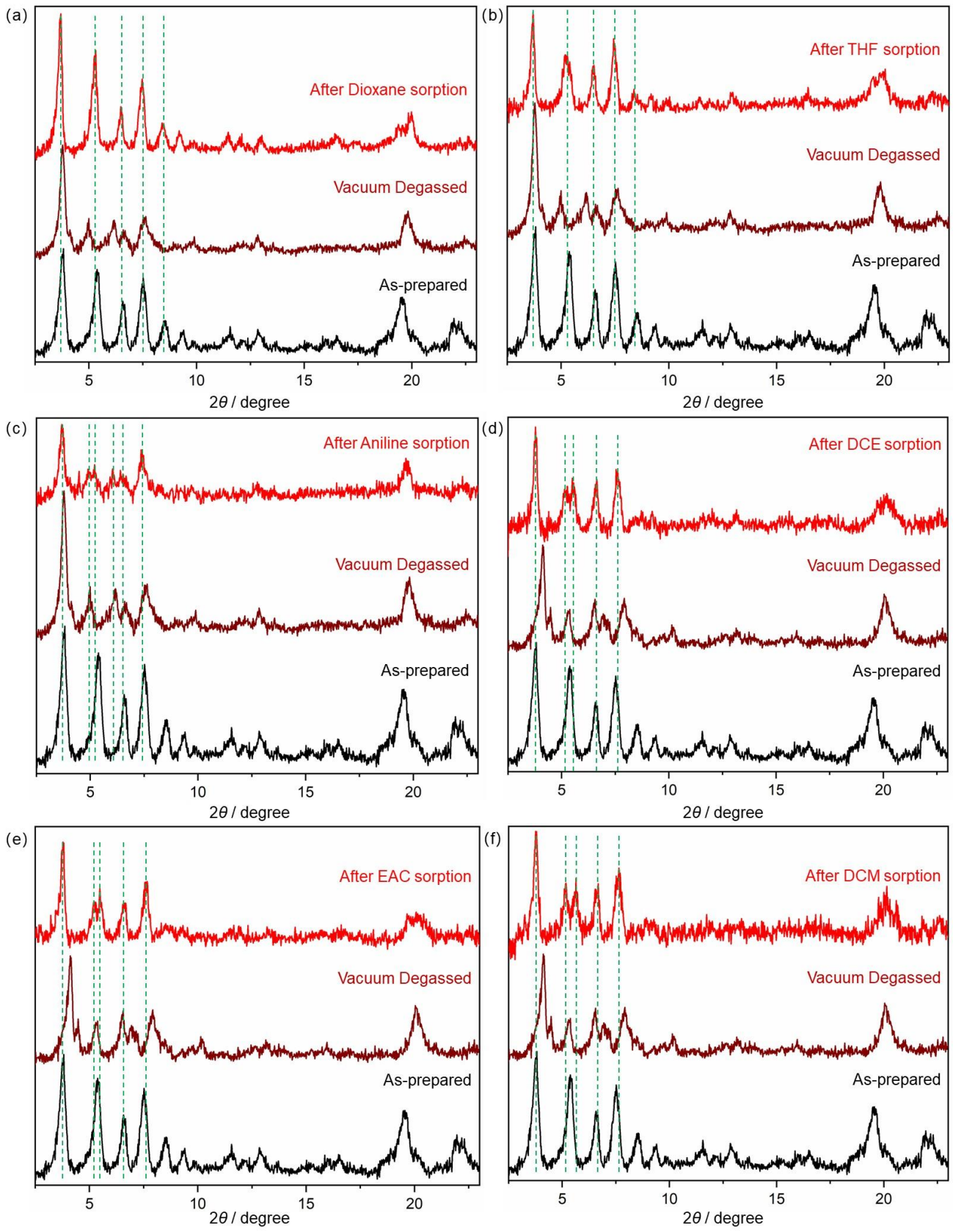

Fig. S38 Comparison of the PXRD patterns of CR·$PMo_{11}V$ assembly: as-prepared, vaccum degassed, and after (a) Dioxane; (b) Tetrahydrofuran (THF); (c) Aniline; (d) Dichloroethane (DCE); (e) Ethyl acetate (EAC); (f) Dichloromethane (DCM) sorption.

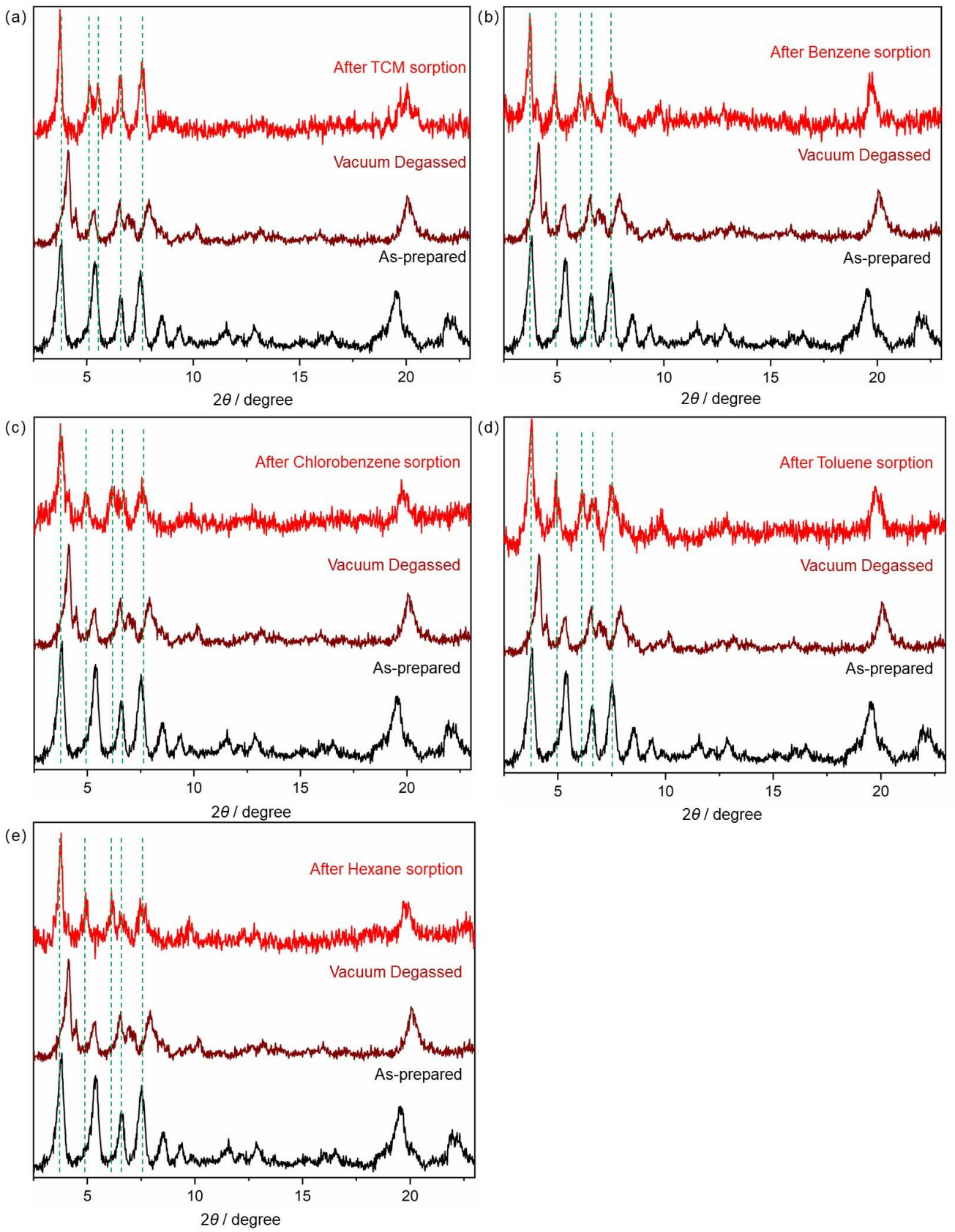

Fig. S39 Comparison of the PXRD patterns of CR·$PMo_{11}V$ assembly: as-prepared, vaccum degassed, and after (a) Trichloromethane (TCM); (b) Benzene; (c) Chlorobenzene; (d) Toluene; (e) Hexane sorption.

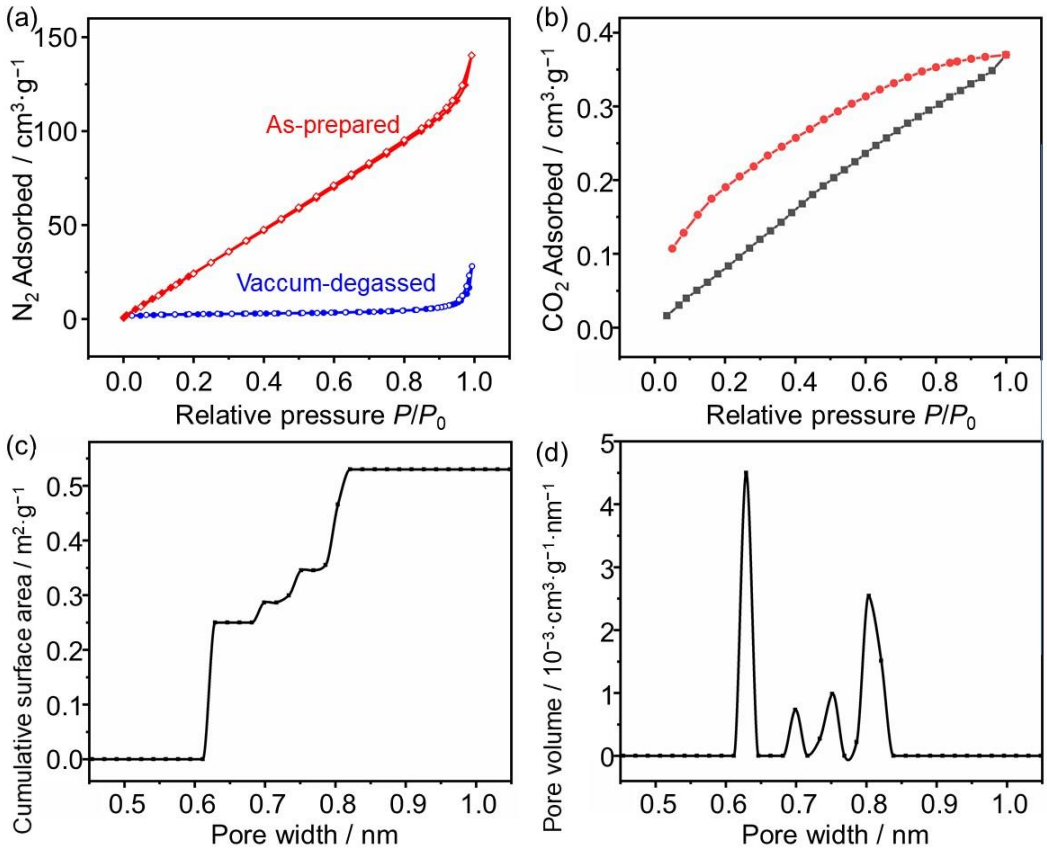

Fig. S40 (a) N_2 gas sorption isotherm for as-prepared and vaccum-degassed CR·PMo$_{11}$V assembly; (b) CO_2 gas sorption isotherm for CR·PMo$_{11}$V assembly (black line, sorption; red line, desorption); Porosity distribution by CO_2 DFT model (c) Cumulative surface area *vs.* pore width; (d) *d*V/*d*W pore volume *vs.* pore width.

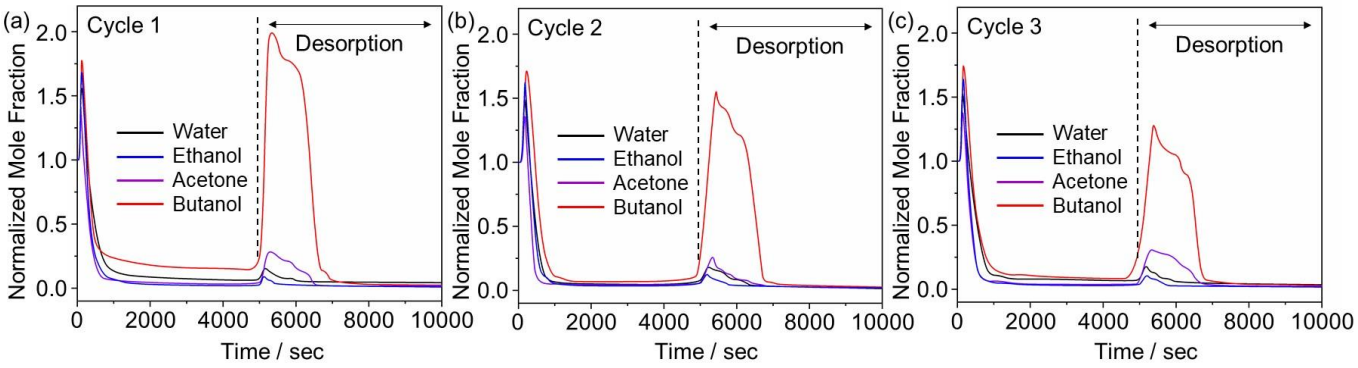

Fig. S41 Desorption profile of CR·PMo$_{11}$V assembly sequentially after an ABE breakthrough run (a–c for 3 cycles).

S7. Reversible crystalline transformation triggered by DMSO

Preparation of CR·PMo$_{11}$V-B single crystal: Method 1: A DMSO/H_2O/CH_3COOH solution of CR·SO_4 (1 mM, 1 mL) was added to a DMSO/H_2O/CH_3COOH solution of $H_4PMo_{11}V$ (0.5 mM, 1 mL), then stewing few days to obtain yellowish needle crystals; Method 2: CR·$PMo_{11}V$ assembly powder was dissolved in DMSO, and slowly evaporated H_2O into it for a few weeks to obtain yellowish needle crystals.
Elemental analysis for $C_{30}H_{60}N_8(C_{36}H_{60}O_{30})_2(PMo_{11}VO_{40})_{0.5}\cdot 20H_2O\cdot 6C_2H_6SO\cdot 4CH_3COOH$ (%): Anal. Calcd: N 2.53, C 33.03, H 6.18, S 4.34, Mo 11.89, V 0.57; Found: N 2.65, C 32.62, H 5.71, S 4.57, Mo 11.50, V 0.62 (Method 1).

Preparation of CR·(SiW_{12}, PMo_{12}, $PMo_{10}V_2$, PMo_9V_3)-B single crystal: The same crystal structure can be obtained by just changing the POM with the same preparation method as CR·PMo_{11}V-B single crystal. Elemental analysis for $C_{30}H_{60}N_8(C_{36}H_{60}O_{30})_2(HPMo_{10}V_2O_{40})_{0.5}\cdot 5H_2O\cdot 6C_2H_6SO$ (%): Anal. Calcd: N 2.87, C 35.07, H 5.85, S 4.93, Mo 12.29, V 1.30; Found: N 2.81, C 35.16, H 5.80, S 4.64, Mo 12.45, V 0.89; Elemental analysis for $C_{30}H_{60}N_8(C_{36}H_{60}O_{30})_2(H_2PMo_9V_3O_{40})_{0.5}\cdot 5H_2O\cdot 6C_2H_6SO$ (%): Anal. Calcd: N 2.89, C 35.27, H 5.89, S 4.96, Mo 11.12, V 1.97; Found: N 2.82, C 35.28, H 5.93, S 5.09, Mo 11.43, V 1.39 (Method 2).

Table S19 Crystal data and structure refinement for CR·PMo_{11}V-B single crystal.

Formula	$(C_{30}H_{60}N_8(C_{36}H_{60}O_{30})_2)_2PMo_{11}VO_{40}\cdot 5.5C_2H_6SO\cdot 33.4H_2O$
CCDC number	2320354
Formula weight	7755.66
Temperature/ K	100.00
Crystal system	Monoclinic
Space group	$P2_1$
color of crystal	yellowish
a/ Å	27.7756(19)
b/ Å	24.3712(13)
c/ Å	31.144(2)
α/°	90
β/°	112.486(2)
γ/°	90
Volume /Å^3	19480(2)
Z	2
ρ_{calc}/ g·cm^{-3}	1.322
μ/ mm^{-1}	0.494
F(000)	8062
Radiation	Mo$K\alpha$ (λ = 0.71073)
2θ range for data collection/°	5.01 to 50.05
Index ranges	$-33 \le h \le 33$, $-29 \le k \le 29$, $-37 \le l \le 37$
Reflections collected	1118342
Independent reflections	68701 [R_{int} = 0.0770, R_{sigma} = 0.0277]
Goodness of fit on F^2	1.138
Final R index.	R_1 = 0.0700, wR_2 = 0.1781
Largest diff. peak/hole/e Å^{-3}	1.47/−1.28

$R_1 = \sum|F_o| - |F_c|/\sum|F_o|$. $wR_2 = \{(F_o{}^2 - F_c{}^2)^2/\sum w(F_o{}^2)^2\}^{1/2}$.

Table S20. Crystal data and structure refinement for CR·SiW/PMo/$PMo_{10}V_2$/PMo_9V_3-B.

Formula	$(C_{30}H_{60}N_8(C_{36}H_{60}O_{30})_2)_2SiW_{12}O_{40}\cdot 2C_2H_6SO\cdot 11H_2O$	$(C_{30}H_{60}N_8(C_{36}H_{60}O_{30})_2)_2PMo_{12}O_{40}\cdot 3.5C_2H_6SO\cdot 19.5H_2O$	$(C_{30}H_{60}N_8(C_{36}H_{60}O_{30})_2)_2PMo_{10}V_2O_{40}\cdot 3C_2H_6SO\cdot 30.5H_2O$	$(C_{30}H_{60}N_8(C_{36}H_{60}O_{30})_2)_2PMo_9V_3O_{40}\cdot 4.4C_2H_6SO\cdot 29.3H_2O$
CCDC number	2320353	2320357	2320355	2320356
Formula weight	7976.13	6800.53	7451.37	7505.65
Temperature/ K	108.00	100.00	100.00	100.00
Crystal system	Monoclinic	Monoclinic	Monoclinic	Monoclinic
Space group	$P2_1$	$P2_1$	$P2_1$	$P2_1$
color of crystal	colourless	blue	orange	orange
a/ Å	27.9885(9)	27.761(2)	27.697(2)	27.719(3)
b/ Å	24.5604(7)	24.3189(16)	24.2992(17)	24.319(3)
c/ Å	31.7007(10)	30.754(3)	30.828(3)	30.950(4)
α/°	90	90	90	90
β/°	112.1159(12)	112.131(3)	112.331(3)	112.509(4)
γ/°	90	90	90	90
Volume/ $Å^3$	20188.0(11)	19233(3)	19192(3)	19274(4)
Z	2	2	2	2
ρ_{calc}/ $g\cdot cm^{-3}$	1.312	1.205	1.289	1.293
μ/ mm^{-1}	3.497	0.488	0.476	0.474
F(000)	7728.0	6834.0	7728.0	7811.0
Radiation	Mo*Kα* (λ = 0.71073)	Mo*Kα* (λ = 0.71073)	Mo*Kα* (λ = 0.71073)	Mo*Kα* (λ = 0.71073)
2θ range for data collection/°	4.944 to 50	5.03 to 50.05	4.834 to 51	5.034 to 51
Index ranges	$-33 \le h \le 33$, $-29 \le k \le 29$, $-37 \le l \le 37$	$-33 \le h \le 33$, $-28 \le k \le 28$, $-36 \le l \le 36$	$-33 \le h \le 33$, $-29 \le k \le 29$, $-37 \le l \le 37$	$-33 \le h \le 33$, $-29 \le k \le 29$, $-37 \le l \le 37$
Reflections collected	458214	944839	400432	802006
Independent reflections	71020 [R_{int} = 0.0984, R_{sigma} = 0.0786]	67823 [R_{int} = 0.1081, R_{sigma} = 0.0463]	71398 [R_{int} = 0.1040, R_{sigma} = 0.0690]	71745 [R_{int} = 0.1073, R_{sigma} = 0.0484]
Goodness of fit on F^2	1.128	1.100	1.114	1.145
Final R index.	R_1 = 0.0727, wR_2 = 0.1795	R_1 = 0.1010, wR_2 = 0.2525	R_1 = 0.1006, wR_2 = 0.2498	R_1 = 0.0799, wR_2 = 0.1942
Largest diff. peak/hole/e $Å^{-3}$	4.86/−2.67	2.43/−1.82	2.84/−1.37	2.51/−1.39

$R_1 = \sum|F_o| - |F_c|/\sum|F_o|$. $wR_2 = \{(F_o^2 - F_c^2)^2/\sum w(F_o^2)^2\}^{1/2}$

Table S21 Mo/V ratio in P–Mo–V polyoxometalates at different stages: precursor, state A, and state B.

	Precursor	State A assemblies	State B crystals
$PMo_{11}V$	$PMo_{10.93}V_{1.07}$	$PMo_{10.83}V_{1.17}$	$PMo_{10.89}V_{1.11}$
$PMo_{10}V_2$	$PMo_{10.04}V_{1.96}$	$PMo_{10.00}V_{2.00}$	$PMo_{10.57}V_{1.42}$
PMo_9V_3	$PMo_{8.92}V_{3.08}$	$PMo_{8.86}V_{3.14}$	$PMo_{9.77}V_{2.23}$

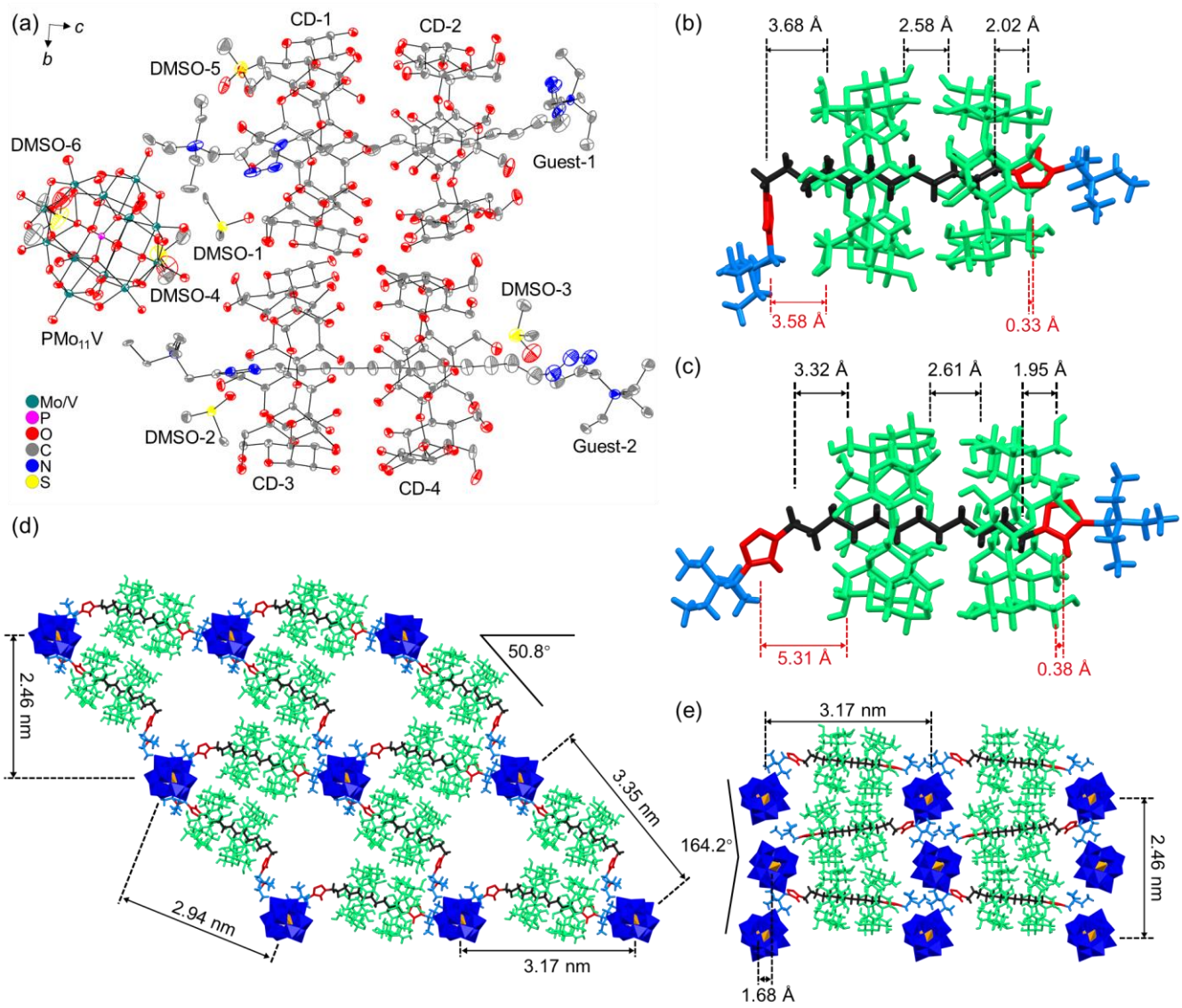

Fig. S42 X-ray crystal structure of CR·$PMo_{11}V$-B. (a) Asymmetric unit (ORTEP Type 30%); (b, c) The relative position between the guest and CD on CRs; (d) Arrangement on the (010) plane; (e) Arrangement on the (100) plane.

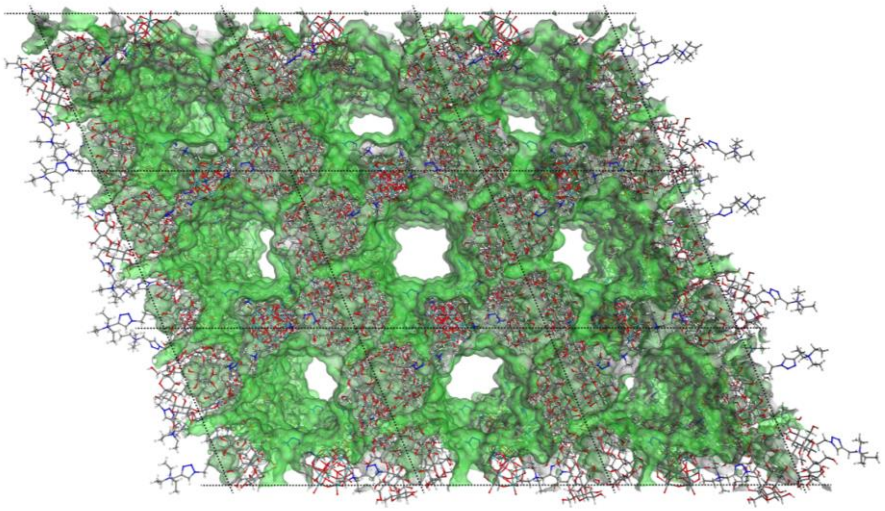

Fig. S43 Voids of CR·$PMo_{11}V$-B single crystal (diameter of 1D channel pore: 1.4 nm).

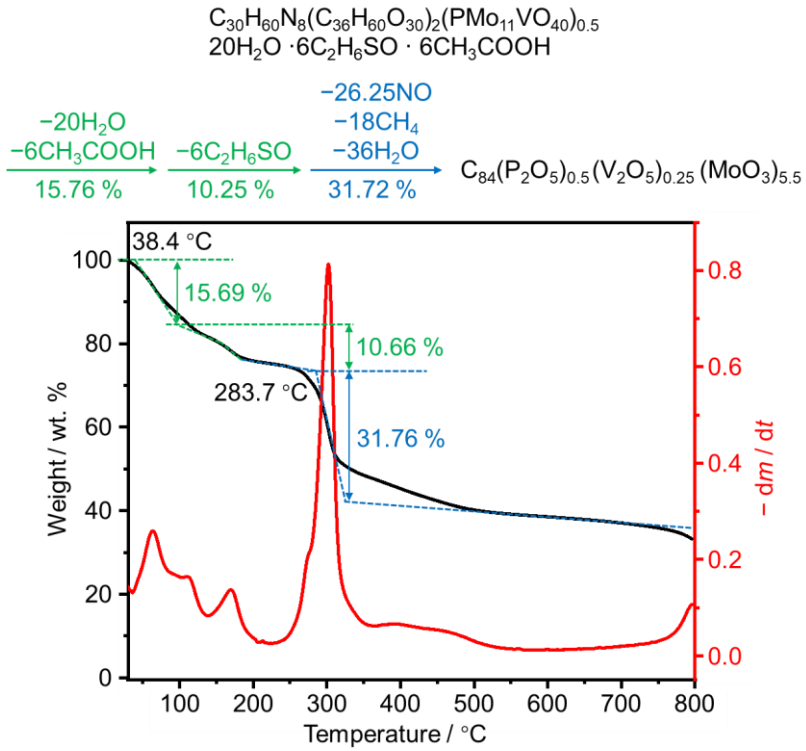

Fig. S44 TGA of CR·$PMo_{11}V$-B single crystal.

Table S22 Solvent mask information for CR·$PMo_{11}V$-B single crystal.

Number	Volume/Å^3	Electron Count	Content/Unit Cell
2	30	0	
3	44	−4	1 H_2O
4	3418	850	13 C_2H_6SO, 24 $C_2H_4O_2$, 12.2 H_2O
7	28	0	

A solvent mask was calculated and 846 electrons were found in a volume of 3520Å^3 in 4 voids per unit cell. This is consistent with the presence of 13[C_2H_6SO], 24[$C_2H_4O_2$], 13.2[H_2O] per Unit Cell which accounts for 1446 electrons per unit cell.

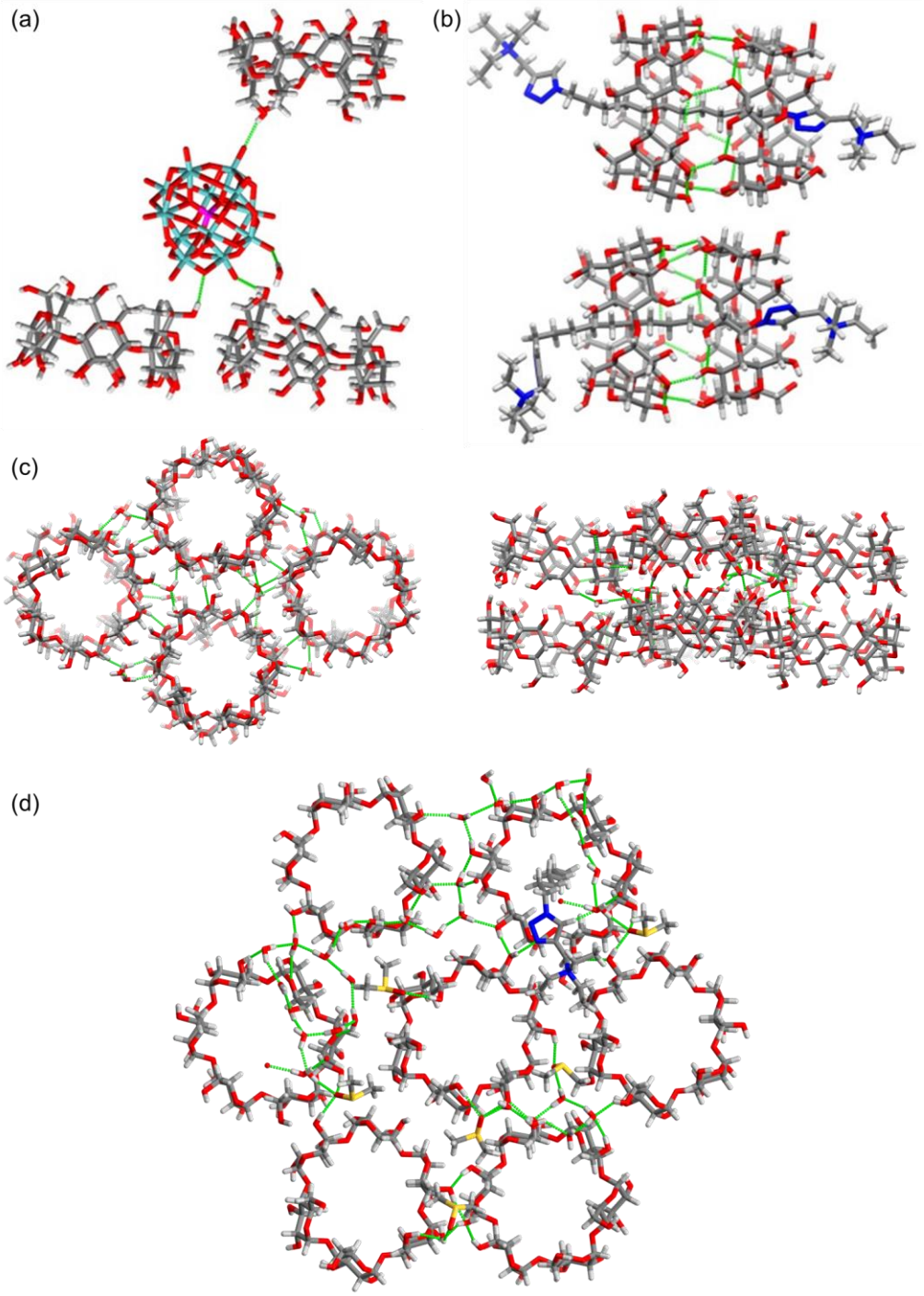

Fig. S45 Hydrogen bonds in CR·$PMo_{11}V$-B. (a) Intermolecular hydrogen bonds among the primary side of cyclodextrins on CR and POM; (b) Intramolecular hydrogen bonds between the secondary side of cyclodextrins on CR; (c) Intermolecular hydrogen bonds among the secondary side of cyclodextrins on CR and crystalline H_2O; (d) Intermolecular hydrogen bonds among the primary side of cyclodextrins on CR, triazole group, and crystalline H_2O.

Table S23 Intermolecular hydrogen bonds list among the primary side of cyclodextrins on CR and POM.

D	A	d(D−A)/Å	D	A	d(D−A)/Å
O305	O8P$^{\#1}$	3.096(11)	O125	O2P$^{\#8}$	2.809(19)
O325	O21P	2.777(12)	O42W	O1P$^{\#9}$	3.01(3)

Symmetry codes: (#1) −x, 0.5+y, 1−z; (#8) −x, −0.5+y, 1−z; (#9) +x, +y, 1+z.

Table S24 Intramolecular hydrogen bonds list between the secondary side of cyclodextrins on CR.

D	A	d(D−A)/Å	D	A	d(D−A)/Å
O307	O303	2.811(11)	O423	O308	2.822(11)
O323	O408	2.782(11)	O427	O423	3.068(11)
O123	O208	2.757(11)	O418	O422	2.884(11)
O302	O328	2.846(11)	O413	O318	2.783(12)
O122	O118	2.950(13)	O402	O428	2.820(12)
O103	O107	2.895(12)	O408	O412	2.792(11)
O102	O128	2.789(11)	O417	O413	2.847(11)
O327	O323	2.874(12)	O403	O407	2.981(13)
O318	O322	2.940(11)	O203	O207	2.879(12)
O308	O312	2.830(11)	O218	O113	2.751(12)
O317	O313	2.985(11)	O227	O223	2.965(14)
O128	O203	2.773(11)	O208	O212	2.786(12)
O328	O403	2.706(11)	O228	O103	2.700(11)
O303	O428	3.051(11)	O223	O108	2.855(13)
O118	O213	2.874(13)	O222	O218	2.837(13)
O113	O117	2.747(12)	O213	O217	2.921(14)
O313	O418	2.822(12)	O108	O112	3.015(13)
O127	O123	2.899(11)	O112	O218	3.033(13)

Table S25 Intermolecular hydrogen bonds list among the secondary side of cyclodextrins on CR and crystalline H_2O.

D	A	d(D−A)/Å	D	A	d(D−A)/Å
O312	O7W	2.702(14)	O6W	O317	2.769(12)
O322	O8W	2.59(3)	O6W	$O423^{\#3}$	2.827(11)
O107	O2W	2.696(14)	O1W	O127	2.761(13)
O117	O5W	2.593(12)	O1W	$O2W^{\#5}$	3.08(2)
O412	$O422^{\#3}$	2.736(11)	O3W	O102	2.732(14)
O428	$O3W^{\#2}$	3.002(13)	O4W	O302	2.734(12)
O407	O108	2.967(13)	O4W	$O228^{\#2}$	2.830(13)
O422	$O8W^{\#4}$	2.90(3)	O7W	$O218^{\#4}$	3.060(15)
O202	$O402^{\#5}$	2.771(11)	O7W	$O8W^{\#4}$	2.68(3)
O207	$O227^{\#5}$	2.844(12)	O2W	$O203^{\#2}$	3.017(16)
O217	$O417^{\#3}$	2.752(11)	O2W	O403	2.926(14)
O212	$O4W^{\#6}$	2.854(15)	O8W	O112	2.69(3)
O5W	$O6W^{\#3}$	2.833(12)	O8W	O408	3.00(3)
O5W	$O307^{\#6}$	2.729(11)			

Symmetry codes: (#2) 1−*x*, 0.5+*y*, 2−*z*; (#3) −*x*, −0.5+*y*, 2−*z*; (#4) −*x*, 0.5+*y*, 2−*z*; (#5) 1−*x*, −0.5+*y*, 2−*z*; (#6) +*x*, −1+*y*, +*z*.

Table S26 Intermolecular hydrogen bonds list among the secondary side of cyclodextrins on CR and crystalline H_2O.

D	A	d(D−A)/Å	D	A	d(D−A)/Å
O105	N7$^{\#2}$	2.772(16)	O9W	O24W$^{\#5}$	2.91(5)
O310	O21W	2.71(2)	O9W	O1W	2.80(3)
O320	O27W$^{\#3}$	2.71(2)	O11W	O10W	2.84(2)
O330	O2S	2.725(12)	O11W	O26W$^{\#5}$	2.70(3)
O315	O43W	2.71(4)	O26W	O430	2.75(2)
O110	O1S	2.815(14)	O15W	O16W$^{\#7}$	3.06(5)
O130	O5S	2.99(4)	O15W	O425	3.10(3)
O415	O309$^{\#3}$	3.177(12)	O29W	O30W	2.80(4)
O415	O310$^{\#3}$	2.797(14)	O29W	O42W	2.60(3)
O420	O199$^{\#4}$	2.50(3)	O17W	O23W	2.84(5)
O420	O29W	2.79(2)	O17W	O18W	2.89(5)
O425	O27W	2.770(16)	O16W	O220	2.93(4)
O405	O26W	2.75(2)	O16W	O32W	3.11(4)
O210	O105$^{\#5}$	2.764(12)	O23W	O224	3.06(3)
O205	O329$^{\#5}$	3.161(11)	O23W	O410	2.54(4)
O205	O330$^{\#5}$	3.111(12)	O25W	O405	2.73(3)
O230	O2S$^{\#5}$	2.749(13)	O20W	O33W	2.78(3)
O215	O15W$^{\#6}$	2.68(2)	O20W	O2S$^{\#5}$	2.934(19)
O225	O19W	2.80(2)	O33W	O34W	2.72(6)
O120	O3S$^{\#3}$	2.93(2)	O33W	O35W	2.71(5)
O220	O17W	2.66(3)	O40W	O229$^{\#5}$	2.85(3)
O430	O14W$^{\#7}$	2.737(18)	O40W	O9W	3.01(4)
O410	O21W$^{\#3}$	2.89(2)	O22W	O16W$^{\#4}$	2.89(5)
O199	O3S$^{\#3}$	2.94(4)	O18W	O225	2.71(4)
O3W	O10W	2.710(16)	O39W	O19W	2.52(5)
O10W	O14W$^{\#2}$	2.688(18)	O39W	O40W$^{\#2}$	3.12(6)
O10W	O210$^{\#2}$	2.741(13)	O24W	O25W	2.74(6)
O14W	O31W	2.75(5)	O24W	O23W	2.51(4)
O14W	O215	2.732(16)	O42W	O3S	2.55(4)
O27W	O28W	2.88(2)	O43W	O6S$^{\#1}$	2.58(5)
O27W	O30W	2.77(3)	O115	O1S	2.903(18)
O21W	O43W	2.72(5)	O198	O40W	2.88(4)
O28W	O420	2.67(2)	O499	O29W	2.54(4)
O28W	O1S$^{\#4}$	2.839(17)	O197	O11W	2.72(5)
O19W	O20W	2.66(2)	O399	O22W	2.87(5)

Symmetry codes: (#2) 1−*x*, 0.5+*y*, 2−*z*; (#3) −*x*, −0.5+*y*, 2−*z*; (#4) −*x*, 0.5+*y*, 2−*z*; (#5) 1−*x*, −0.5+*y*, 2−*z*; (#6) +*x*, −1+*y*, +*z*; (#7) +*x*, 1+*y*, +*z*.

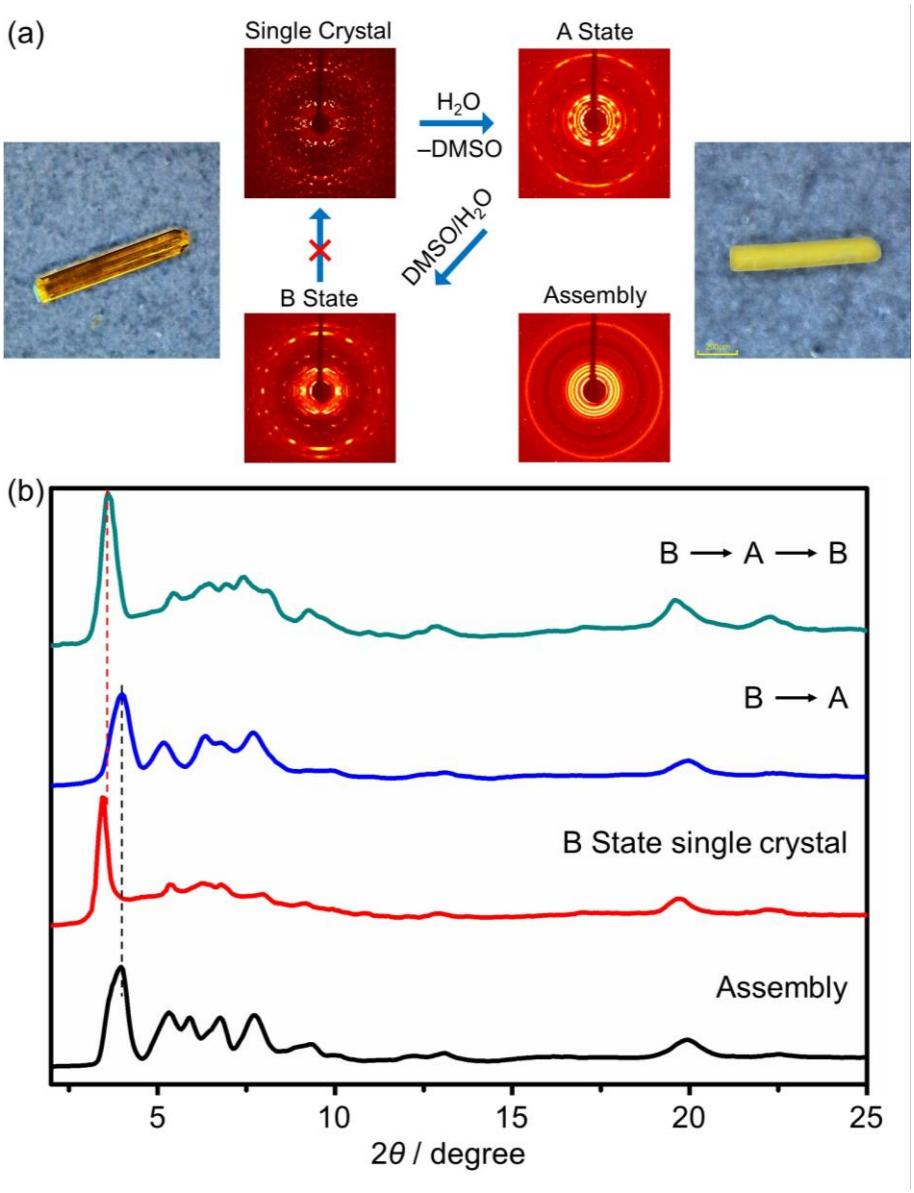

Fig. S46 *In situ* reversible crystalline transformation. (a) Optical picture and 2D XRD pattern of CR·$PMo_{11}V$-A/B single crystal; (b) XRD pattern by integrating 2D XRD image of CR·$PMo_{11}V$ assembly, CR·$PMo_{11}V$-B single crystal, CR·$PMo_{11}V$-B single crystal treated with water, and CR·$PMo_{11}V$-B single crystal treated with water first and then treated with DMSO/H_2O solution (from down to up).

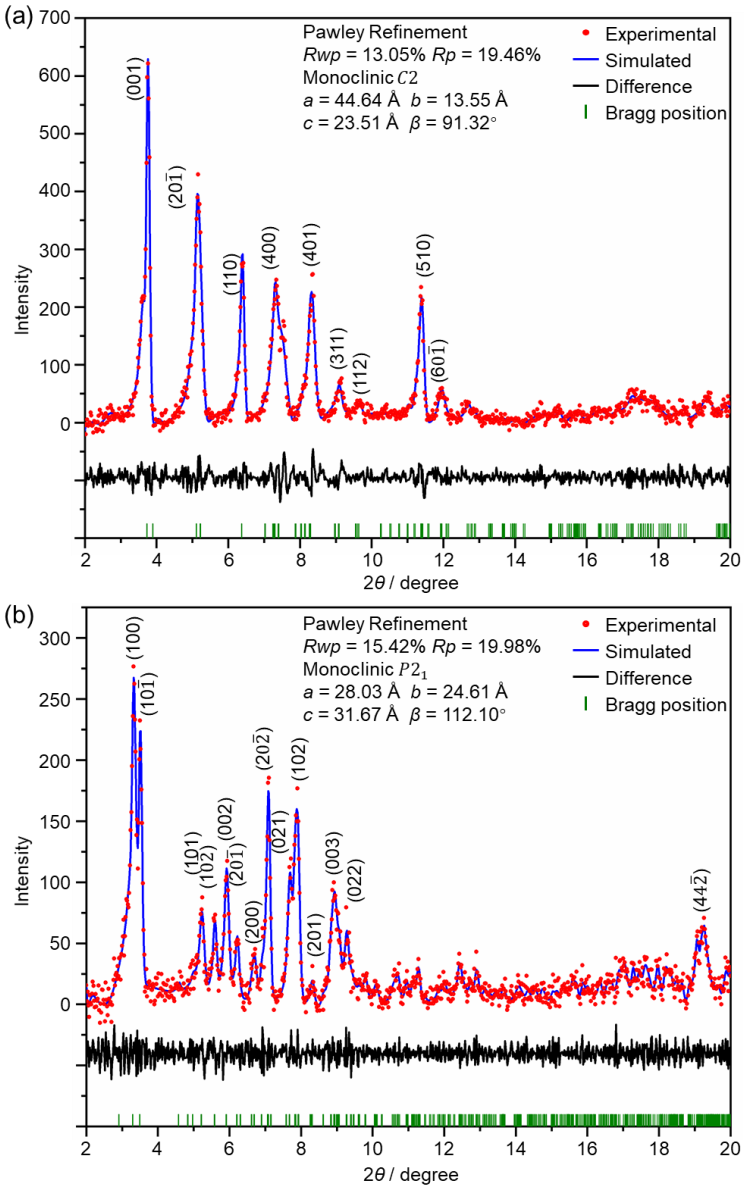

Fig. S47 PXRD Pawley refinement of (a) CR·PMo_{11}V-B single crystal treated with water; (b) CR·PMo_{11}V assembly treated with DMSO/H_2O solution.

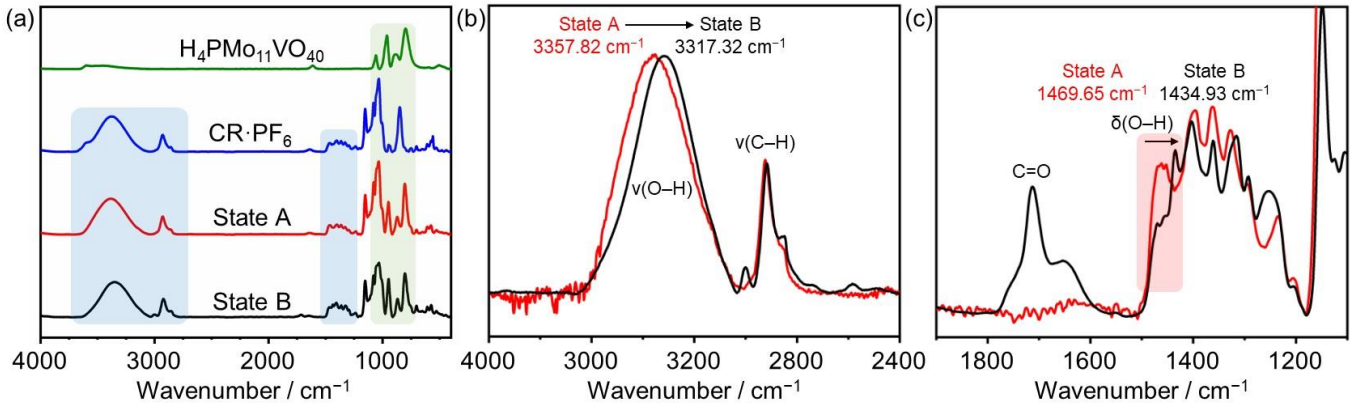

Fig. S48 (a) The IR spectra of $H_4PMo_{11}VO_{40}$, CR·PF_6, CR·PMo_{11}V-A, and CR·PMo_{11}V-B; *in situ* ATR-IR spectra of CR·PMo_{11}V-A, and CR·PMo_{11}V-B with range of (b) 2400 cm^{-1}–4000cm^{-1}; (c) 2400 cm^{-1}–4000cm^{-1}.

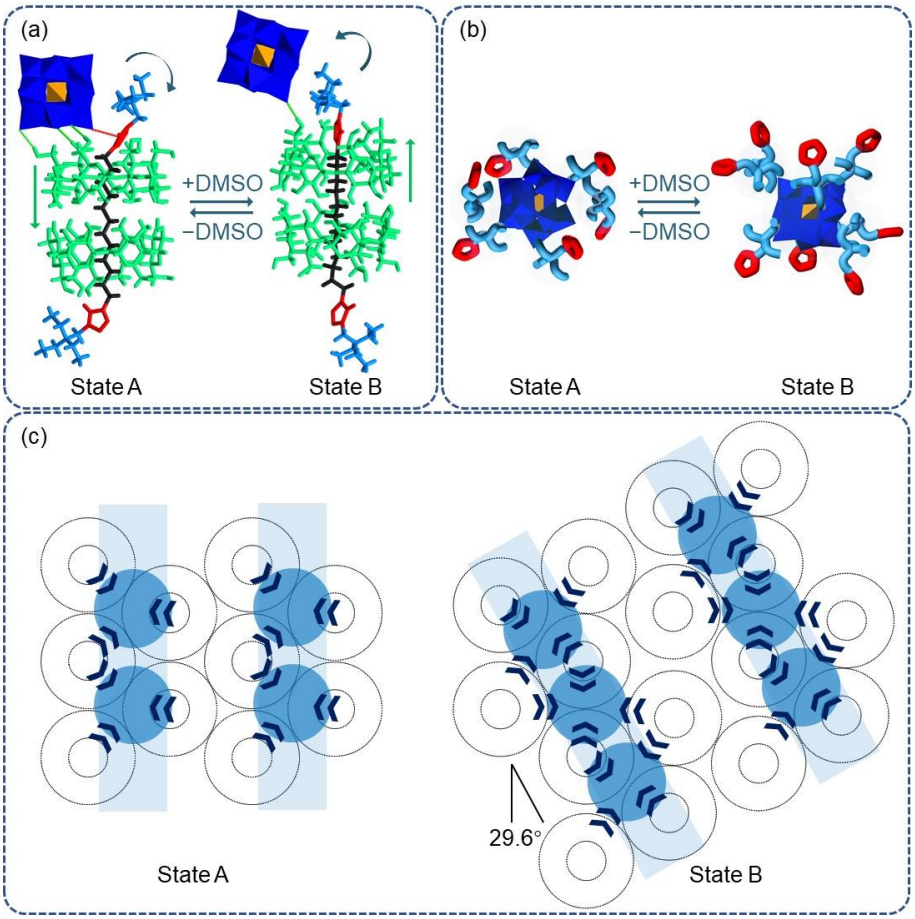

Fig. S49 Reversible crystalline transformation accompanied by (a) rotaxane conformation switching, (b) modulation of ion-binding modes, and (c) top-view structural evolution of the ionic layer.

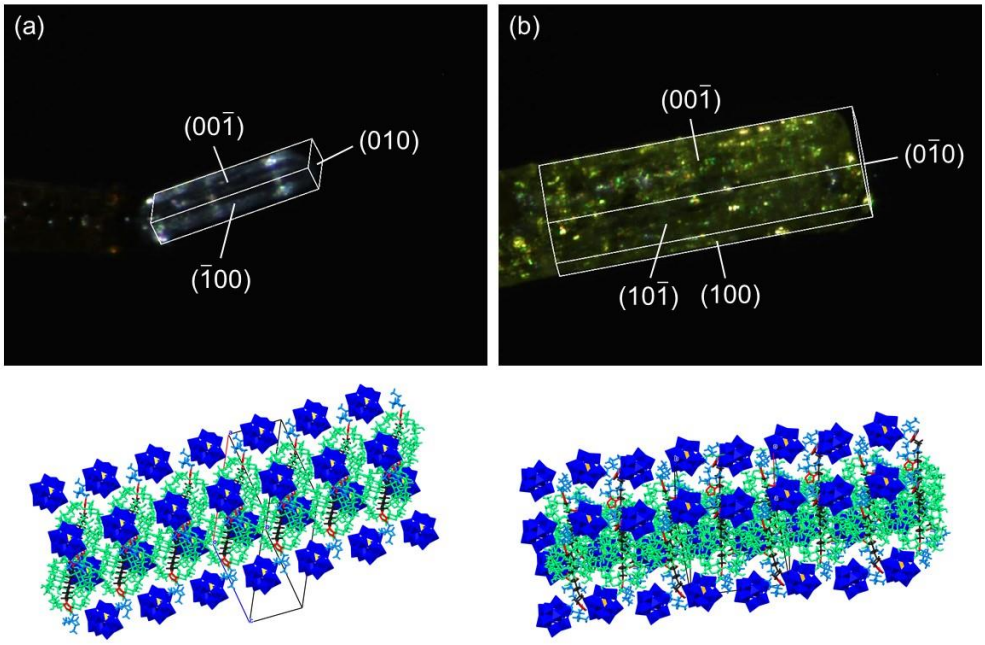

Fig. S50 Facet indexing and corresponding molecular packing arrangement in (a) State A and (b) State B single crystal.

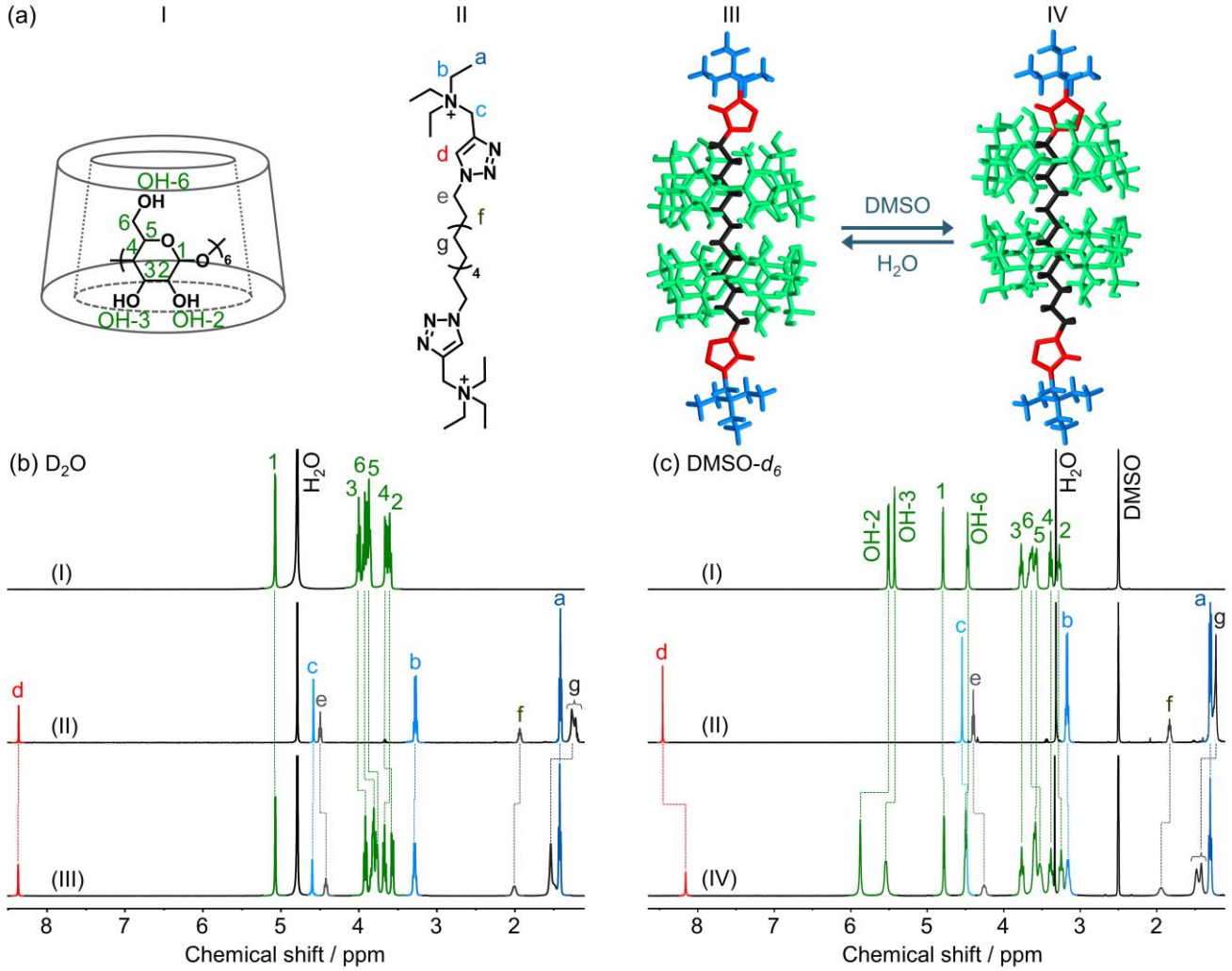

Fig. S51 (a) The chemical structures of (I) α-cyclodextrin, (II) guest molecule, and the bistable states of (III)/(IV) CR in various solvents; Comparison of ^{1}H NMR spectra (b) in D_2O. (c) DMSO-d_6.

S8. Computational details

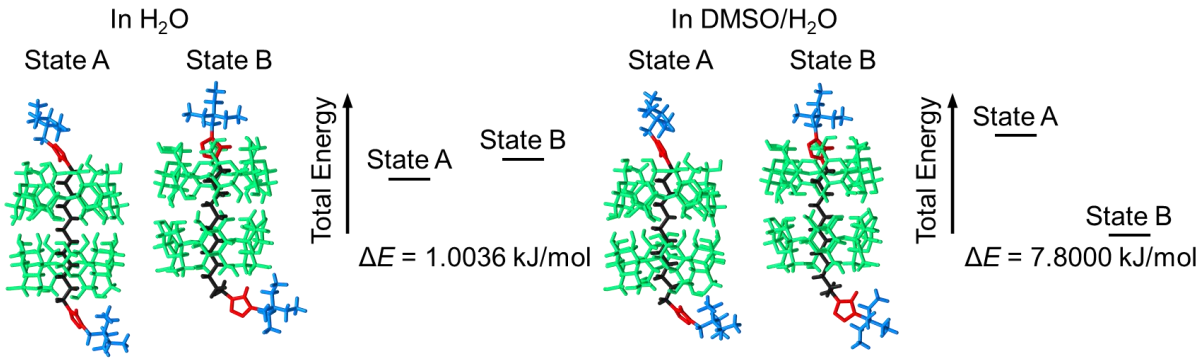

Fig. S52 Geometry optimizations and system energy differences of CR state A and B with different implicit solvation model by DFT calculation.

Table S27 Total energy of CR state A and B with different implicit solvation model by DFT calculation.

E_{tot} / Hatree	In H_2O	In DMSO/H_2O
State A	−8942.590612	−8942.577788
State B	−8942.590226	−8942.580788

Table S28 Total energy, vacancy(without anions) energy, anion energy and absorption energy (binding energy between anions and CRs) of the CR·SiW-A.

	In H_2O	In DMSO/H_2O
E_{tot} / Hatree	−10258.05792	−10258.89995
E_{vac} / Hatree	−7334.793198	−7335.650863
E_{ion} / Hatree	−1461.551184	−1461.552877
E_{abs} / Hatree	−0.16236	−0.14333

$E_{abs} = E_{tot} - E_{vac} - 2E_{ion}$

Table S29 Total energy, vacancy (without anions) energy, anion energy and absorption energy (binding energy between anions and CRs) of the CR·SiW-B.

	In H_2O	In DMSO/H_2O
E_{tot} / Hatree	−10327.83922	−10328.10584
E_{vac} / Hatree	−7404.570089	−7404.827028
E_{ion} / Hatree	−1461.551184	−1461.552877
E_{abs} / Hatree	−0.16677	−0.17306

$E_{abs} = E_{tot} - E_{vac} - 2E_{ion}$

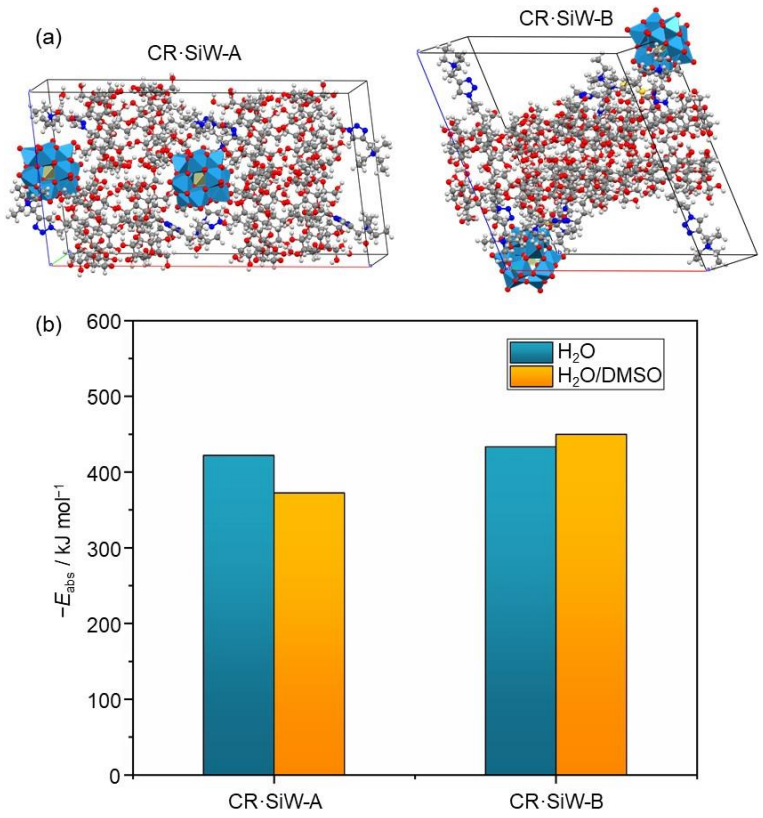

Fig. S53 Geometry optimizations and system energy differences of CR·SiW-A/B. (a) Optimized CR·SiW-A/B crystals in GFN1-xTB level. (b) Adsorption energy difference of CR·SiW-A/B with different self-consistent continuum solvation.

S9. Induced proton conductivity variations

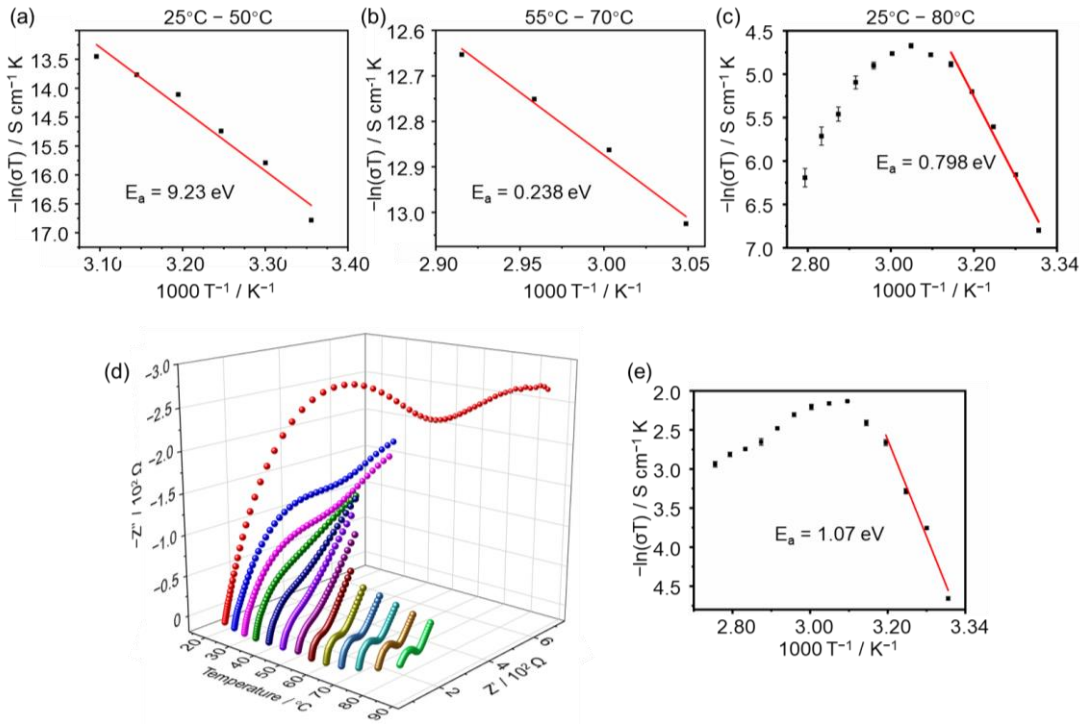

Fig. S54 Arrhenius plots of (a) CR·$PMo_{11}V$ assembly from 25 to 50 ˚C; (b) from 55 to 70 ˚C; (c) CR $PMo_{11}V$-B from 25 to 80˚C; (d) Nyquist diagrams of CR PMo_9V_3-B; (e) Arrhenius plots of CR PMo_9V_3-B from 25 to 80˚C.

S10. Reference

1. Tsigdinos, G. A.; Hallada, C. J. Molybdovanadophosphoric acids and their salts. I. investigation of methods of preparation and characterization. *Inorg. Chem.* **1968**, *7* (3), 437–441.
2. Domaille, P. J. The 1- and 2-dimensional tungsten-183 and vanadium-51 NMR characterization of isopolymetalates and heteropolymetalates. *J. Am. Chem. Soc.* **1984**, *106* (25), 7677–7687.
3. Krause, L.; Herbst-Irmer, R.; Sheldrick, G. M.; Stalke, D. Comparison of silver and molybdenum microfocus X-ray sources for single-crystal structure determination. *J. Appl. Crystallogr.* **2015**, *48* (1), 3–10.
4. Dolomanov, O. V.; Bourhis, L. J.; Gildea, R. J.; Howard, J. A. K.; Puschmann, H. OLEX2: a complete structure solution, refinement and analysis program. *J. Appl. Crystallogr.* **2009**, *42* (2), 339–341.
5. Sheldrick, G. A short history of SHELX. *Acta Crystallogr. Sect. A* **2008**, *64* (1), 112–122.
6. Sheldrick, G. Crystal structure refinement with SHELXL. *Acta Crystallogr. Sect. C-Struct. Chem.* **2015**, *71* (1), 3–8.
7. Spek, A. PLATON SQUEEZE: a tool for the calculation of the disordered solvent contribution to the calculated structure factors. *Acta Crystallogr. Sect. C-Struct. Chem.* **2015**, *71* (1), 9–18.